

PHOSPHORYLATION OF MYOSIN-1C BY cAMP-DEPENDENT PROTEIN
KINASE

By

Emilie Diane Miller

A DISSERTATION

Presented to the Neuroscience Graduate Program

and the Oregon Health & Science University

School of Medicine

in partial fulfillment of

the requirements for the degree of

Doctor of Philosophy

June 26, 2007

School of Medicine
Oregon Health & Science University

CERTIFICATE OF APPROVAL

This is to certify that the Ph.D. dissertation of
Emilie Diane Miller
has been approved

School of Medicine
Oregon Health & Science University

CERTIFICATE OF APPROVAL

This is to certify that the Ph.D. dissertation of
Emilie Diane Miller
has been approved

Advisor

Member

Member

Member

Member

CONTENTS

<u>LIST OF FIGURES</u>	viii
<u>LIST OF ABBREVIATIONS</u>	x
ACKNOWLEDGEMENTS	xiii
ABSTRACT	xiv
<u>INTRODUCTION</u>	1
THE INNER EAR	1
HAIR CELL STRUCTURE	5
MECHANOTRANSDUCTION	10
ADAPTATION	17
HAIR CELL MYOSINS	25
MYOIC STRUCTURE, CALCIUM, AND CALMODULIN	27
MYOSIN MECHANICS	30
MYOSIN V	33
REGULATION OF MYOSIN V by CALCIUM AND CALMODULIN	34
MYOSIN VI	36
PKA AND SPONTANEOUS OSCILLATIONS	39
REGULATION OF TRANSDUCTION CURRENT BY PKA	40
SERINE 701 AND ITS ROLE IN MYOIC FUNCTION	45
<u>MATERIALS AND METHODS I</u>	50
PHOSHO-S701 MYOIC ANTIBODY	50
AUTOSPOT PEPTIDE ARRAY ASSAYS	50

SF9 PROTEIN EXPRESSION	51
PURIFICATION OF MYOIC EXPRESSED IN SF9 CELLS	53
MODIFICATIONS TO THE SF9 PURIFICATION PROTOCOL	54
SDS-PAGE	55
PKA CATALYTIC SUBUNIT EXPRESSION AND PURIFICATION	56
SF9 PROTEIN PHOSPHORYLATION	58
STOICHIOMETRY MEASUREMENTS	58
CONSTRUCTION OF IQ1 PEPTIDES	59
IQ1 PEPTIDE PHOSPHORYLATION	59
ALEXA-CAM BINDING TO IQ1 PEPTIDES	60
TRYPTOPHAN FLUORESCENCE MEASUREMENTS	61
IMMUNOPRECIPITATION OF MYOIC	61
CONJUGATING DAR TO SEPHAROSE	61
BINDING ANTIBODIES TO DAR SEPHAROSE	62
COS-7 CELL STIMULATION AND EXTRACTION	63
IMMUNOPRECIPITATION	64
WESTERN BLOT ANALYSIS	65
<u>MATERIALS AND METHODS II</u>	67
CONSTRUCTION OF S701 MUTATIONS OF HN	67
<i>IN VITRO</i> MOTILITY ASSAY	67
ACTIN PREPARATION	67
ACTIN CYCLING OF MYOSIN	69

ACTIN LABELING	69
PREPARATION OF FLOW-THROUGH CHAMBERS	70
ANALYSIS OF MOTILITY	71
ALPHA-ACTININ <i>IN VITRO</i> MOTILITY ASSAYS	72
ATPASE ASSAY	73
<u>MATERIALS AND METHODS III</u>	<u>74</u>
NMB-ADP INHIBITION OF <i>IN VITRO</i> MOTILITY	74
<u>RESEARCH OBJECTIVES IA</u>	<u>75</u>
<u>RESULTS IA</u>	<u>76</u>
PKA PHOSPHORYLATION OF S701	76
MYOIC CONSTRUCTS	80
MYOIC CONSTRUCTS ARE PHOSPHORYLATED BY PKA	83
<u>DISCUSSION IA</u>	<u>86</u>
<u>FUTURE DIRECTIONS IA</u>	<u>89</u>
<u>RESEARCH OBJECTIVES IB</u>	<u>90</u>
<u>RESULTS IB</u>	<u>91</u>
PHOSPHORYLATION OF MYOIC IN THE PRESENCE OF VESICLES	91
CALCIUM PROMOTES HN PHOSPHORYLATION	96
CALMODULIN PROMOTES IQ1 PEPTIDE PHOSPHORYLATION	99
CALCIUM INHIBITS IQ1 PHOSPHORYLATION	102

ALEXA-CALMODULIN BINDING TO IQ1 PEPTIDES	105
CALMODULIN TITRATION OF IQ1 PEPTIDES	108
<u>DISCUSSION IB</u>	111
<u>FUTURE DIRECTIONS IB</u>	117
<u>RESEARCH OBJECTIVES IC</u>	118
<u>RESULTS IC</u>	119
PHOSPHO-MYOICS701 ANTIBODY	119
IMMUNOPRECIPITATION OF MYOIC FROM COS-7 CELLS	122
IONOMYCIN TREATMENT OF COS-7 CELLS	125
IMMUNOPRECIPITATION OF MYOIC FROM SF9 CELLS	128
<u>DISCUSSION IC</u>	131
<u>FUTURE DIRECTIONS IC</u>	133
<u>RESEARCH OBJECTIVES II</u>	137
<u>RESULTS II</u>	138
S701 AMINO ACID SUBSTITUTIONS	138
<i>IN VITRO</i> MOTILITY OF S701 SITE MUTANTS	141
<i>IN VITRO</i> MOTILITY IN THE PRESENCE OF α -ACTININ	146
ACTIN CYCLING OF HNS701D COMPARED TO HN	149
<u>DISCUSSION II</u>	152
<u>FUTURE DIRECTIONS II</u>	156

RESEARCH OBJECTIVES III	159
RESULTS III	160
<i>IN VITRO</i> MOTILITY OF HN COMPARED TO WT MYOIC	160
INHIBITION OF MOUSE Y61G MYOIC BY NMB-ADP	163
DISCUSSION III	166
FUTURE DIRECTIONS III	168
SUMMARY AND CONCLUSIONS	169
REFERENCES	172

LIST OF FIGURES

FIGURE 1.	THE INNER EAR	3
FIGURE 2.	BULLFROG HAIR CELLS	7
FIGURE 3.	HAIR CELL STRUCTURE	9
FIGURE 4.	HAIR CELL TRANSDUCTION	13
FIGURE 5.	TIP LINK STRUCTURE	15
FIGURE 6.	MODEL OF THE TRANSDUCTION APPARATUS	19
FIGURE 7.	FAST AND SLOW ADAPTATION	21
FIGURE 8.	MODEL OF SLOW ADAPTATION	24
FIGURE 9.	MYOIC FUNCTIONAL DOMAINS	29
FIGURE 10.	MYOSIN ATPASE CYCLE	32
FIGURE 11.	PKA ACTIVATORS AND INHIBITORS AFFECT THE CURRENT-DISPLACEMENT CURVE	42
FIGURE 12.	PKA INHIBITION AND ADAPTATION	44
FIGURE 13.	CONSERVATION OF S701	48
FIGURE 14.	PKA PHOSPHORYLATION OF S701	79
FIGURE 15.	MYOIC CONSTRUCTS	82
FIGURE 16.	PHOSPHORYLATION OF MYOIC CONSTRUCTS	85
FIGURE 17.	LOCATION OF S701 IN MYOIC	93
FIGURE 18.	PS VESICLES AND MYOIC PHOSPHORYLATION	95
FIGURE 19.	CALCIUM AND MYOIC PHOSPHORYLATION	98
FIGURE 20.	PHOSPHORYLATION OF IQ1	101
FIGURE 21.	CALCIUM TITRATION OF IQ1 PHOSPHORYLATION	104

FIGURE 22.	ALEXA-CAM BINDING TO IQ1 AND PHOS-IQ1	107
FIGURE 23.	CAM TITRATION OF NATIVE CAM BINDING	110
FIGURE 24.	MODEL FOR CALCIUM AND CAM REGULATION	114
FIGURE 25.	PHOSHO-MYOICS701 ANTIBODY	121
FIGURE 26.	IP OF MYOIC FROM COS-7 CELLS	124
FIGURE 27.	IP OF MYOIC FROM IONOMYCIN-TREATED CELLS	127
FIGURE 28.	IP OF MYOIC FROM SF9 ELUATES	130
FIGURE 29.	SCANSITE MYOIC PHOSPHORYLATION SITES	136
FIGURE 30.	AMINO-ACID SUBSTITUTIONS FOR S701	140
FIGURE 31.	<i>IN VITRO</i> MOTILITY ASSAY	143
FIGURE 32.	<i>IN VITRO</i> MOTILITY OF S701 MUTANTS	145
FIGURE 33.	FORCE MEASUREMENTS OF S701 MUTANTS	148
FIGURE 34.	ACTIN CYCLING OF HN AND HNS701D	151
FIGURE 35.	<i>IN VITRO</i> MOTILITY OF HN AND WT MYOIC	162
FIGURE 36.	<i>IN VITRO</i> MOTILITY OF Y61G AND WT MYOIC	165

ABBREVIATIONS

AC1	adenylate cyclase 1
AKAP	A-kinase anchoring protein
APS	ammonium persulfate
ATP	adenosine triphosphate
ADP	adenosine diphosphate
BCA	bicinchoninic acid
BSA	bovine serum albumin
C	catalytic
CaM	calmodulin
CAMKII	Ca ²⁺ /calmodulin kinase II
cAMP	Cyclic adenosine monophosphate
CAPS	N-Cyclohexyl-3-aminopropanesulfonic acid
CP	cuticular plate
CREB	cAMP response element-binding protein
DAR	donkey anti-rabbit
DEGs	degenerins
DMEM	Dulbucco's modified Eagle's medium
DMP	dimethylpimelimidate
DTT	dithiothreitol
EDTA	ethylenediamine tetraacetic acid
EGTA	ethylene glycol tetraacetic acid
FBS	fetal bovine serum

FERM	fodrin, ezrin, radixin, moesin
GM	Grace's Media
GCM	Grace's Complete Media
HB	hair bundle
HEPES	N-(2-Hydroxyethyl)piperazine-N'-(2-ethanesulfonic acid)
HN	head-neck Myolc
HRP	horse radish peroxidase
IBMX	3-isobutyl-1-methylxanthine
IP	immunoprecipitate
ITPG	isopropylthio-beta-D-galactoside
I-X	current-displacement
K	kinocilium
LB	Luria broth
Myolc	myosin-1c
MT	mitochondria
N	nucleus
NCCC	National Cell Culture Center
NMB-ADP	(2-methylbutyl) adenosine diphosphate
NMB-ATP	(2-methylbutyl) adenosine triphosphate
NT	neck-tail Myolc
OM	otolithic membrane
PBS	phosphate buffered saline
pfu	plaque forming units

PH	pleckstrin homology
Pi	inorganic phosphate
PIP ₂	phosphoinositide
PKA	protein kinase A
PKC	protein kinase C
PMCA	Ca ²⁺ -dependent ATPase pump
PMSF	phenylmethylsulfonyl fluoride
PS	phosphoserine
PVDF	polyvinylidene fluoride membrane
R	regulatory
Rh-Ph	rhodamine-phalloidin
rpm	repetitions per minute
RT	room temperature
SB	sample buffer
SC	supporting cells
SD	standard deviation
SDS	sodium dodecyl sulfate
SDS-PAGE	sodium dodecyl sulfate - polyacrylamide gel electrophoresis
SE	standard error
SH3	src homology domains
TEMED	N,N,N,N -Tetramethyl-Ethylenediamine
TRP	transient potential receptor
TTBS	Tris-Tween buffered saline

ACKNOWLEDGEMENTS

This work wouldn't have been possible without the support of my mentor, Peter Gillespie. It has been several years since I began work in his lab, but he has always kept my enthusiasm for science high through the trials and tribulations of research.

The members of the Gillespie lab have offered countless hours of help and have kept me going throughout the years. Kevin Nusser has come to my rescue many times through the difficulty of working with Sf9 cells. I thank members of the John Scott lab for their generous help with phosphorylation protocols, PKA expression, and generation of the peptide arrays by their AutoSpot machine. I also thank the Farrens lab and Steve Mansoor for their help and use of the fluorescence spectrophotometer for the calmodulin-binding experiments.

I thank my parents, sister, and Kevin McCabe for their encouragement, I would have never made it through this without them. Lastly, I want to thank my thesis committee for their support and helpful advice with this project.

ABSTRACT

In hair cells of the inner ear, the process of adaptation resets the open probability of the transduction channel to its resting value restoring hair-cell sensitivity. Determining how the adaptation motor, myosin-1c (Myo1c), is regulated is critical for understanding how sensitivity is controlled in hair cells. Previous research has shown that activators of Protein Kinase A (PKA) can reduce channel open probability, suggesting a decrease in force production by the adaptation motor. Consistent with these results, a PKA phosphorylation site (RRXS) is located at serine 701 (S701) in a hinge region between the head and neck of Myo1c, a prime location to affect mechanics of the motor.

The experiments herein demonstrate that Myo1c could be phosphorylated by PKA at S701. Short peptides of Myo1c containing the PKA consensus site at S701 were strongly phosphorylated by PKA. Sf9 cell-expressed constructs of Myo1c containing either the head or tail domains in addition to the neck domains were also phosphorylated by PKA, though stoichiometry measurements showed only 10-15% of the protein was phosphorylated. Phosphorylation levels of long constructs were increased in the presence of Ca^{2+} . Phosphorylation of short peptides containing only the first IQ domain and PKA consensus site were phosphorylated by PKA strongly in the presence of calmodulin (CaM), but inhibited when Ca^{2+} was present. CaM also bound with equal affinity to the first IQ domain of both phosphorylated and unphosphorylated short peptides of

Myolc. These results suggest that the absence of CaM from either the second, third, or fourth IQ domain may be ideal for phosphorylation.

In an attempt to determine the phosphorylation state of Myolc in hair cells, the Myolc phosphorylation states in COS-7 cells and purified Myolc from Sf9 cells were measured. Cells were exposed to reagents to stimulate or inhibit phosphorylation, or no treatment, and then immunoprecipitated with an antibody specific for phosphorylated Myolc. When immunoprecipitated eluates were probed with a general Myolc antibody, no Myolc was recognized. These results show that Myolc is unphosphorylated both in COS-7 and Sf9 cells. These results confirm that Myolc is difficult to phosphorylate, or may require other undetermined conditions for efficient phosphorylation.

To determine the importance of the S701 site for Myolc function, the ATPase and *in vitro* motility activities were investigated in head-neck (HN) Myolc mutants that mimic the phosphorylated (HNS701D) and unphosphorylated (HNS701A) states of Myolc. Preliminary results show that HNS701D had slower ATPase rates than HNS701A or HN. Both HN701D and HNS701A translocated actin at slower rates than HN, with HN701D displaying the slowest velocities. In an assay of force production, the actin-binding protein α -actinin was introduced into the *in vitro* motility experimental set-up. Predictably, HN was stalled with increasing concentrations α -actinin. The velocities of both HN701D and HN701A remained constant with increasing amounts of α -actinin. These results suggest that both HN701A and HN701D have greater force-producing capabilities than

HN. These results also illustrate that importance of the S701 site for MyoIc mechanics.

Finally, *in vitro* motility studies showed that wild-type MyoIc had a greater velocity than the truncated version HN. These results suggest the tail region is potentially critical for the myosin step size or force production and may play a role in stabilization or unfolding of the protein to effectively translocate actin. MyoIc was also determined to be a key component in the process of fast adaptation. To support *in vivo* studies in mice, *in vitro* motility studies were conducted with the *in vitro* motility assay. NMB-ADP, the mutant-specific inhibitor of Y61G MyoIc, effectively slowed down motor velocity and had no effect on wild type mouse MyoIc, as expected. Ca^{2+} was also able to inhibit velocity of both wild type and Y61G MyoIc.

These results illustrate the complicated nature of phosphorylating MyoIc. We have determined that the presence of CaM at IQ1 and Ca^{2+} is crucial for phosphorylation of both short and long constructs of MyoIc. These results suggest that CaM at IQ2 or an intermediate Ca^{2+} occupied state of CaM may influence PKA phosphorylation of S701. Mutations of S701 also affected ATPase rate, *in vitro* motility velocities, and force-producing properties of MyoIc confirming that S701 is critical for MyoIc mechanics. Taken together, these results support the preliminary effects of PKA inhibitors and activators on hair cell open probability.

INTRODUCTION

The Inner Ear

Within the inner ear are several organs that enable us to respond to auditory stimuli and maintain balance. The spiral-shaped cochlea is sensitive to both high- and low-frequency auditory stimuli, while the vestibular organs—the sacculus, utricle, and three semicircular cristae—detect angular accelerations and head motion in several planes of sensitivity (Figure 1A).

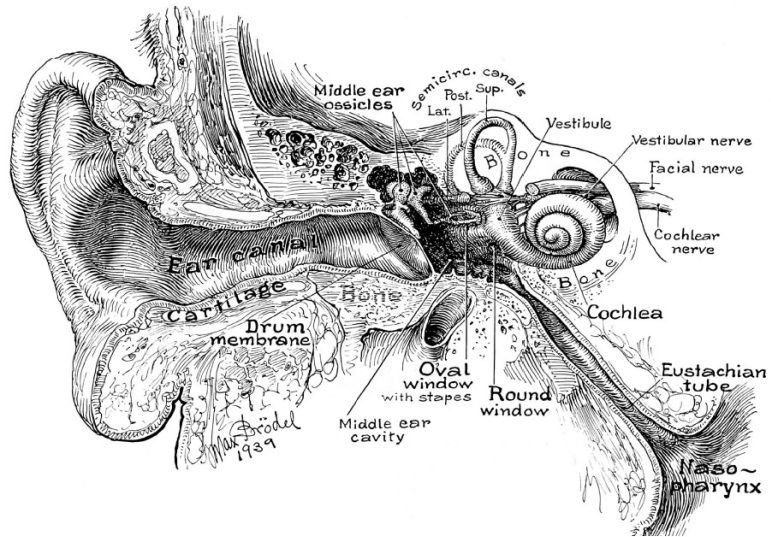
The cochlea is divided into three compartments: the scala tympani, the scala media, and the scala vestibuli (Figure 1B). The scala vestibuli and scala media are separated by Reissner's membrane, while the scala media and scala tympani are separated by the reticular laminae. The potassium-rich endolymph, produced by the stria vascularis, fills the scala media (Wangemann P, 1995). The perilymph, a potassium-poor yet sodium-rich fluid, bathes the scala vestibuli and tympani.

Sound waves vibrate the three ossicles of the middle ear, the malleus, incus, and stapes, which transmit vibrations to the oval window. The motion of the oval window causes movement of the perilymph and basilar membrane of the organ of Corti. Movement of the basilar membrane relative to the overlying tectorial membrane stimulates mechanically sensitive cells of the organ of Corti.

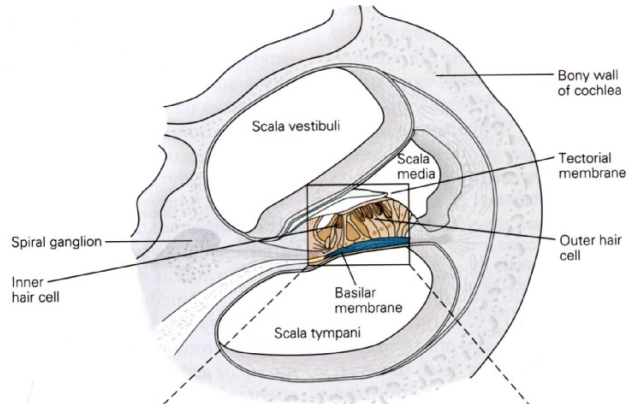
In the organ of Corti, there are four parallel rows of mechanically sensitive cells called hair cells (Figure 1C). There are approximately 15,000 hair cells in

Figure 1. The inner ear. A. Sound waves are transmitted to the fluid-filled cochlea via vibrations of the middle ear ossicles. The sensory cells are located in the organ of Corti. B. Cross section through the cochlea. The cochlea is divided into three chambers; the scala vestibuli, scala tympani, and scala media. The sensory cells dwell within the basilar membrane of the scala media. C. Three rows of outer hair cells and one row of inner hair cells sit in the organ of Corti. Hair cells are stimulated when the basilar membrane oscillates relative to the tectorial membrane. The inner hair cells are primarily innervated by afferent fibers while the outer hair cells are enervated by efferent fibers. The pillar cells provide structural support to the organ of Corti (Fain, 1999).

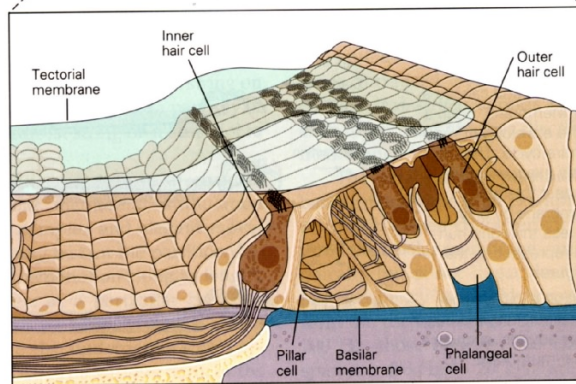
A



B



C



the human cochlea, which are tonotopically arranged; low frequency cells are located at the apex, while high frequency cells are found at the base (G., 1960). Three rows of outer hair cells are essential for signal amplification and receive primarily efferent innervation. The single row of inner hair cells transmits signals to afferent fibers which transmits sensory information to the brain. The rows are separated by the pillar cells, while Deiters' cells cup the outer hair cells; both provide stability and support to the hair cells. The tectorial membrane lies over the organ of Corti, to which the outer hair cells are mechanically coupled (Lim, 1986). In the scala tympani, fluid movement stimulates activity of the basilar membrane and organ of Corti. Shear between the organ of Corti the overlying tectorial membrane stimulates the bundles of the hair cells resulting in mechanotransduction.

The sacculus is a vestibular organ specialized for detecting acceleration in the vertical plane at low frequencies. The bullfrog sacculus, an important model for hair cell function, also detects ground-borne vibrations. The frog sacculus contains approximately 3000 hair cells which are surrounded by nonsensory supporting cells (Jacobs and Hudspeth, 1990). The saccular hair cells sit in the sensory macula, a kidney-shaped structure while the otolithic membrane lies on top of the hair cells. Calcium carbonate crystals, the otoconia, are situated on top of the otolithic membrane. Because otoconia are dense, they move more slowly than the hair cells, deflecting the otolithic membrane and stimulating the hair cells (AV, 2001). The utricle is similar to the sacculus in structure, but detects acceleration in the horizontal plane.

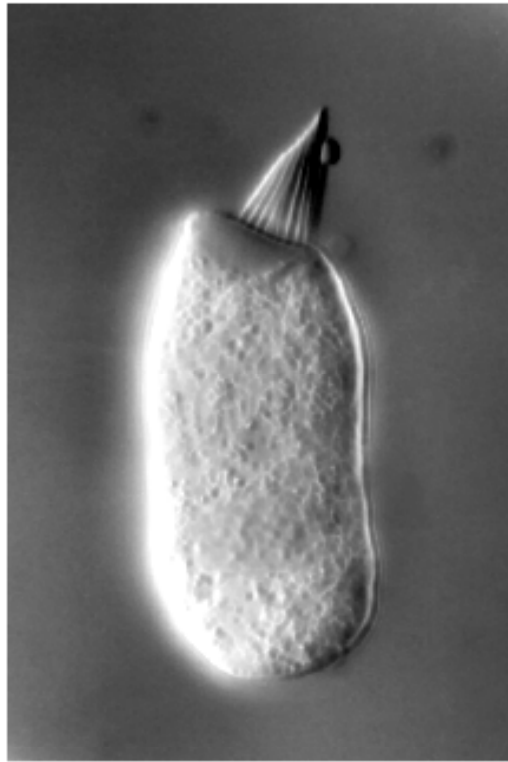
The three semicircular canals are arranged 90° orthogonal to one another and are stimulated by angular acceleration in three orthogonal planes. Within each of the semicircular canals dwells the ampulla, an enlarged area that contains the hair cells situated on a ridge in the ampulla known as the crista ampullaris (Lewis, 1985). The hair bundles are embedded in the gelatinous cupula that overlies the hair cells (Lewis, 1985). Changes in angular acceleration produce movement of the endolymph in the semicircular canals. This movement deflects the cupula, which in turn stimulates hair cells.

Hair Cell Structure

The unique structure of hair cells carries out the conversion of mechanical stimulus into an electrical signal. They are exquisitely sensitive and can respond to deflections as small as 0.3 nm (Sellick et al., 1982). Hair cells of auditory and vestibular organs are topped by 30-300 actin-filled stereocilia, arranged in rows of ascending height; together, they constitute the hair bundle (Figure 2). Among the stereocilia is one true microtubule-containing cilium, the kinocilium, which is thought to play a role in the patterning of the hair bundle (Kelley MW, 1992; Montcouquiol M, 2003). Although the kinocilium is present in hair cells during development, it is not necessary for transduction (Hudspeth and Jacobs, 1979). Stereociliary actin filaments, crosslinked by fimbrin and espin, taper at the base of the stereocilia and insert into the actin-dense cuticular plate of the cell body (Baylor and Fetiplace, 1975; Tilney et al., 1983; Zheng et al., 2000). Stereocilia tapering facilitates pivoting of the bundle as a unit and allows the stereocilia to

Figure 2. Bullfrog hair cells. A. A differential interference contrast micrograph showing an isolated bullfrog hair cell and the mechanosensitive hair bundle (W. M. Roberts and A. J. Hudspeth, unpublished). B. Electron micrograph of the frog saccular hair bundle. The bundle is composed of individual stereocilia and one true cilium, the kinocilium. The stereocilia are arranged in ascending height.

A



B

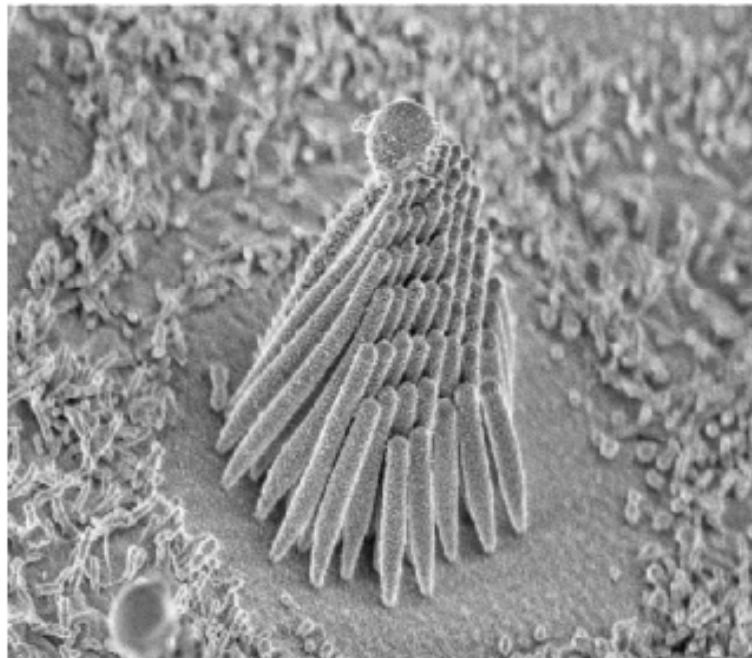
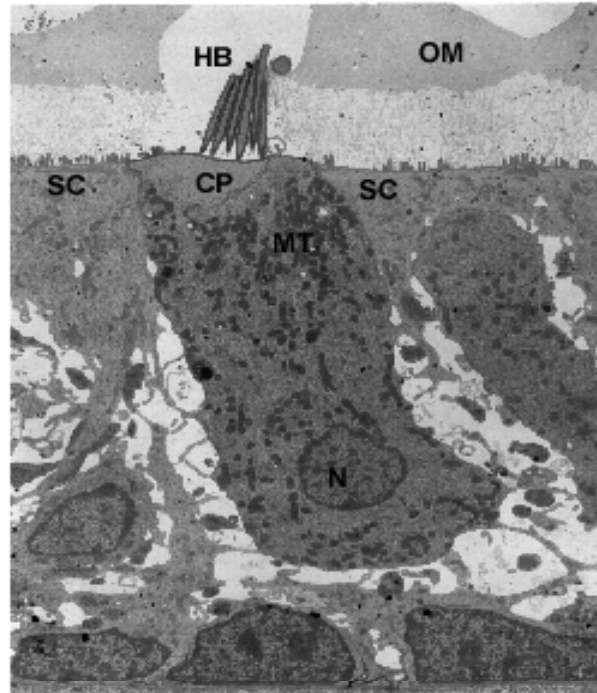
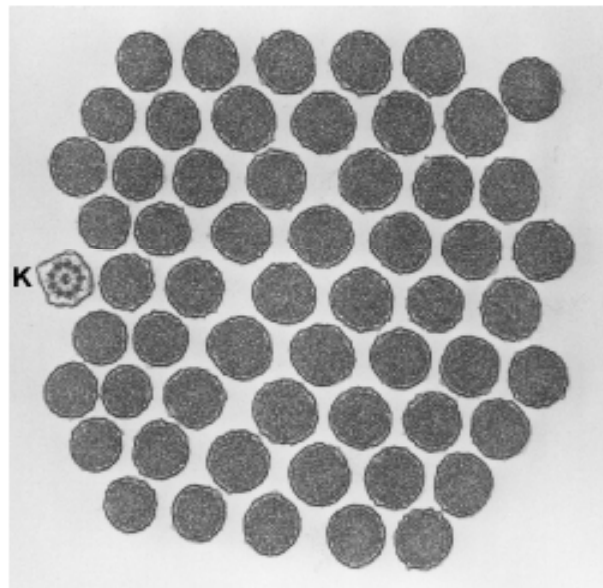


Figure 3. Hair cell structure. A. Transmission electron micrograph of a hair cell and sensory epithelium from the bullfrog sacculus. The otholithic membrane (OM) overlies and is coupled to the hair bundle (HB). Actin filaments comprise the cuticular plate (CP) into which the stereocilia are anchored. The mitochondria (MT) and nucleus (N) are noted. Hair cells are surrounded by supporting cells (SC) (Jacobs and Hudspeth, 1990). B. Cross section through the hair bundle. Each stereocilium is packed with actin filaments while the kinocilium (K) contains microtubules.

A



B



slide along one another (Howard and Ashmore, 1986). Several crosslinks function to keep the bundle together as a cohesive unit (Goodyear et al., 2005). Lateral links attach adjacent stereocilia along their shafts, ankle links attach the basal regions of neighboring stereocilia, and tip links connect neighboring stereocilia near the tips of the bundle (Goodyear et al., 2005).

Mechanotransduction

Deflections of the hair bundle toward the tallest stereocilia open cation-selective channels and depolarize the hair cell (Figure 4). Because the hair bundle is surrounded by high-potassium endolymph, the inward depolarizing current is carried primarily by potassium, and less so by Ca^{2+} and Na^+ (Bosher and Warren, 1978). The resultant cell depolarization triggers neurotransmitter release from synapses at the basolateral membrane of the hair cell. At rest, 10-20% of channels are open; further channel opening results in increased release of neurotransmitter. When the bundle is deflected towards the shortest stereocilia, channels close, the cell hyperpolarizes, and consequently, neurotransmitter release is decreased (Howard et al., 1988). These movements were defined to be along the axis of sensitivity, as perpendicular bundle movements have no effect on transduction (Shotwell et al., 1981).

The opening of channels is very fast, which argues against the presence of a second messenger cascade (Corey and Hudspeth, 1983). Instead, direct gating by the mechanical stimulus is thought to open the channel. The gating-spring

model is the dominant model for hair cell transduction (Corey and Hudspeth, 1983). This model proposes that positive-directed deflection of the bundle causes tension in a gating spring, which results in an increased open probability of the transduction channel (Corey and Hudspeth, 1983).

Recently, considerable effort has been put into the identification of two key components of the transduction machinery, the tip link and the transduction channel. The tip link is composed of two helical filaments that stretch from the side of one stereocilium to the lateral wall of the next tallest neighboring stereocilium (Baylor and Fettiplace, 1975; Pickles et al., 1984). The tip link splits to form two insertions into the wall of the taller stereocilium and several insertions on the tip of its shorter neighboring stereocilium. Recently, cadherin 23 and protocadherin-15 have been identified as components of the tip link (Siemens et al., 2004; Sollner et al., 2004; Ahmed et al., 2006). Cadherin 23 assembles as a dimer, which is consistent with data from electron micrographs of the stereocilia (Kachar et al., 2000; Siemens et al., 2004). Significantly, tip links and transduction disappear in low- Ca^{2+} conditions and when exposed to the Ca^{2+} chelator, BAPTA (Assad et al., 1991; Zhao et al., 1996). Cadherin 23 is similarly sensitive to low Ca^{2+} and protocadherin-15 is lost from the hair bundle with Ca^{2+} chelation (Siemens et al., 2004; Ahmed et al., 2006). These data further support the proposal that these two proteins are part of the tip-link structure. Based upon its location and structure, the tip link was hypothesized to gate the transduction channel (Pickles et al., 1984). It was initially thought also to be the gating spring but analysis of scanning electron micrographs and mechanical models have

Figure 4. Hair cell transduction. Only the cuticular plate and stereocilia are illustrated for simplicity. At rest 10-20% of channels (yellow) are open, allowing minimal amount of K^+ and Ca^{2+} entry. A positive displacement puts tension on the gating spring, allowing all channels to open and more K^+ and Ca^{2+} to enter. Negative displacements slacken the gating spring and all channels are closed (Gillespie, 1995; Corey and Hudspeth, 1983)

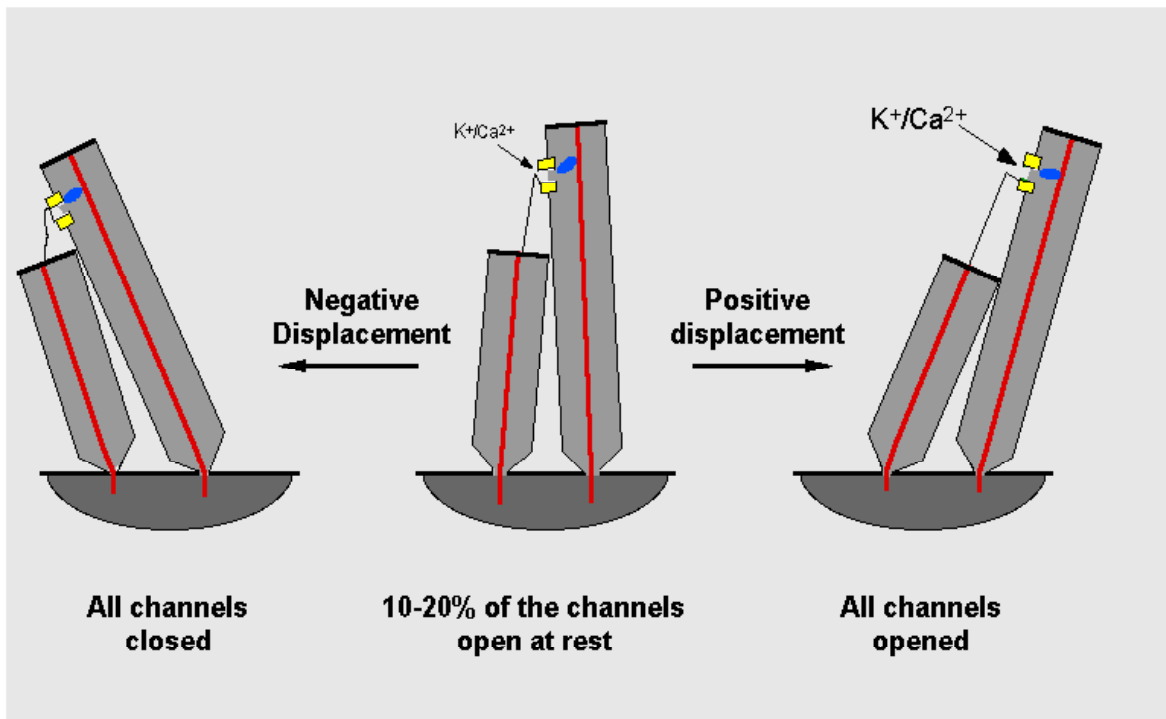
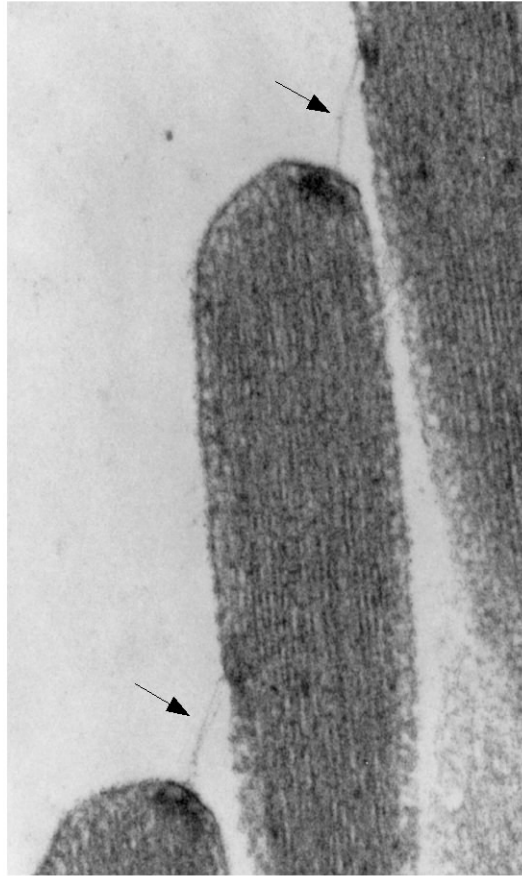
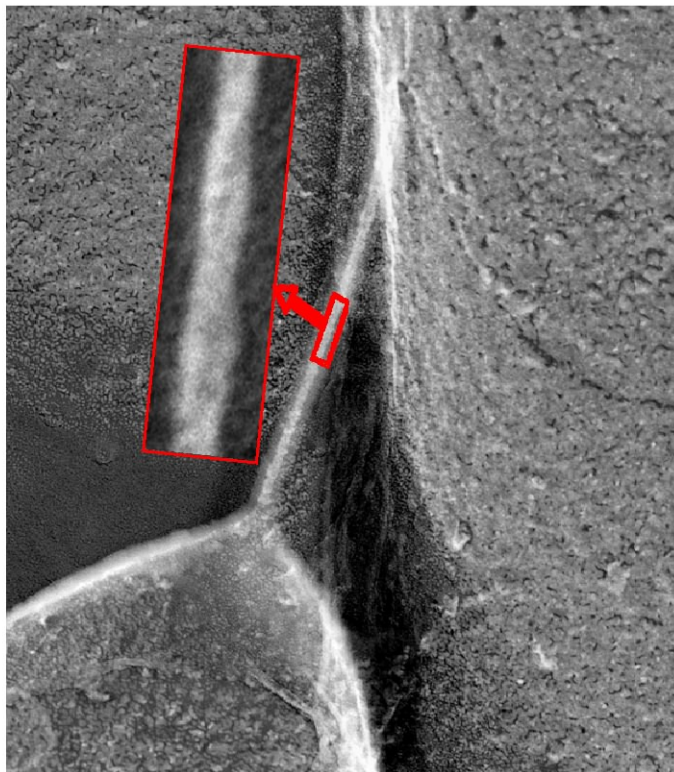


Figure 5. Tip link structure. A. Transmission electron micrograph of a stereocilia from a bullfrog saccular hair cell from R. A. Jacobs and A. J. Hudspeth, unpublished. Tip links are indicated (arrows). B. Freeze-etch SEM image of a bullfrog tip link. Tip links are attached from the tip of the shorter stereocilia to the side of the next tallest neighbor. The helical structure is highlighted (inset) (Kachar et al., 2000).

A



B



argued against this idea due to the proposed rigidity of the tip link (Kachar et al., 2000). The gating spring is believed to be a separate element or protein within the bundle in series with the tip link.

The identity of the transduction channel also is unknown. Large-scale genetic screens of candidate genes have identified several members of the DEG/ENaC family that are necessary for nematode mechanotransduction (O'Hagan R, 2005). Degenerins (DEGs), channels related to epithelial sodium channels in vertebrates, and ENaCs have been investigated in other organisms; however, these have both been ruled out as the transduction channel due to inconsistencies in electrophysiological profiles and the finding that knockout mice have normal hearing (Rusch and Hummler, 1999).

Transient potential receptor (TRP) channels have been promising candidates for the transduction channel due to their similar conductance properties (Nagata et al., 2005). In *Drosophila*, NompC, a gene encoding TRPN1 of the TRP channel family, was shown to be important for fly bristle mechanotransduction (Walker et al., 2000). Because of this key finding, considerable effort has been focused on finding similar TRP channels in other systems. A homolog of TRPN1 was identified in zebrafish (Sidi et al., 2003), but is not present in mouse and human genomes. The TRPA1 channel has been proposed as a candidate for the transduction channel in mammals (Corey et al., 2004). siRNA interference of TRPA1 channels decreased transduction currents and Ca²⁺-sensitive labeling was present at the tips of the stereocilia, kinocilium, and in the pericuticular necklace (Corey et al., 2004). Similar to TRPN1, TRPA1 has a series of ankryin

repeats near the N- terminal, which have been proposed to be the gating spring. When critical exons were deleted from the mouse TRPA1, however, the mice retained vestibular and auditory function including normal transduction and adaptation. (Bautista et al., 2006; Kwan et al., 2006). Though initial research on TRPA1 was disappointing, TRP channels remain the most attractive candidates for the transduction channel due to the zebrafish and *Drosophila* data.

Adaptation

In order to maintain sensitivity, hair cells must adapt to constant stimuli. If a stimulus is sustained, the process of adaptation causes channels to close and readies the cell for subsequent stimuli. In hair cells, adaptation is described by a shift in the position of the displacement-response curve, which reflects the dependence of channel open probability on bundle displacement (Eatock et al., 1987). Adaptation has a fast component and a slow component; Ca^{2+} is required for and controls the time constants of each (Baylor and Fettiplace, 1975; Eatock et al., 1987; Assad and Corey, 1992; Wu et al., 1999). To regulate Ca^{2+} , hair cells rely on mobile Ca^{2+} buffers, diffusion, and the plasma membrane Ca^{2+} -dependent ATPase pump (PMCA2a) (Ricci et al., 1998; Yamoah et al., 1998; Dumont et al., 2001).

The motor Myosin-1c (Myo1c) is present in the actin-rich hair cells and localized at tips of stereocilia, a prime location to influence transduction (Gillespie et al., 1993; Steyger et al., 1998; Garcia et al, 1998}. Myo1c is hypothesized to be linked with both the channel and the actin core and has been shown to play a

Figure 6. Model of the transduction apparatus. In the current model of the transduction apparatus, a myosin cluster (blue), serving as the adaptation motor, is bound to both the actin core and plasma membrane. The transduction channel is connected in series with the tip link, and attached in series to the adaptation motor.

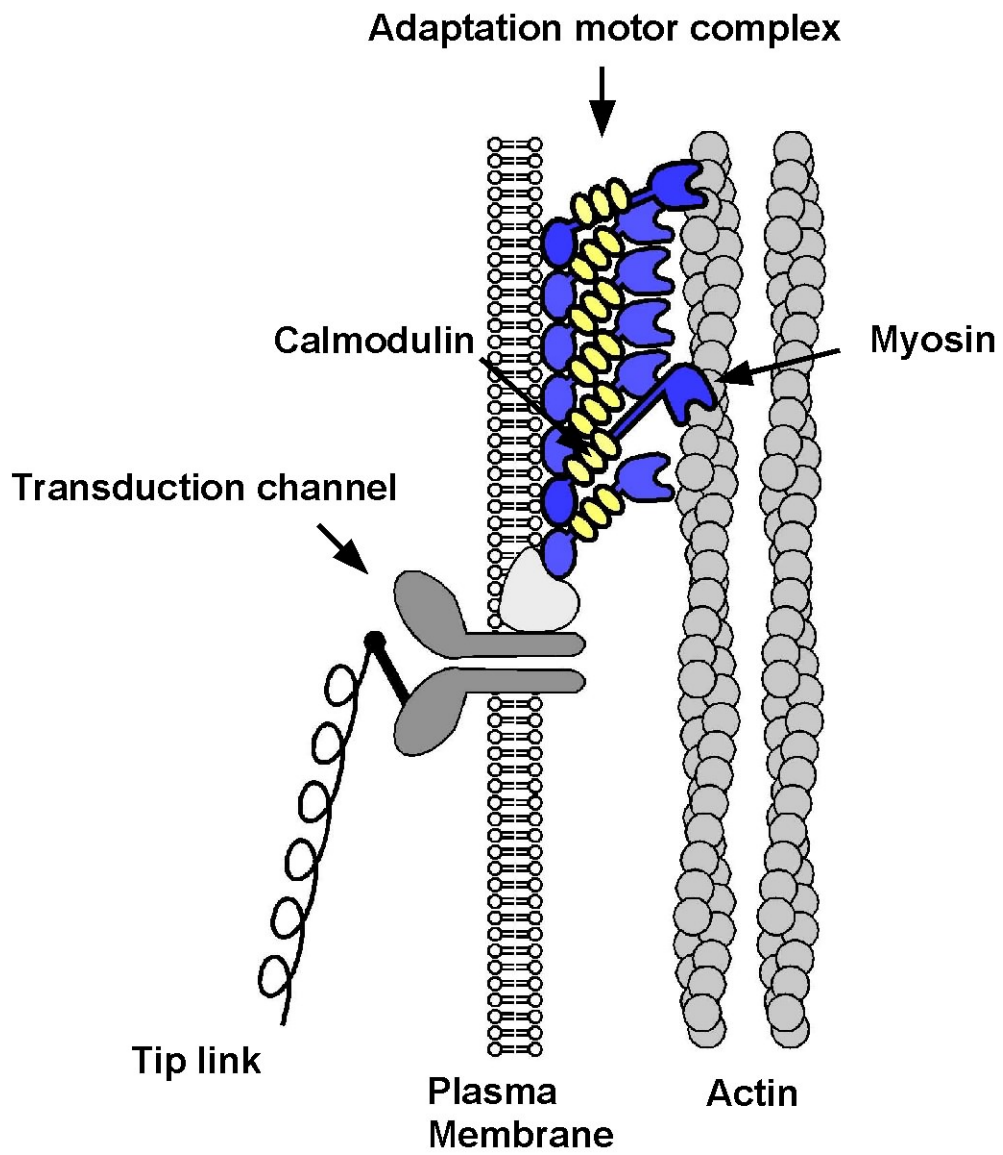
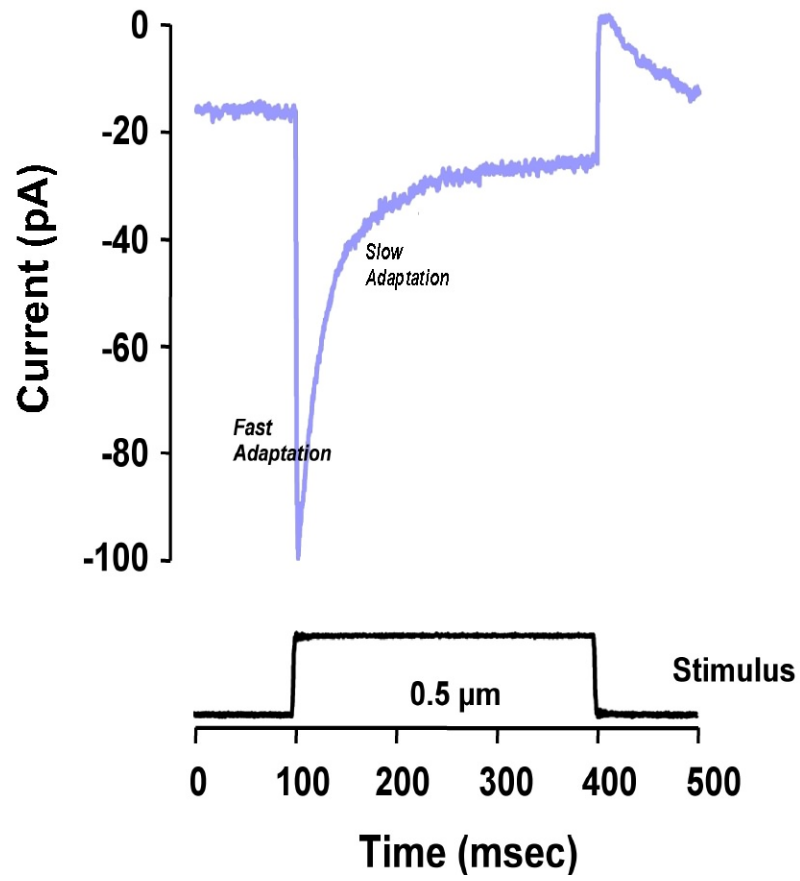


Figure 7. Fast and slow adaptation. A transducer current from a bullfrog saccular hair cell for a step deflection of 0.5 μm for 300 ms. Prolonged positive deflections produced an inward current that adapted. Fast and slow components of adaptation are noted (Howard and Hudspeth, 1987).

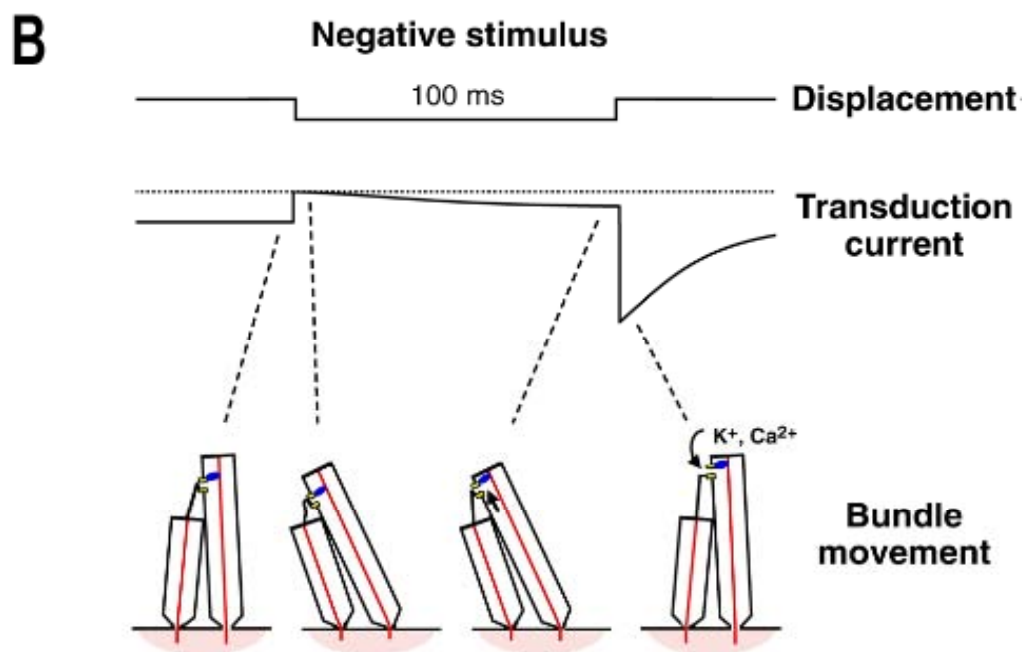
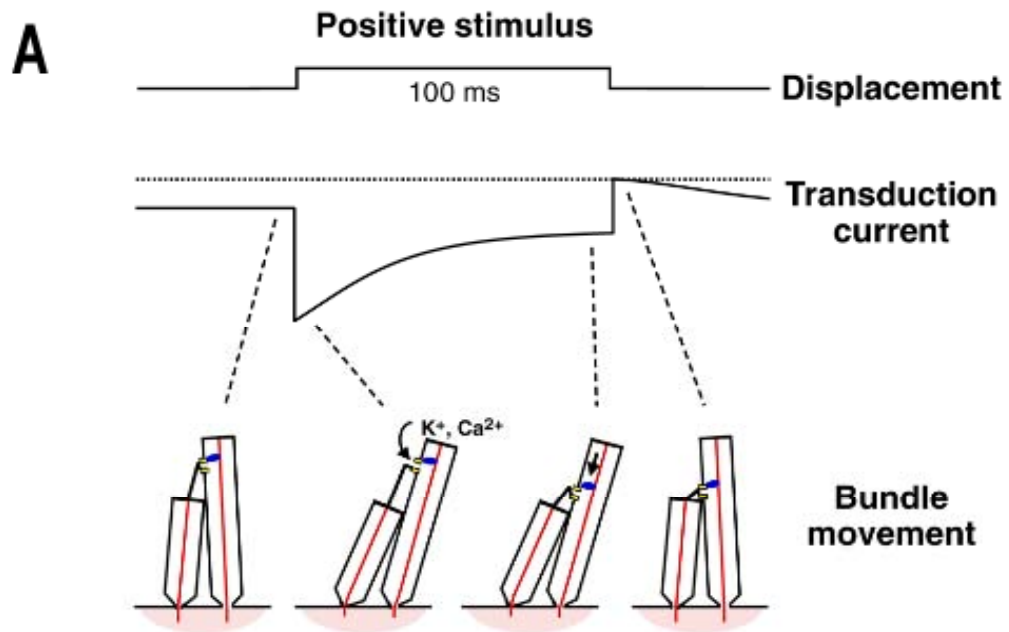


key role in both the fast and slow components of adaptation (Baylor and Fettiplace, 1975; Holt et al. 2002; Gillespie and Cyr, 2004; Stauffer et al., 2005). In addition to hair cell adaptation, Myo1c also plays roles in stimulated insulin uptake in adipocytes and neuronal growth cone extension due to its force-producing properties (Wang et al., 1996; Bose et al., 2002).

Fast adaptation, seen in both turtles and mammals, has a time constant of 0.05-1 ms and is proposed to result from Ca^{2+} binding to or near the channel to induce rapid closure (Figure 7) (Ricci and Fettiplace, 1997; Ricci et al., 1998; Kennedy et al., 2003). Closure of the channel increases tip link tension and as a result displaces the bundle in the negative direction. By contrast, a second model proposes that Ca^{2+} binds an element in series with the tip link. Ca^{2+} causes a conformational change and lengthening of this protein, proposed to be Myo1c, and results in a decrease in tip link tension (Stauffer et al., 2005).

A model for slow adaptation was proposed where a cluster of Myo1c motors exerts modest tension (~10 pN) on the gating spring and tip link (Figure 7) (Hudspeth, 1992). When tension of the gating spring is high, the channels open, allowing K^+ and Ca^{2+} influx (Figure 8). Ca^{2+} can alter motor force production by promoting slipping of Myo1c down the actin core. (Howard and Hudspeth, 1987; Assad and Corey, 1992; Gillespie and Corey, 1997; Holt et al., 2002). Slipping of Myo1c reduces tension, channels close, and Ca^{2+} influx is reduced. When the bundle is moved so that gating-spring tension is low, Myo1c can climb to restore resting tension (Figure 8B). Myo1c is a low-duty ratio motor

Figure 8. Model of slow adaptation. Positive (A) and negative (B) step deflections applied to hair bundles and transducer current recorded for the step stimuli. **A.** Positive deflections increase tip link tension and allow greater current entry. The adaptation slips down the actin core to reclose channels. **B.** Negative deflections result in a slackening of the tip link. The motor complex climbs up the actin core to restore resting open probability. The position of the transduction machinery of the hair cells in relation to hair bundle movement is also shown (Hudspeth and Gillespie, 1994).



as defined by transient binding to actin during the ATPase cycle; however, it is hypothesized to form clusters and could perform effectively as the adaptation motor (Gillespie et al., 1999; Howard, 2001; Gillespie and Cyr, 2004).

Using a mutant-inhibitor approach, it was shown that Myo1c participates in slow adaptation (~15 ms) (Holt et al., 2002; Gillespie and Cyr, 2004). Mice were created with a Y61G mutation in the ATP-binding pocket. Normal adaptation was observed in wild-type mice when either NMB-ADP or ATP was applied to hair cells. Adaptation was also normal in Y61G mice exposed to ATP. However, as hypothesized, slow adaptation was inhibited in hair cells of the Y61G mice when exposed to NMB-ADP. This experiment, along with work conducted by Stauffer et al., (2005), confirmed that Myo1c plays a key role in *both* fast and slow adaptation, using a Y61G knock-in mouse.

Hair Cell Myosins

Because hair cells are abundant in actin, myosins are good candidate motors for hair-cell functions, because they require actin to perform their distinct actions (Tilney et al., 1980). Hair cells have four actin-rich domains: the hair bundle, the cuticular plate, the cortical actin cytoskeleton, and the circumferential actin belt (Gillespie et al., 1996). Myosins generate force along actin filaments by hydrolyzing ATP, producing mechanical work. Myosins have three key domains: the motor head, the neck, and the tail. The head binds ATP and actin, while the neck consists of several IQ motifs that bind light chains or calmodulin (CaM) (Friedman et al., 1999). There are eighteen different classes of myosins, based

on highly conserved amino acid sequences in the motor domains (Mooseker and Cheney, 1995; Mermall et al., 1998; Friedman et al., 1999; Berg et al., 2001). The tail regions of myosins contain various domains, including membrane-binding domains, src homology domains (SH3), pleckstrin homology domains (PH), zinc binding domains, and fodrin, ezrin, radixin, moesin (FERM) domains, among others (Friedman et al., 1999; Oliver et al., 1999).

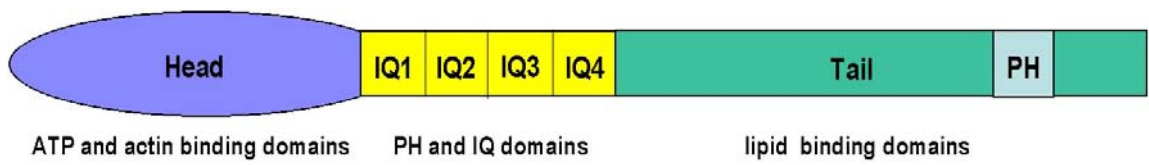
In the hair cell, a variety of myosins are necessary for auditory and vestibular function. Myo1c, as described in the previous section, myosin 7a (Myo7a), myosin 15a (Myo15a), among others are all found in distinct regions of the hair cell (Hasson et al., 1997). Myo7a is associated with the basal ankle links and thought to play a role in tip link tension (Kros et al., 2002). Myo7a is also an A-kinase anchoring protein (AKAP), binding the RI subunit of cAMP-dependent PKA (Küssel-Andermann P, 2000). Myo15a is located at stereocilia tips and is hypothesized to play a role in actin polymerization (Rzadzinska AK, 2004). Mice with mutant Myo15a have abnormally short stereocilia (Anderson DW, 2000). Myosin 6 (Myo6) is located in the pericuticular necklace and also the taper regions of stereocilia (Hasson et al., 1997). This motor has unique amino acid sequence in the motor core domain, thought to contribute to minus-end directed movement of Myo6 (Homma K, 2001). Mice with null Myo6 have decreased viability, decreased vestibular function, and fused stereocilia detectable immediately after birth (Avraham et al., 1995). These features suggest that Myo6 functions to hold the stereocilia down at the base, providing stability and maintaining the pivot points of the bundle. Myosin 3a (Myo3a) is localized to

stereocilia tips and may regulate stereocilia length and shape (Schneider et al., 2006). Though not present in the hair cell, Myosin 5 (Myo5) is found at the synaptic terminals of hair cell afferents and is likely to play a role in synaptic vesicle transport (Stowers et al., 2002).

MyoIIc Structure, Calcium, and Calmodulin

MyoIIc can be regulated by several binding partners. Similar to a number of myosins, MyoIIc contains an ATP (GESGAGKT) and actin-binding domain (RCIKPN) in the globular head domain, 3-4 IQ domains in the neck, and a membrane-binding tail (Baylor and Fettiplace, 1975; Metcalf et al., 1994; Solc et al., 1994). The IQ sequences of IQ1 and IQ2 adhere closely to the general consensus sequence IQX₃RGX₃R, while IQ3 and IQ4 are less well conserved (Cyr et al., 2002). MyoIIc has 2-3 CaM molecules bound to the IQ domains in the presence of the Ca²⁺ chelator EGTA (1 mM), but in the presence of Ca²⁺ (0.1 mM), at least 2 CaM molecules are released (Zhu et al., 1996; Gillespie and Cyr, 2002). MyoIIc can bind to its receptors through its IQ domains when they are free of CaM (Cyr et al., 2002). Ca²⁺ stimulates MyoIIc ATPase activity, but inhibits *in vitro* motility rates (Zhu T, 1996). CaM is hypothesized to play a role in stabilization of the neck domain during force generation, as CaM dissociation destabilizes the neck. The IQ domains of frog MyoIIc bind phosphoinositide (PIP₂) present in hair cell membranes in a Ca²⁺-dependent manner; this interaction is reduced in the presence of excess CaM (Cyr et al., 2002; Hirono et al., 2004).

Figure 9. Myolc functional domains. Myolc is composed of three primary domains: the head, neck, and tail. The head contains ATP and actin binding sites. The neck contains four IQ domains which bind CaM molecules, and also contain pleckstrin homology (PH) domains. At the C-terminus is the basic tail domain which bind lipids with an additional PH domain.



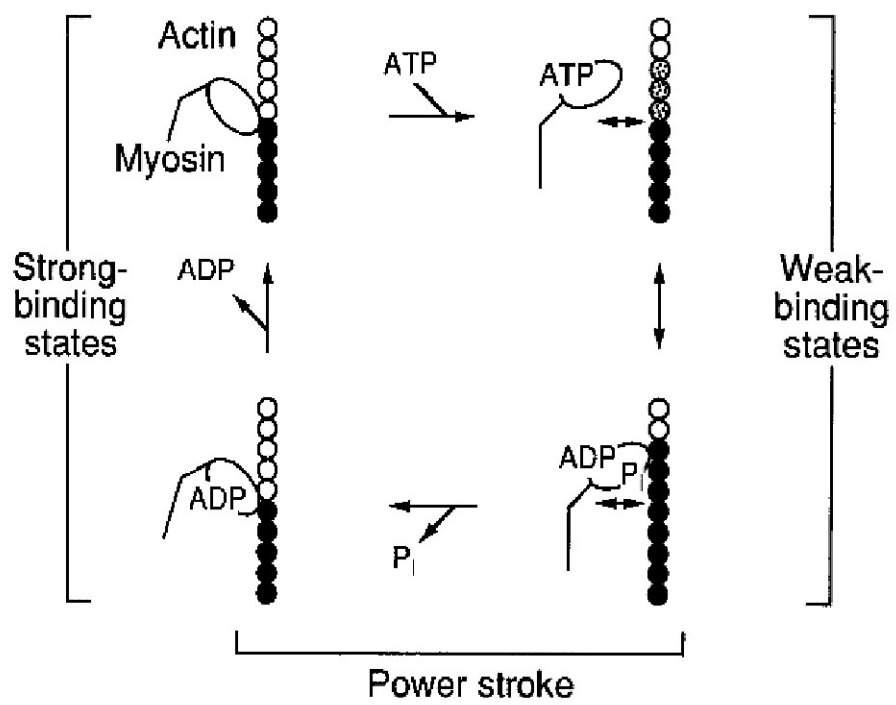
The MyoIc tail is highly basic in charge and also binds PIP₂ through a PH domain (Reizes et al., 1994). Because Ca²⁺ and CaM are required for adaptation, it will be necessary to further explore their dynamic interactions with MyoIc in the hair cell (Fettiplace, 1992; Walker and Hudspeth, 1996).

Myosin Mechanics

Studies of MyoII provide key information about the motor's ATPase cycle. Isoforms of MyoII were first isolated from striated muscle and are the best characterized of myosin family. Myosin II has a head domain, a converter domain, two IQ domains that bind the essential and regulatory light chains, and a tail. They are assembled as hexamers consisting of a pair of heavy chains and two pairs of light chains. MyoII isoforms are involved in muscle contraction, cytokinesis, cell motility, and transport (Sellers et al., 2006).

Myosin force production results from small changes in the protein's motor domain that are amplified by the head's converter domain, which is responsible for converting ATP hydrolysis into a rotation of the neck region (Volkman N, 2003). In the absence of ATP, myosin strongly binds to actin in the rigor state. During the ATPase cycle, ATP binds to the nucleotide-binding pocket; ATP binding reduces actin-myosin affinity and resets the myosin lever-arm - the domain responsible for movement - into a position to exert force. ATP is then hydrolyzed to ADP and inorganic phosphate (P_i), with myosin remaining in a weak-binding state with actin (Figure 10).

Figure 10. Myosin ATPase cycle. In the absence of ATP, myosin binds tightly to actin. The addition of ATP puts myosin into a weak-binding state with actin. Myosin hydrolyzes ATP to ADP and P_i . P_i leaves first followed by ADP, allowing myosin to rebind tightly to actin.



The powerstroke of MyoIc, a non-processive motor, occurs in two phases as it simultaneously binds tightly to actin, as determined using optical tweezers on single MyoIc molecules (Batters et al., 2004a). The first phase, corresponding to P_i release, is 3.1 nm in length, while the second, 1.1 nm, occurs with ADP release. Electron micrographs of MyoIc decorated with actin showed there was a large difference in the position of the neck relative to motor domain between the ADP-bound and nucleotide-free states. From these experiments it was estimated that the neck pivots 33° after ADP release with a displacement of 5 nm (Batters et al., 2004b). Because the two powerstroke distances are not equal to 5 nm, it was suggested that MyoIc has a range of possible displacements during translocation. These studies also confirm that the MyoIc neck moves as a rigid structure relative to the head after the ADP release step. As the powerstroke is in two phases, this data suggests that MyoIc can bear significant tension, and may stall before releasing from actin during its ATPase cycle (Gillespie and Cyr, 2004).

Myosin V

MyoV, another well-characterized myosin, and may be regulated in a similar mode as MyoIc. MyoV, unlike MyoIc, is a processive motor (Menta, et al., 2000). Processive motors function as a pair of monomers and take several steps along actin before detachment. MyoV is involved in organelle transport, transporting melanosomes, synaptic vesicles, vacuoles, and mRNA (Reck-Peterson et al., 2000). MyoV has six CaM-binding IQ domains in addition to

dimerization domains in the tail, while the neck is an alpha-helix. MyoV takes 36 nm steps as it moves towards the barbed end of the actin filaments (Sakamoto, et al., 2003; Purcell et al., 2005).

When visualized at low ATP concentrations on F-actin by electron microscopy, MyoV appears to move in a hand-over-hand fashion, where the two heads communicate with each other by a strain-dependent mechanism (Yildiz et al., 2003; Sellers JR, 2006). To move processively, both heads of MyoV are initially attached to actin; the leading head has ADP bound, while the trailing head is in a rigor ATP-free state. ATP binding to the trailing head promotes dissociation from actin. The forward motion of the released trailing head releases molecular strain, hydrolyzes ATP, and binds actin. This is now the leading head (Veigel et al., 2005). A pre-powerstroke attachment was shown illustrating that the detached head cannot approach the next actin binding site while the attached head is in a pre-power stroke position (Coureux et al., 2004). This also suggests that the junction between the heads is flexible.

Regulation of Myosin V by Ca^{2+} and CaM

The interaction of Ca^{2+} with bound CaM appears to be an important mode of MyoV regulation. In the absence of Ca^{2+} , the six IQ domains of MyoV are fully occupied by CaM (Sellers JR, 2006). MyoV purified from tissue has low ATPase activity and affinity for actin (Tauhata., et al. 2001; Cheney et al., 1993; Nascimento et al., 1996). In this state the motor is in a folded and inactive conformation with the cargo-binding domain interacting with the motor domain.

Exposure to low Ca^{2+} or cargo binding regulates the structure and activates MyoV. Electron microscopy has also shown that Ca^{2+} changes the position of the lever arm and also causes conformational changes in the motor domain (Trybus et al., 2007). It was demonstrated that low amounts of Ca^{2+} changes the conformation of CaM bound at the first two IQ domains suggesting a partial occupancy of CaM by Ca^{2+} (Trybus et al., 2007). Also, MyoV constructs containing only the motor domain and first two IQ domains show little change in activity in the presence of either EGTA or Ca^{2+} . By contrast, full length MyoV has very low activity when exposed to EGTA, supporting the hypothesis that Ca^{2+} causes MyoV to unfold by a Ca^{2+} -CaM interaction.

In MyoV purified from baculovirus-expressing cells, high Ca^{2+} inhibits *in vitro* motility (Cheney et al., 1993; Trybus et al., 1999; Homma et al., 2000; Wang et al., 2000). Ca^{2+} dissociates CaM from one or more of the IQ domains and inhibit the motor's processivity. Because IQ2 of MyoV has a lower affinity for CaM, Ca^{2+} binds to and removes CaM from IQ2 first. Removal of CaM is proposed to render the lever arm less stable and abolish MyoV's strain-dependent motility. ADP release does not appear to be affected by Ca^{2+} due to the observation that the run length decreases while the velocity remains constant (Krementsov et al., 2004). Motility can also be restored when the motor is supplemented with excess CaM (Trybus et al., 1999).

Other motors may be regulated in a similar manner as MyoV. Smooth muscle myosin II is in a folded monomeric conformation displaying little activity when its regulatory light chain is unphosphorylated (Trybus et al., 1991). Also,

kinesin appears to be in a compact conformation with low activity when unbound to cargo (Coy et al., 1999; Stock et al., 1999; Hachway and Stock., 2000). It is also a possible regulation mechanism for MyoIc.

MyoV is also regulated by CaMKII phosphorylation at serine 1650 in the globular tail region which allows release of the motor from vesicles (Karcher et al., 2001). The tail also binds CaMKII leading to autophosphorylation of the kinase and phosphorylation of the tail in the presence of Ca^{2+} (Coelho MV, 1993; Costa et al., 1999). Costa et al. also proposed that MyoV may use its own CaM in addition to free Ca^{2+} to bind to and activate CaMKII.

Myosin VI

MyoVI, another unconventional In contrast to other myosins, may also share some traits with MyoIc. MyoVI is a moves toward the pointed end of actin, a unique feature of this motor. It is localized in the golgi complex, plasma membrane, membrane ruffles, vesicles, clathrin-coated pits, and hair cells (Bahloul et al., 2004). MyoVI is composed of a motor domain, and a single IQ domain, followed by a cargo-binding tail domain composed of both a coiled coil and globular domain (Wells et al., 1999). MyoVI contains two unique inserts; a 22 amino acid insert near the ATPase site in the head which may slow the rate of ADP release, and a 53 amino acid insert located near the converter domain which contains a CaM-binding motif (Bahloul et al., 2004; Menetrey et al., 2005). It was originally thought that the first domain determines the directionality of the motor, but recent optical trapping experiments have demonstrated the second

insert to be the sole determinant of directionality (Homma et al., 2001; Bryant et al., 2007; Sweeney et al., 2007).

Based on the short lever arm length of MyoVI, this motor is estimated to have a short step size of 6-8 nm. Instead, it has a large two-step working stroke of 17 nm associated with phosphate release and an additional 1 nm with ADP release (Veigel et al., 1999; Veigel C, 2002). The large working stroke may be possible due to the size of the lever arm in addition to the orientation of lever arm in relation to the actin filament (Wells AL, 1999; Lister, I, 2004). Another hypothesis is that a short flexible element near the lever arm may also contribute to the large step size of the motor, or possible decoupling of the second insert from the converter domain (Rock et al., 2005).

MyoVI was originally believed to exist only as a dimer based on a region of the tail predicted to form a coiled coil (Kellerman TA. 1992; Hasson and Mooseker, 1994). Induced dimers with a leucine zipper motif or smooth muscle rod domain of head-neck monomers, had functional *in vitro* motility and ATPase activity *in vitro* (Rock et al., 2001; Nishikawa et al., 2002). Baculovirus-expressed MyoVI revealed that MyoVI is also functional as a monomer (Lister, 2004). In addition, electron microscopy visualization confirmed that MyoVI can exist as a monomer (Howard et al., 1989). Artificial MyoVI dimers have a large step size of 30 nm raising the possibility that MyoVI may be both a monomer and dimer *in vivo* (Nishikawa, S, et al. 2002; Rock et al., 2001). A possibility is that dimerization may be controlled by post-translational modifications or binding partners similar to kinesins. Recent studies have proposed that when MyoVI

monomers are in close proximity, such as when associated with cargo, dimerization will result to result in processivity (Park et al., 2006). A similar theory has been proposed for MyoX and MyoVIIa (Knight et al., 2005; Yang et al., 2007).

To move processively, MyoVI is proposed to walk in a hand-over-hand method along actin filaments (Nishikawa et al., 2002; Rock et al., 2005). MyoVI has a high duty ratio and the heads are hypothesized to communicate with each other by a strain-dependent mechanism. The leading head is strongly bound to actin with the trailing head in a weak-binding state with actin. The leading head can not release ADP and phosphate until the trailing head detaches from actin (De La Cruz et al., 2001; Morris et al., 2003). Using optical trapping experiments, MyoVI can also bind strongly to actin in the presence of ATP when presented with large forces, suggesting an important anchoring role in the cell (Altman et al., 2004).

Phosphorylation is another important mode of MyoVI regulation. MyoVI has three phosphorylation sites. In addition to two tail phosphorylation sites, MyoVI can be phosphorylated at Threonine 406 by PAK, a member of the G-protein rac and cdc42 activated kinase family, shown to be involved in fibroblast cell motility (Buss et al., 1998; Sells et al., 1999). This site is located in the actin binding cardiomyopathy loop and obeys the TEDS (Threonine, Glutamate, Aspartate, Serine) rule for phosphorylation proposed by Bement and Mooseker, 1995. Initial mutational analysis of threonine 406 with glutamate or alanine substitutions have failed to reveal any effect on MyoVI activity *in vivo* (Buss et al.,

1998). The Ostap lab, however, has shown that phosphorylation of Threonine 406 affects the K_{ATPase} but not the V_{max} of MyoVI (De La Cruz EM et al., 2001). The Morris lab also showed that T406E had an increase in phosphate release and an increase in affinity for ADP. Phosphorylation is also consistent with recruitment of MyoVI into membrane ruffles suggesting that cytoskeletal dynamics are affected (Buss et al., 1998). Based on the increase in ADP affinity and slow dissociation from actin, phosphorylation of T406 may be a potential regulator of motor dimerization and membrane anchoring.

PKA and Spontaneous Oscillations

Under the right ionic conditions, bullfrog hair bundles spontaneously oscillate (Martin et al., 2003). In frogs and turtles, spontaneous oscillations of the hair bundle range in frequency from 5-40 Hz *in vitro* (Art et al., 1985; Martin and Hudspeth, 1999; Martin et al., 2003). These oscillations are hypothesized to arise from a combination of negative stiffness of the hair bundle and the force generated by myosin motors undergoing adaptation (Hudspeth et al., 1994; Martin et al., 2000). When transduction channels rapidly close, an increase in tension is transferred to the tip link which causes the bundle to move towards the stimulus. An input of an oscillatory stimulus will permit the increased tip link tension to increase movement of the bundle. Stimulating a hair cell with a sinusoidal wave at its characteristic frequency has been shown to result in an output greater than the input, and may represent a form of amplification (Martin and Hudspeth, 1999).

There are few known regulators of MyoIc, though experiments with kinase stimulators and inhibitors have produced some intriguing leads. In the bullfrog

sacculus, enhancers of PKA activity such as forskolin, 8-Br-cAMP, Sp-cAMP, okadaic acid, and 3-isobutyl-1-methylxanthine (IBMX) all decreased the frequency of spontaneous oscillations, while the PKA inhibitor Rp-cAMP increased oscillation frequency (Martin et al., 2003). Interestingly, a myosin inhibitor, butanedione monoxime, blocked spontaneous oscillations. These results support the hypothesis that PKA phosphorylation influences the mechanics of the hair bundle.

Regulation of Transduction Current by PKA

The relationship between displacement of the hair bundle and current entry is depicted with the current-displacement (I-X) curve. This relationship can be described by a sigmoidal Boltzmann curve. From the I-X curve one can infer how much force is exerted through the tip links by the transduction machinery to open transduction channels. The tip link tension (5-20 pN) is reasonably high at rest, and is generated mainly by the adaptation motor (Hudspeth, 1992). At rest, the channels carry 15% of their maximal current; displacement of the bundle in the positive direction allows additional current entry. A shift of the I-X curve to the right indicates that more displacement of the bundle is needed to allow the same amount of current entry. This curve shift is indicative of less force exerted through the tip links by the transduction machinery to keep channels open. Similarly, a shift of the curve to the left shows that tension on the tip link is high, and little deflection of the hair bundle is needed to achieve a large level of current entry. Under these conditions we infer that the adaptation motor exerts

Figure 11. PKA activators and inhibitors affect the current-displacement curve. A. In the Corey lab, the addition of 8-Br-cAMP to hair bundles shifted the I-X curve to the right by 375 nm while washout returned the curve to near resting values. B. The addition of Rp-cAMP shifted the I-X curve to the left by 425 nm. The curve returned to resting values with washout (Corey, D, unpublished).

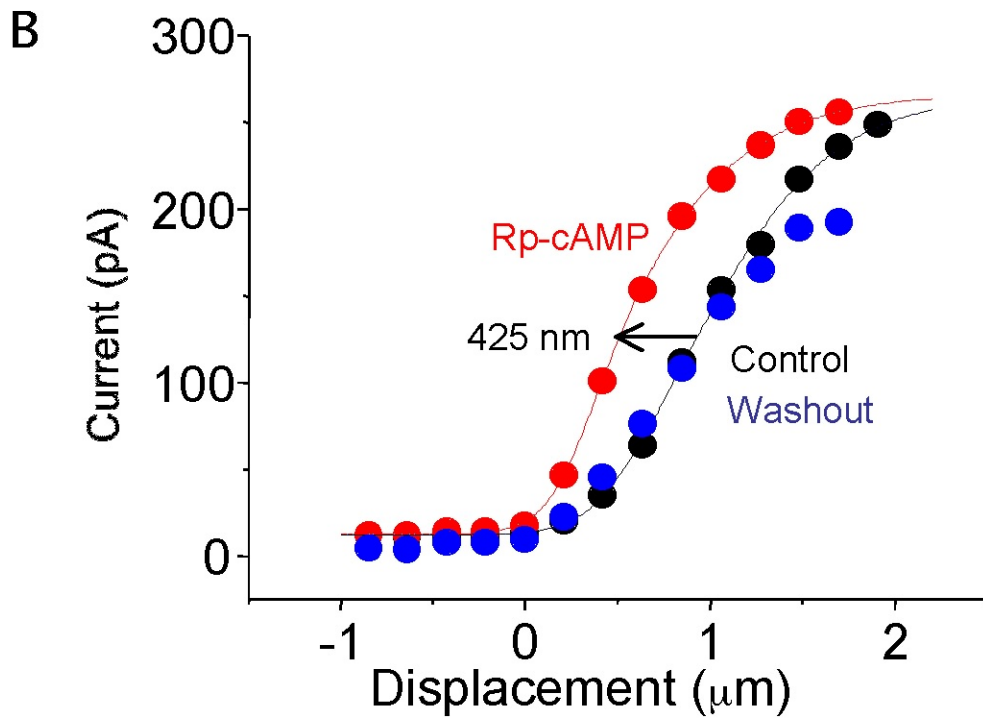
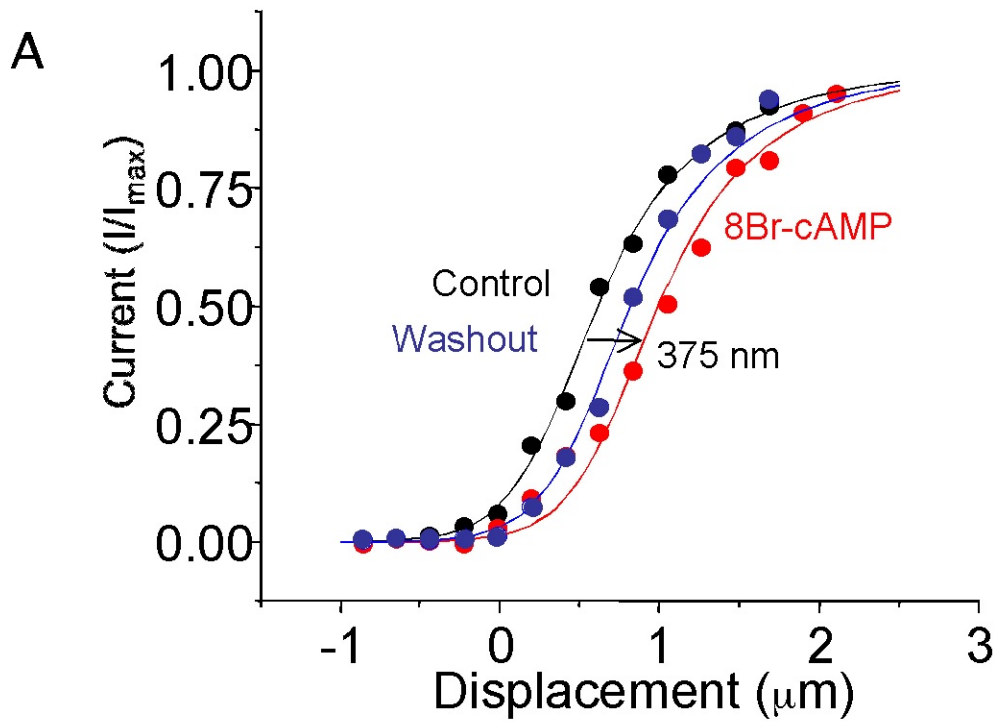
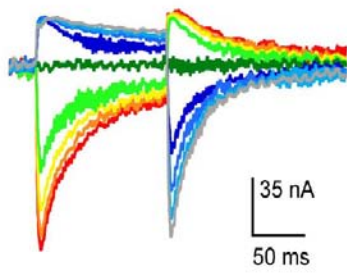
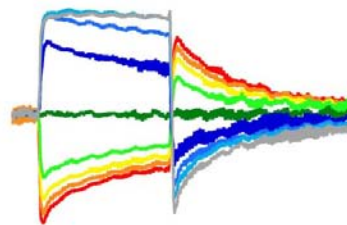


Figure 12. PKA inhibition and adaptation. H89 was applied to bullfrog hair cells while the cells were stimulated with a family of step displacements. The PKA inhibitor H89 decreased the rate of slow adaptation in bullfrog hair bundles, while washout did not fully return the curve to resting current (Gillespie, P., unpublished).

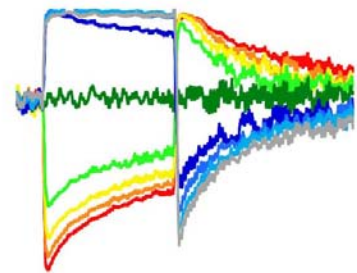
Control



H89



Washout



large amounts of force on the gating spring.

Agents that affect PKA can alter the I-X curve of a hair cell, suggesting that PKA phosphorylation is an important regulator of tip link tension. For example, the membrane-permeant cAMP analog 8-Br-cAMP induced a positive shift in the I-X curve in both turtle and mouse vestibular hair cells, which reversed upon washout (Figure 10A; Ricci et al., 1998; Geleoc et al., 2001) consistent with decreased force production by MyoIc. Intracellular application of (0.1 mM) cAMP had similar results. IBMX, a phosphodiesterase inhibitor that should raise cyclic nucleotide levels, also produces the same rightward shift in turtle hair cells (Ricci and Fettiplace, 1997). Conversely, the PKA inhibitors H89 and Rp-cAMP cause the curve to shift in the negative direction, indicating an increase in motor force production (Baylor and Fettiplace, 1975; Geleoc, 2001). H89 also decreased the rate of adaptation and increased open probability in frog hair bundles (Gillespie P., unpublished; Figure 12). This increase in force with PKA inhibition suggests that a target protein is phosphorylated when at rest. Inhibiting PKA would allow endogenous phosphatases to dephosphorylate their target proteins. Potential targets could include the transduction channel, an unidentified protein in series with the tip link, or a myosin. We propose that PKA is activating a protein or protein cascade that reduces force production by the transduction apparatus.

Serine 701 and its Role in MyoIc Function

MyoIc contains a strong PKA consensus site at serine 701 (S701). This site is conserved among human, mouse, and rat, while the sequence deviates

slightly in chicken and frog (Figure 13). In addition, a high-stringency Scansite (<http://scansite.mit.edu/>) search of the Myolc amino acid sequence supports that S701 is a strong candidate for PKA phosphorylation. Scansite scores start at 0 and increase as a particular sequence diverges from being an optimal match (Obenauer JC, 2003). For Myolc, the PKA phosphorylation site at S701 in human, mouse, and rat has a percentile score of 0.2839, the lowest (best) of all predicted kinase phosphorylation sites for Myolc. The chicken and frog sequences are predicted to be phosphorylated by PKA, albeit with slightly higher scores of 0.400 and 0.380. By comparison, known PKA substrates cAMP response element-binding protein (CREB) and L-type Ca²⁺ channels have scores of 0.2210 for S133, and 0.3143 for S1897 respectively (Fiol CJ, 1987; Davare MA, 2000). The consensus PKA site of rat and mouse includes S701, which is sandwiched between the ATP-hydrolyzing head region and the three CaM-binding IQ domains of Myolc.

The PKA holoenzyme is composed of a dimer of two regulatory (R) subunits that keep two catalytic (C) subunits in an inhibited state. cAMP binds to two sites in each of the regulatory subunits of PKA, leading to dissociation of active catalytic subunits (Taylor et al., 2004). The activated catalytic subunits can phosphorylate serine or threonine residues on target substrates. There are three C subunits: α , β , and γ , and four types of regulatory subunits, RI α , RI β , RII α , and RII β . PKA holoenzymes containing RI α or RI β are found in the cytoplasm, where those containing RII α or RII β are mostly found at intracellular locations where

Figure 13. Conservation of S701. Alignment of Myolc sequences from rat, mouse, human, bullfrog, and chicken. S701 is conserved across species. The PKA consensus site is conserved in rat, mouse, and human while less conserved in bullfrog and chicken.

	688	701	711
rat	LFATEDSLEVRRQSLATKIQAAR		
mouse	LFATEDSLEVRRQSLATKIQAAR		
human	LFATEDALEVRRQSLATKIQAAR		
bullfrog	LFATEDALEVRKHSIATFLQARWR		
chicken	LFATEDALEVRKQSLATKMQATWR		

they are bound to anchoring proteins (Taylor et al., 2004). In one model for PKA regulation, Ca^{2+} stimulates cAMP synthesis through an adenylyl cyclase; for example, adenylyl cyclases 1 and 8 are both regulated by Ca^{2+} . The mRNA transcripts for adenylyl cyclases 1, 6, 9 have been identified in the organ of Corti (Drescher MJ, 1997; Kumagami H, 1999). The presence of adenylyl cyclases in the ear further supports the possibility that cAMP can activate hair cell PKA.

The identification of a strong PKA consensus sequence in Myo1c at S701 leads us to propose that Myo1c is the target of PKA-altering agents. Due to the placement of S701 between the head and neck domains at a flexible region, we hypothesize that Myo1c mechanics can be altered by the addition of a phosphate.

MATERIALS AND METHODS I

Phospho - S701 Myolc Antibody

In order to determine the phosphorylation state of Myolc in various experiments, an antibody specific for phosphorylated S701 in Myolc was produced by Open Biosystems (Huntsville, AL). The peptide, EVRRQ(phospho-S)LATKIQ was synthesized on a 50- μ M scale and injected into 2 rabbits using the SPF 90-day immunization protocol (<http://www.openbiosystems.com/antibodies/custom/polyclonal/2rabbit90day/>) (Sleeman, M. et al., 2004). To deplete the antibodies to non-phosphorylated S701, the analog non-phosphorylated peptide was also synthesized and used in affinity enrichment chromatography.

AutoSpot Peptide Array Assays

To determine if S701 in Myolc was recognized by PKA, an array of peptides were covalently synthesized on cellulose membrane by an AutoSpot robot ASP222 (ABiMED, Langenfeld, Germany) in the John Scott lab. The membrane was dipped in 100% ethanol and incubated in 10 ml pre-incubation buffer (20 mM N-(2-Hydroxyethyl)piperazine-N'-(2-ethanesulfonic acid) [HEPES] pH 7.4, 100 mM NaCl, 5 mM MgCl₂, 1 mM EDTA, 1 mM DTT, 0.2 mg/ml bovine serum albumin (BSA)) overnight. The buffer was then replaced by 10 ml blocking buffer (20 mM HEPES pH 7.4, 100 mM NaCl, 5 mM MgCl₂, 1 mM EDTA, 1 mM

DTT, 1 mg/ml BSA, 100 μ M ATP) and incubated for 1 hr at 30° C. The membrane was placed in 10 ml pre-warmed kinase assay buffer (20 mM HEPES pH 7.4, 100 mM NaCl, 5 mM MgCl₂, 1 mM EDTA, 1 mM DTT, 0.2 mg/ml BSA, 50 μ M ATP, PKA, 1:10,000 dilution of 10 μ Ci/ μ l γ -³²P-ATP) for 20 minutes at 37°C with gentle agitation. The membrane was then washed 3 x 10 minutes with 1 M NaCl + 0.2% Tween-20, rinsed 3 times in dH₂O, washed 3 x 10 minute in 1 M NaCl, rinsed 3 more times in dH₂O, and finally rinsed 3 times in Tween-Tris Buffered Saline (TTBS; .5M Tris-Cl and 0.15M NaCl, 0.5 ml Tween-20, 1 L dH₂O, pH to 7.4). The membrane was exposed to film (X-Omat Blue, Kodak, Rochester, NY) and developed.

Sf9 Protein Expression

To express MyoIc protein from baculoviruses, we used the BaculoDirect Baculovirus Expression System (Invitrogen, Carlsbad, CA). Log phase Sf9 insect cells were plated at 0.7×10^6 cells/ml in 35-mm tissue culture dishes and allowed to adhere for 20 minutes. A DNA transfection mixture was prepared containing 0.34 ml Grace's Media (Invitrogen) 0.17 μ g Bac-N-Blue DNA (Invitrogen), 1.3 μ g plasmid DNA, 6.8 μ l of vortexed Insectin liposomes (Invitrogen), and then allowed to incubate at room temperature (RT) for 15 minutes. The cells were washed with Grace's Media and then the transfection mixture was added dropwise to the cells and incubated with rocking for 4 hours at RT. After incubation, 0.64 ml of Grace's Complete Media (GCM; Grace's Media, 10% Fetal Bovine Serum (FBS), 25 mg/ml gentamicin) was added to the cells. The cells

were then centrifuged at 12,000 x g for 5 minutes at 4°C. The supernatant (P1) was collected and stored at 4°C. To prepare the first round of viral amplification, 1×10^6 cells were plated in 30 ml GCM in a 150 cm² tissue culture flask (Fisher). The next day, the cells were infected with 200 µl of the P1 stock. After 7 days, the media was removed and centrifuged at 10,000 x g for 15 minutes at 4°C. The supernatant (P2) was removed and stored in a 50 ml conical tube at 4°C. To amplify the virus a second time, 200 ml of 1.5×10^6 Sf9 cells were grown in a Kiss flask at 27°C at 100 rpm. The cells were infected with 3 ml of P2 stock or a multiplicity of 0.25 virus per cell. After 7 days, the media and cells were poured into 50 ml conical tubes and centrifuged at 12,000 x g at 4° C. The supernatant (P3) was collected into new sterile tubes and stored at 4°C. To determine the viral titer of the P3, a plaque assay was performed by first plating 1.8×10^6 cells into 60 mm tissue culture plates (Fisher) in GCM and allowed to adhere for 20 minutes. Dilutions of the P3 stock were made of 1×10^{-7} and 2.5×10^{-7} virus in GCM. From the seeded plates, 1 ml of media was removed, and replaced with 1 ml of the virus dilutions. The plates were allowed to sit at RT for 2 hours with gentle rocking every half hour. After 4 hours, the media was aspirated from the cells and 4 ml of the agarose overlay was added. The agarose overlay contained 3.2% low melting agarose in dH₂O, diluted to 0.8% with GCM and 150 µg/ml X-gal. The overlay was allowed to harden for 1 hour and then stored in a humid container at 27°C for 7 days. Blue plaques were counted in order to estimate the plaque-forming units per ml (pfu/ml). To express Myolc constructs, cells were grown to a density of 1.8×10^6 in 400 ml of GCM in a Kiss flask and infected with

~30 ml P3 Myolc stock and 4 ml *Xenopus* CaM P3 virus at a multiplicity of infection of 4:2 (Gillespie et al., 1999). The cells were incubated at 27°C with gentle shaking at 100 rpm and harvested after 56-70 hours. The cells were centrifuged at 3000 rpm, the supernatant removed, and the cells were stored at -80°C.

Purification of Myolc Expressed in Sf9 Cells

Myosin was purified at 4°C or on ice.. Frozen cell pellets were resuspended with 9 ml of chilled lysis buffer (25 mM Tris pH 8, 0.5 mM MgCl₂, 0.5 mM EGTA, 0.2 mM phenylmethylsulfonyl fluoride (PMSF), 1 µM leupeptin, 1 µM pepstatin, and 2.4 mM β-mercaptoethanol). Using a 10-ml Luer-lock syringe, the cell resuspension was passed through a 22 g needle twice and then 3 times through a 25 g needle. To the mixture, 1440 µl of 5 M NaCl was added in addition to 240 µl of 100 mM ATP. The volume of the lysate was adjusted to 18 ml with lysis buffer and then centrifuged for 30 minutes at 256,000 x g at 4°C. The Ni-NTA column was prepared by adding 1.2 ml of a 50% slurry of Ni-NTA-agarose resin (Qiagen, Valencia, CA) to a column. The resin was washed with 10 ml dH₂O followed by 15 ml wash buffer (300 mM NaCl, 25 mM Tris pH 8, 0.5 mM MgCl₂, 0.5 mM EGTA, 0.2 mM PMSF, 1 µM leupeptin, 1 µM pepstatin, and 2.4 mM β-mercaptoethanol). Following the centrifugation, clarified supernatant was loaded on the Ni-NTA column. After the supernatant had flowed through, the column was washed with 20 ml wash buffer. The myosin was then eluted from the column with 5 x 300 µl aliquots of elution buffer (125 mM imidazole pH 8, 200

mM KCl, 15 mM HEPES pH 8, 1 mM MgCl₂, 0.1 mM EGTA, 0.2 mM PMSF, 1 μM leupeptin, 1 μM pepstatin, and 2.4 mM β-mercaptoethanol) into 1.7 ml Eppendorf tubes. A Bradford assay was used to determine relative protein concentrations by adding 8 μl of each eluted fraction to 175 μl Bradford reagent in 5 glass test tubes. The elution fractions corresponding to the tubes that were most blue in color were pooled and stored at 4°C. The concentration of MyoIc was also evaluated by a standard Bradford plate assay and by absorption using extinction coefficient (<http://expasy.org/>) (Wilkins MR, et al., 1999).

Modifications to the Sf9 Protein Purification Protocol

To achieve higher yields of head-neck (HN) MyoIc protein, we had the National Cell Culture Center (NCCC, Minneapolis, MN) coexpress HN with CaM in Sf9 cells. We were able to purify substantially more HN (~1 μg/μl vs. ~0.2μg/μl) from NCCC cell pellets using the standard purification protocol. To increase yields of all other protein, we used 2 other techniques in the purification process: IPER lysis reagent and batch-binding. We added 100 ml IPER Insect Cell Protein Extraction Reagent, (Pierce, Rockford, IL) with 0.2 mM PMSF, 1 μM leupeptin, 1 μM pepstatin, and 2.4 mM β-mercaptoethanol per 800 ml of pelleted Sf9 cells. The resuspended cells were incubated on ice for 10 minutes with intermittent vortexing followed by addition of 8 ml 5 M NaCl and 1.333 ml 100 mM ATP. The lysate was centrifuged for 30 minutes at 256,000 x g at 4°C. The Ni-NTA resin (Qiagen) was prepared by washing 1.2 ml of the 50% slurry with dH₂O followed by wash buffer (300 mM NaCl, 25 mM Tris pH 8, 0.5 mM MgCl₂, 0.5 mM EGTA,

0.2 mM PMSF, 1 μ M leupeptin, 1 μ M pepstatin, and 2.4 mM β -mercaptoethanol). Following the centrifugation, clarified supernatant was added to the Ni-NTA resin in an Erlenmeyer flask and stirred with a magnetic stir-bar overnight at 4°C. The next day, the resin was centrifuged for 5 minutes at 12,000 x g at 4°C and the supernatant was removed. The resin was then resuspended in 50 ml wash buffer and re-centrifuged for 5 minutes at 12,000 x g at 4°C. The resin was further resuspended in 3 ml wash buffer and transferred to a column. The residual wash buffer was allowed to drip through, and then the protein was eluted from the resin with 5 x 300 μ l aliquots of elution buffer (125 mM imidazole pH 8, 200 mM KCl, 15 mM HEPES pH 8, 1 mM MgCl₂, 0.1 mM EGTA, 0.2 mM PMSF, 1 μ M leupeptin, 1 μ M pepstatin, and 2.4 mM β -mercaptoethanol) into 1.7 ml Eppendorf tubes. A quick Bradford assay was used to determine relative protein concentrations by adding 8 μ l of each eluted fraction to 175 μ l Bradford reagent in 5 glass test tubes. The elution fractions corresponding to the tubes that were most blue in color were pooled and stored at 4°C. The concentration of MyoIc was also evaluated by a standard Bradford plate assay and by an OD₂₈₀ nm measurement.

SDS-PAGE

Proteins were separated on a 15% resolving - 4% stacking sodium dodecyl sulfate - polyacrylamide gel electrophoresis (SDS-PAGE) gel. The resolving gel consisted of 2.2 ml dH₂O water, 3.75 ml 30% 150 acrylamide to 1 bis, 1.43 ml 2 M Tris pH 8.9, 37.5 μ l 200 mM EDTA, 37.5 μ l 20% sodium dodecyl

sulfate (SDS), 50 μ l 15% ammonium persulfate (APS) and 6 μ l N,N,N',N'-Tetramethylethylenediamine (TEMED; BioRad, Hercules, CA). The stacking gel consisted of 5.79 ml water, 1.07 ml 29% acrylamide/1% bis, 1 ml 1 M Tris pH 6.8, 40 μ l 200 EDTA, 40 μ l 20% SDS, 60 μ l 15% APS, and 8 μ l TEMED. The gel was run at 200 V for 1 hour in running buffer (25 mM Tris pH 7.5, 192 mM glycine, 0.1% SDS, and 1 mM EDTA). The protein samples prepared in 4x sample buffer (4x SB; 20% glycerol, 250 mM Tris, 0.7 M β -mercaptoethanol, 0.016% bromophenol blue, 12% SDS, 20 mM EDTA) and heated for 5 minutes at 95°C. To determine the relative size of proteins, molecular weight markers were run alongside experimental samples. Perfect Protein Markers, 10-225 kDa range (Novagen, Madison, WI) and Benchmark Prestained Protein Markers, 10-190 kDa range (Life Technologies) were used.

PKA Catalytic Subunit Expression and Purification

To obtain PKA, the pET-15b-PKA plasmid was transformed into 50 ml BL-21 cells overnight at 37°C with shaking, and then 10 ml of these cells were inoculated into 1 L of Luria Broth (LB) supplemented with ampicillin. Once the cells reached an OD of 0.6, 1 ml of 1 M isopropylthio-beta-D-galactoside (IPTG) was added and the cells were incubated 4 hours at 37°C with shaking. The culture was centrifuged at 12,000 x g for 5 minutes, and the pelleted cells were resuspended in 15 ml of lysis buffer (50 mM Tris pH 7.5, 150 mM NaCl, 0.1 mM EDTA, 0.1 mM EGTA, 0.15 Triton X-100, 0.2 mM PMSF, and 0.07% β -mercaptoethanol). The cells were sonicated for 8 x 15 seconds with cooling and

then centrifuged at 256,000 x g for 30 minutes at 4°C. To prepare the resin, 1.5 ml of a 50% slurry of Ni-NTA agarose (Qiagen) was centrifuged 1 minute at 10,000 x g in a 1.7 ml Eppendorf tube. The liquid was removed, and the resin was washed several times with equilibration buffer (50 mM Tris pH 7.5, 0.5 M NaCl, 0.1% Triton X-100, 0.07% β -mercaptoethanol, 0.2 mM PMSF). The clarified lysate was added to the equilibrated Ni-NTA agarose in a 50 ml conical tube and incubated on a roller at 4°C for 2 hours. The resin was centrifuged and resuspended in high salt buffer (50 mM Tris pH 7.5, 0.5 M NaCl, 10 mM imidazole, 0.1% Triton X-100, 0.07% β -mercaptoethanol, and 0.2% PMSF). It was then loaded onto a column and washed with 30 ml high salt buffer followed by 30 ml of low salt buffer (50 mM Tris pH 7.5, 150 mM NaCl, 10 mM imidazole, 0.1% Triton X-100, 0.07% β -mercaptoethanol, and 0.2% PMSF) at 4°C. The protein was eluted from the column with 10 aliquots of 300 μ l elution buffer (50 mM Tris pH 7.5, 150 mM NaCl, 0.1 mM EGTA, 300 mM imidazole, 0.2 mM PMSF, and 0.1% β -mercaptoethanol). The elution fractions were separated by SDS-PAGE and stained with 100 ml Coomassie stain (2.5 g Coomassie Brilliant blue, 455 ml methanol, 455 ml dH₂O, 90 ml glacial acetic acid) for 30 minutes with rocking followed by incubation in 100 ml destain solution (455 ml methanol, 455 ml dH₂O, 90 ml glacial acetic acid) for 2 hours to identify the fractions with the highest PKA concentration. The pooled fractions were then dialyzed against dialysis buffer (50 mM Tris pH 7.5, 150 mM NaCl, 0.1 mM EGTA, 0.03% Brij-35, 50% glycerol, 0.2 mM PMSF, 0.1% β -mercaptoethanol) overnight at 4°C. The protein was stored at -20°C.

Sf9 Protein Phosphorylation

To determine conditions permitting MyoIc phosphorylation by PKA, a series of *in vitro* reactions was performed with Sf9-expressed protein. Phosphorylation mixtures were assembled on ice in 1.7 ml Eppendorf tubes and reactions initiated by placing tubes in a 30°C water bath. Individual reactions contained ~1 µg of MyoIc protein, 0 - 100 µM CaCl₂, 0 - 100 µM EGTA, 15 mM HEPES pH 7.5, 150 mM KCl, 1 mM MgCl₂, 10 -1000 µM [γ -³²P] ATP, PKA, and dH₂O for a total volume of 10 µl. After 30 minutes, the reactions were stopped by addition of 3.3 µl 4x SB. Samples were separated on a 15% resolving - 4% stacking SDS-PAGE gel, stained with Coomassie stain and destained. The gel was dried for 2 hours with heating and exposed to film (X-Omat Blue, Kodak) at -80°C for 2 days. The hot ATP stock was made by mixing 10 µl of a 1 mM ATP stock with 10 µl of 10 mCi/ml [γ -³²P] ATP and 80 µl dH₂O to result in a 100 µM stock. In one experiment, calmidazolium, a CaM inhibitor, (Compound R24571, Sigma, Saint Louis, MO) was also included in the reaction.

Stoichiometry Measurements

To measure the stoichiometry of phosphorylation, the individual myosin bands were cut out of the dried Coomassie-stained gels. Each band was placed in a scintillation vial along with 0.5 ml H₂O₂ overnight. The following day, 2.5 ml scintillation fluid (EcoLite, MP Biomedicals, Solon, OH) was added to vials and counted in a scintillation counter.

Construction of IQ1 Peptides

To investigate the interaction of CaM at IQ1 with S701, two peptides were synthesized by GeneMed synthesis (South San Francisco, CA). The native form included the amino acid sequence: DSLEVRRQSLATKIQA
AAWRGFHWRQKFLRC, while the phosphorylated form contained: DSLEVRRQ(phospho-S)LATKIQA
AAWRGFHWRQKFLRC.

IQ1 Peptide Phosphorylation

For each reaction, a 2 x 2 cm square of 0.2- μ m nitrocellulose paper (PROTRAN, Schleicher and Schuell, Keene, NH) paper was cut and labeled with a pencil. Reaction mixtures were assembled in 1.7 ml Eppendorf tubes on ice and reactions initiated by placing tubes in a 30°C water bath for 30 minutes. The hot ATP stock was made by mixing 10 μ l of a 1 mM ATP stock with 10 μ l of 10 mCi/ml [γ -³²P] ATP and 80 μ l dH₂O to give a 100 μ M stock. Each reaction contained 1 μ l of the labelled ATP stock, 1 μ l PKA, 1 μ l of 1 mM of short peptide, and 1 μ l of 10x assay buffer (10 mM MgCl₂, 150 mM HEPES pH 7.5, 1.5 M KCl). When indicated, reactions also included 1 μ l of 250 μ M CaCl₂, 1 μ l of 1 mM EGTA, or 1 μ l of 250 μ M CaM. To bring the volume of each reaction up to 10 μ l, reactions were supplemented with dH₂O. Following incubation at 30°C, the entire reaction from each tube was pipetted onto nitrocellulose squares and allowed to air dry for 5 minutes. The squares were washed simultaneously by placing them in a beaker with 200 ml 75 mM orthophosphoric acid and stirring the contents

with a magnetic stir-bar for 5 minutes. The squares were washed a total of 5 times 5 minutes each. The squares were washed for a final time in acetone for 5 minutes. Squares were allowed to air dry for 10 minutes, then placed in scintillation vials with 1 ml dH₂O. Cerenkov radiation was then counted. The counts were analyzed with Excel software (version 11.1, Microsoft) and graphed in Kaleidograph (version 3.6, Synergy Software).

Alexa-CaM Binding to PKA-1Q1 Peptides

To determine if CaM could equally bind to both phosphorylated and dephosphorylated IQ1 peptides, Alexa-CaM quenching experiments were conducted. Samples were assembled in a 96-well plate (Fisher) in triplicate. Negative controls contained no peptide, while our positive control was an *E. Coli* - expressed IQ1 domain. The wells contained CaM assay buffer (150 mM KCl, 15 mM Hepes pH 7.5, 1 mM MgCl₂, 1 mM DTT, 15 mM CaCl₂, 500 µg/ml BSA), and peptide (0-100 µM) for a final well volume of 100 µl. The Alexa-CaM was prepared by adding 120 µl PBS to 200 µg of Alexa 488-CaM (Molecular Probes, Eugene, Oregon) and further diluted to 1:1000 with CaM assay buffer. To each well, 100 µl of the diluted Alexa-CaM was added to give a final CaM concentration of 50 nM. The plate was then covered with foil and incubated for 30 minutes at RT. The plate was read in a spectrofluorometer with an excitation of 494 nm and emission of 520 nm. The results were analyzed with Excel software and graphed with Kaleidograph.

Tryptophan Fluorescence Measurements

To further investigate if native CaM could bind to the two states of PKA-IQ1 peptides, fluorometer readings were acquired under a variety of conditions. Reactions comparing phosphorylated peptide to native peptide were prepared in 1.7 μ l Eppendorf tubes. Endogenous tryptophan fluorescence of the peptide was observed with a Photon Technologies QM-1 steady-state fluorescence spectrophotometer with an excitation of 295 nm and emission of 300-500 nm. The spectra were analyzed using the PTI software program Felix. For the CaM quenching experiment, sample tubes contained 5 μ M peptide, 15 mM HEPES pH 7.5, 150 mM KCl, 1 mM $MgCl_2$, +/- 1 mM EGTA, and +/- 100 μ M $CaCl_2$ for a final volume of 750 μ l. To the cuvette, 375 μ l of the sample was added and measurements taken after individual additions of 1 μ M CaM for a final concentration of 21 μ M CaM. The fluorescence spectra of Ca^{2+} and CaM without peptide was subtracted from samples. Results were analyzed with Excel software and results plotted with Kaleidograph.

Immunoprecipitation of MyoIc

Conjugating DAR to Sepharose

Immunoprecipitation of MyoIc was conducted to determine the state of phosphorylation in COS-7 cells and Sf9 cell extracts with the hope of translating these methods to hair cells. The Two ml of phosphate buffered saline (PBS; 137 mM NaCl, 2.7 mM KCl, 4.3 mM Na_2HPO_4 , 1.4 mM KH_2PO_4 , pH 7.3) was added

to a 1 mg vial of donkey anti-rabbit (DAR) IgG (Jackson ImmunoResearch, West Grove, PA), and dialyzed in a slide dialyzer (Pierce) against two 1 L changes of coupling buffer (100 mM sodium bicarbonate, 500 mM NaCl, pH 8.5) at 4°C. Following dialysis, 0.5 ml of hydrated CNBr-Sepharose was washed for 15 minutes with 1 mM HCl followed by a quick rinse with coupling buffer. The DAR IgG was then added to the CNBr-Sepharose and coupling was allowed to take place for 2 hours at RT with tumbling. The beads were washed briefly with coupling buffer then blocked with 100 mM Tris pH 8 and 500 mM NaCl at RT for 2 hours. The beads were washed with a high pH buffer (100 mM CAPS pH 10.5, 500 mM NaCl, 100 mM sodium acetate pH 4.5, 500 mM NaCl), then with a low pH buffer (150 mM NaCl, 5 mM EDTA, 50 mM Tris pH 7.5, 0.05% NaN₃), and stored as a 50% slurry at 4°C in the low pH buffer.

Binding Antibodies to DAR Sepharose

We incubated 200 µl of the 50% Sepharose-DAR slurry with 100 µg of either 2652, an antibody directed against a region of the Myo1c tail, or anti-phospho-Myo1c-S701 in 1 ml PBS for 2 hours with tumbling at RT. The liquid was removed from the Sepharose and then the antibody complex was washed three times with 1 ml 0.2 M sodium borate pH 8. To prepare conjugation buffer, 65 mg of dimethylpimelimidate (DMP) was added to 5 ml 0.2 M sodium borate pH 8, followed by pH adjustment to 8.2 with NaOH. To the antibody complex, 1 ml of freshly-prepared conjugation buffer was added and then the mixture was incubated at RT for 45 minutes with tumbling. The beads were then centrifuged,

the liquid removed, and another 1 ml of fresh conjugation buffer was added for a second 45 minute incubation. The beads were washed with 50 mM Tris pH 8.9 to block the remaining DMP molecules, then washed 3 x 5 minutes with PBS.

COS-7 Cell Stimulation and Extraction

COS-7 cells were grown in a 12-well plate (Fisher) in Dulbecco's Modified Eagles' Medium (DMEM; Invitrogen) supplemented with 10% FBS and penicillin/streptomycin. To stimulate phosphorylation, 20 μ M Forskolin (Sigma) and 75 μ M 3-isobutyl-1-methylxanthine (IBMX; Sigma) was added along with phosphatase inhibitors (10 μ M sodium pyruvate, 50 mM sodium fluoride, 1 mM sodium orthovanadate (Sigma), 1 μ M okadaic acid (Calbiochem, San Diego, CA), 1 μ M microcystin (Calbiochem), 1 μ M cyclosporin A (Calbiochem)). PKA activity was also stimulated by adding 500 μ M 8-Br-cAMP or 1 μ M ionomycin in addition to phosphatase inhibitors. To inhibit PKA activity, we added 100 μ M H89 (Sigma). The cells were stimulated or inhibited for 15 minutes, then the media was removed and the cells were washed quickly with PBS (+/- stimulators/inhibitors), then removed with a cell scraper in the presence of 1 ml lysis buffer (25 mM Tris pH 8, 0.5 mM MgCl₂, 0.5 mM EGTA, 0.2 mM PMSF, 1 μ M leupeptin, 1 μ M pepstatin, +/- activators/inhibitors). SDS was added to a final concentration of 1% and then the tubes were heated at 95°C for 10 minutes. The cells were then centrifuged at 256,000 x g for 30 minutes at 4°C. The total protein concentration of the extract was measured by a standard bicinchoninic acid (BCA) assay. The MyoIc concentration was estimated by separating the extract

on a SDS-PAGE gel along with Myolc standards (0.1 μ g-1 μ g) and immunoblotting with 2652

Immunoprecipitation

For each immunoprecipitation, 15 μ g of COS-7 cell extract was used. Samples were diluted to 30 μ l using 1% SDS, followed by addition of 10 μ l 4x SB and heated to 95°C for 10 minutes. To each sample 80 μ l water was added to reduce the SDS concentration to 0.2%, and then samples were diluted with 440 μ l of 1.25% Triton X-100, 187.5 mM NaCl, 6.25 mM EDTA, and 62.5 mM Tris pH 7.5. The samples were centrifuged for 10 minutes at 12,000 x g at RT and the supernatants were transferred to new Eppendorf tubes along with 15 μ l of the 50% slurry of DAR-antibody-Sepharose. DAR-anti-phospho-Myolc-S701-Sepharose was used to precipitate phosphorylated Myolc; DAR-2652-Sepharose was used as a positive control to also precipitate total Myolc. DAR-Sepharose-anti-adenylate cyclase 1 (AC1), and DAR-Sepharose alone were used as negative controls. The mixtures were incubated overnight at 4°C on a rotator and then centrifuged at 12,000 x g at RT for 1 minute. The supernatant was removed in 2 x 270 ml aliquots in 1.7 ml Eppendorf tubes. To these tubes, 1.25 ml acetone was added and then tubes were incubated for 1 hour at -20°C. The pelleted Sepharose was washed 4 x 1 ml with wash buffer (0.1% Triton X-100, 0.02% SDS, 150 mM NaCl, 5 mM EDTA, 50 mM Tris pH 7.5). To the washed Sepharose, 2.5 μ l of 4x SB and 10 μ l of 1x SB was added to each tube and the mixture was heated to 65°C for 20 minutes. The Sepharose was centrifuged

briefly and the supernatant removed and placed into a fresh tube. Another 10 μ l aliquot of 1x SB was added to the Sepharose and heated to 65°C for 20 minutes. The two supernatants were pooled and saved to be run on a SDS-PAGE gel. Following the 1 hour incubation at -20°C, the acetone precipitates were centrifuged at 12,000 x g at 4°C for 20 minutes. The supernatant was removed and the pellets were resuspended in 30 μ l 1x SB, per pair. The acetone pellets and precipitated protein were both separated on a 15% resolving/4% stacking SDS-PAGE gel, transferred to polyvinylidene fluoride membrane (PVDF) membrane (Immobilon P, Millipore, Billerica, MA), and probed with either 2652 or anti-phospho-MyoIc S701.

Western Blot Analysis

Transfer buffer was made by combining 100 ml methanol, 29.75 ml of 500 mM N-Cyclohexyl-3-aminopropanesulfonic acid (CAPS) buffer pH 10.55, and 1870 ml of cold water. After the protein was separated by SDS-PAGE, the gel was incubated in 50 ml transfer buffer for 5 minutes. Gels were transferred to PVDF for 1 hr at 100 V in transfer buffer with cooling and left overnight with stirring. The membrane was blocked for 2 hours at RT with 25 ml blocking buffer (5% Liquid Block (Amersham Biosciences, UK) in PBS). The membrane was incubated for 1 hour in primary antibody in block buffer at RT with rocking, then washed 3 x 5 minutes in 0.3% Tween-20/PBS with vigorous shaking. The blots were then incubated with 1:10,000 secondary antibody in block buffer for 1 hour at RT with gentle rocking. To detect the Perfect Protein Markers, 1:10,000 S-

protein HRP conjugate was included with the secondary antibody. The blots were washed 3 x 5 minutes with 0.3% Tween-20/PBS and developed for 5 minutes with HRP substrate (SuperSignal West Pico, Pierce, Rockford, IL). The blots were finally exposed to film (X-Omat Blue XB-1, Kodak) for 10 sec - 2 hours depending on intensity of the signal.

MATERIALS AND METHODS II

Construction of S701 Mutations of HN

Site mutations of S701 were constructed for functional studies of Myolc. Residue S701 of the HN sequence of rat Myolc (amino acids 1-791) was converted to either alanine or glutamate by site-directed mutagenesis and inserted into the pBBHis2B vector (Invitrogen). The primers for HNS701A were: Forward (CTGGAAGTCCGACGGCAGGCGCTAGCCACCAAGATCCAGG) and Reverse (CCTGGATCTTGGTGGCTAGCGCCTGCCGTCGGACTTCCAG). The primers for HNS701D were: Forward (CTGGAAGTCCGACGGCAGG-ATCTAGCCACCAAGATCCAGG) and Reverse: (CCTGGATCTTGGTGG-CTAGATCCTGCCGTCGGACTTCCAG). To confirm the presence of the mutation, the vectors were sequenced through the mutation site.

In Vitro Motility Assay

Actin Preparation

The *in vitro* motility assay was used to determine the rate Myolc and S701 mutants could translocate actin. For use in ATPase and *in vitro* motility assays, actin was extracted from rabbit muscle. To prepare actin, 10 ml buffer A (2 mM Tris pH 8, 0.2 mM ATP, 0.5 mM DTT, 0.1 mM CaCl₂, 1 mM NaN₃) was added to 0.5 g rabbit skeletal muscle acetone powder (Pel-Freez Biologicals, Rogers, AR). The mixture was stirred in a small beaker in an ice bath for 30 minutes. The liquid

was squeezed through pre-soaked (buffer A) cheesecloth. The extraction was repeated with an additional 10 ml of buffer A added to the remaining muscle, stirred in an ice bath for 1 hour, and squeezed through cheesecloth. The pooled extracts were centrifuged at 8000 x g for 20 minutes at 4°C. The supernatant was adjusted to 50 mM KCl and 2 mM MgCl₂ and allowed to polymerize for 1 hour with constant stirring in an ice bath. The KCl concentration of the mixture was adjusted to 800 mM and the actin allowed to polymerize for an additional 30 minutes. The actin was then pelleted with a spin at 200,000 x g at 4°C for 30 minutes. The pellet was washed with 1 ml buffer A and then resuspended with a chilled glass homogenizer in 2 ml buffer A. The resuspended actin was then dialyzed against 1 L buffer A with a slide dialyzer (Pierce) for 48 hours with 4 buffer changes total. The polymerized actin was then removed from the dialyzer and centrifuged at 200,000 x g for 30 minutes. The unpolymerized actin in the supernatant was repolymerized by adjusting the final concentrations to 50 mM KCl and 1 mM MgCl₂ and then stirred in an ice bath for 1 hour. The F-actin was dialyzed against ATPase buffer (15 mM HEPES pH 7.5, 50 mM KCl, 1 mM MgCl₂, 0.1 mM EGTA, 0.005% NaN₃) overnight at 4°C, and then it was centrifuged at 200,000 x g for 30 minutes. The pelleted F-actin was homogenized with 1 ml ATPase buffer and stored at 4°C. Actin concentration was determined by assuming 38.5 μM/A₂₉₀ nm optical density for a 1 mg/ml solution.

Actin Cycling of Myosin

To remove MyoIc unable to bind and release actin in the presence of ATP, the MyoIc eluates were actin cycled. To the Ni-NTA eluate, 100 μ M F-actin was added and the mixture was incubated for 30 minutes on ice. A sucrose pad was made by adding 0.34 g sucrose to 1 ml dH₂O. To a micro centrifuge tube, 75 μ l of the sucrose pad was added and then overlaid with the actin and myosin mixture. The tube was centrifuged at 256,000 x g for 30 minutes. The supernatant was removed and the pellet was washed briefly with 100 μ l of Ni-NTA elution buffer. The pellet was resuspended with 100-200 μ l ATP resuspension buffer (50mM KCl, 1 mM MgCl₂, 0.1 mM EGTA, 15 nM HEPES pH 8, 5 mM ATP, 5 mM MgCl₂, 0.3% Tween 20, 0.2 mM PMSF, 1 μ M leupeptin, 1 μ M pepstatin). The resuspended actin and myosin was centrifuged for 10 minutes at 256,000 x g and the supernatant containing the cycled myosin was collected and stored at 4°C. The myosin separated on an SDS-PAGE gel against a set of BSA standards in order to estimate protein concentration.

Actin Labeling

To prepare rhodamine-labeled actin, 66 μ l of 3.3 μ M rhodamine-phalloidin (Rh-Ph) was dried for 10 minutes in a speed-vacuum. The Rh-Ph was then resuspended in 87 μ l buffer A (2 mM Tris pH 8, 0.2 mM ATP, 0.5 mM DTT, 0.1 mM CaCl₂, 50 mM KCl) and added to 10 μ l of 20 μ M F-actin and then incubated overnight at 4°C. This stock was then diluted 1:400-1:800 in buffer A and stored at 4°C wrapped in foil to prevent photobleaching.

Preparation of Flow-Through Chambers

Glass coverslips (15 mm, #1) were washed with detergent, dH₂O, and then stored in 70% ethanol in a 50 ml conical tube. To construct the flow-through chambers the coverslips were allowed to air dry and then coated with 8 μ l of nitrocellulose (Ernest F. Fullam, Latham, NY). Two narrow strips of double-sided Scotch tape were laid down on a glass slide parallel to each other. The nitrocellulose-coated glass coverslips were then laid on top of the parallel strips of tape. Chambers were washed with 50 μ l 1x PBS followed by flow-through of 10 μ l 2.5 mg/ml Protein A (Santa Cruz Biotechnology, Santa Cruz, CA) and incubated for 30 minutes at RT in a humid container. To the chamber, 50 μ l of block buffer (1 mg/ml BSA in PBS) was flowed through and allowed to incubate at RT for 10 minutes in a humid container. Next, 5 μ l of the mouse monoclonal antibody 9E10 (anti-myc) was flowed through the chamber and allowed to bind overnight in a moist chamber at 4°C. The chambers were washed with 50 μ l block buffer and bound with 5 μ l of 0.2 μ g/ml Myolc for 1 hr at 4°C in a humid container. The chamber was washed with 50 μ l of block buffer and 5 μ l of diluted Rh-Ph-actin was flowed into the chamber and incubated for 2 minutes at RT. While the actin was incubating, a 100 μ l aliquot *in vitro* motility assay buffer (see below) was assembled and then flowed into chamber. The ends of the chamber were sealed with a small amount of high-speed vacuum grease (Dow Corning, Midland, MI). The slides were immediately imaged with a Plan Apo 100x oil lens on a Nikon Eclipse E800 upright microscope equipped with a Photometrics

CoolSnap CCD camera. Images were collected with the Metamorph Imaging system (version 6.1r4, Molecular Devices, Sunnyvale, CA).

Solutions for *In Vitro* Motility Assay

	2 mM ATP	250 μ M NMB-ADP	0.1 mM CaCl ₂	2 mM NMB-ATP
H ₂ O	75	72.5	75	75
10x ATPase Buffer	10	10	10	10
1 M DTT	5	5	5	5
100 mM ATP	2	2	2	0
100 mM NMB-ATP	0	0	0	2
25 mM NMB-ADP	0	2.5	0	0
0.5 M MgCl ₂	1	1	1	1
150 mg/ml Glucose	2	2	2	2
25 mg/ml Glucose Oxidase	1	1	1	1
5 mg/ml Catalase	1	1	1	1
500 μ M CaM	2	2	2	2
100 mM EGTA	1	1	0	1
10 mM CaCl ₂	0	0	1	0

* Amounts noted in μ l.

Analysis of Motility

Movies of Rh-Ph actin translocation were captured as consecutive images at 5 second intervals for a total of 5 minutes per movie. Actin velocities were analyzed with Metamorph software as follows. An image of a 100 μ m grated slide was acquired to allow a pixels/ μ m conversion measurement to be applied to each movie. Each movie to be analyzed was then "thresholded" by using the Metamorph tracking feature, 30-60 randomly-selected actin filaments were tracked per movie. This tracking gave an average velocity per filament in μ m/sec. One flaw with the analysis is that Metamorph will provide a velocity for filaments that are "dead" or not moving. To address this problem, the velocities of 10

identified non-moving filaments were averaged per movie; this value was subsequently subtracted from each collected velocity for that movie. The adjusted velocities were analyzed with Excel software and graphed in Kaleidograph. Because of the diversity of data for each condition in the HN vs. HNS701A and HNS701D, the cumulative probability was calculated and graphed for each group of data.

Alpha-Actinin *In Vitro* Motility Assays

To order to assess force production by various MyoIc mutants, a stalling protein was added in the *in vitro* motility assay. To stall myosin motility, α -actinin (Cytoskeleton, Denver, CO) was included in the *in vitro* motility set-up. Stocks of protein A/ α -actinin were made by combining 1.25 mg/ml Protein A and a range of α -actinin concentrations. Next, 5 μ l of Protein A/ α -actinin stocks were added to the nitrocellulose-coated coverslips in the flow-through chambers and allowed to incubate 30 minutes at RT. The coverslips were then blocked as described in the *in vitro* motility protocol. The velocities per MyoIc/ α -actinin ratio were plotted as a mean +/- standard deviation (SD) or standard error (SE). The "protein friction" model for myosin motility was illustrated by Tawada and Sekimoto (1991). To fit the data, the following formula was used in Kaleidograph:

$$V = \frac{V_1 \gamma x}{1 + (\gamma - 1)x}$$

V is the velocity without α -actinin, x is the ratio of α -actinin/MyoIc. and τ is a fit parameter describing the viscosities of each state but weighted by the probability of the holding state of each, $P_{\text{MyoIc}}/P_{\alpha\text{-actinin}}$.

ATPase Assay

To determine ATP hydrolysis by MyoIc, the ATPase assay was performed. 1 mM stock of hot ATP was made by mixing 10 μl of 100 mM ATP, 3 μl of $[\gamma\text{-}^{32}\text{P}]$ ATP, and 987 μl of water. Assay components were assembled in 1.7 ml Eppendorf tubes and kept on ice. Each reaction contained 15 mM HEPES pH 7.5, 1 mM MgCl_2 , 0.1 mM EGTA, 50 mM KCl, and 100 μM ATP from the hot stock. Reactions were initiated by adding water, actin, or actin and myosin. The reactions were immediately vortexed, centrifuged, and placed in a 37°C water bath. Hydrolysis was allowed to progress for 30 minutes, then terminated by the addition of 67 μl stop solution (2 parts 10 N sulfuric acid and 5 parts silicotungstic acid) and vortexed briefly. To recover $[\gamma\text{-}^{32}\text{P}]$ ATP, 250 μl of isobutanol:benzene and 25 μl of ammonium molybdate were added and then the mixture was vortexed for 20 seconds. The tubes were centrifuged for 12,000 x g at RT for 5 minutes and then 100 μl of the organic phase was transferred to a scintillation vial with 2.5 ml scintillation fluid (EcoLite). The counts per minute were measured with a scintillation counter. Controls included 1 μl of $[\gamma\text{-}^{32}\text{P}]$ ATP stock, and also actin and $[\gamma\text{-}^{32}\text{P}]$ ATP to account for intrinsic ATPase activity of actin.

MATERIALS AND METHODS III

NMB-ADP Inhibition of *In Vitro* Motility

To determine the effect of the tail domain on myosin function, and also if (2-methylbutyl) adenosine diphosphate (NMB-ADP) could inhibit Y61G mouse MyoIc, *in vitro* motility assays were performed. Protein purification, actin cycling and *in vitro* motility assays were conducted as described in Materials and Methods I and II. Y61G experiments were carried out using 2 mM ATP, 1 mM EGTA; 2 mM ATP, 250 μ M NMB-ADP; or 2 mM (2-methylbutyl) adenosine triphosphate (NMB-ATP), 1 mM EGTA; 2 mM ATP, 0.1 CaCl₂; 2 mM NMB-ATP, 1 mM EGTA. Filaments were quantified and binned and the data fit with a Gaussian-distribution curve.

RESEARCH OBJECTIVES IA

This thesis investigates the impact of S701 phosphorylation on function of the motor and the conditions necessary for MyoIc phosphorylation. The MyoIc sequence includes a strong consensus sequence for PKA phosphorylation located at the junction of the head and first IQ domain of the motor at S701.

Chapter IA confirms that MyoIc can be phosphorylated by PKA at S701. PKA phosphorylated the PKA consensus sequence at S701 in a short peptide array and also in MyoIc purified from Sf9 cells. While the stoichiometry of phosphorylation was low, conditions that affect phosphorylation will be explored in Results IB.

RESULTS IA

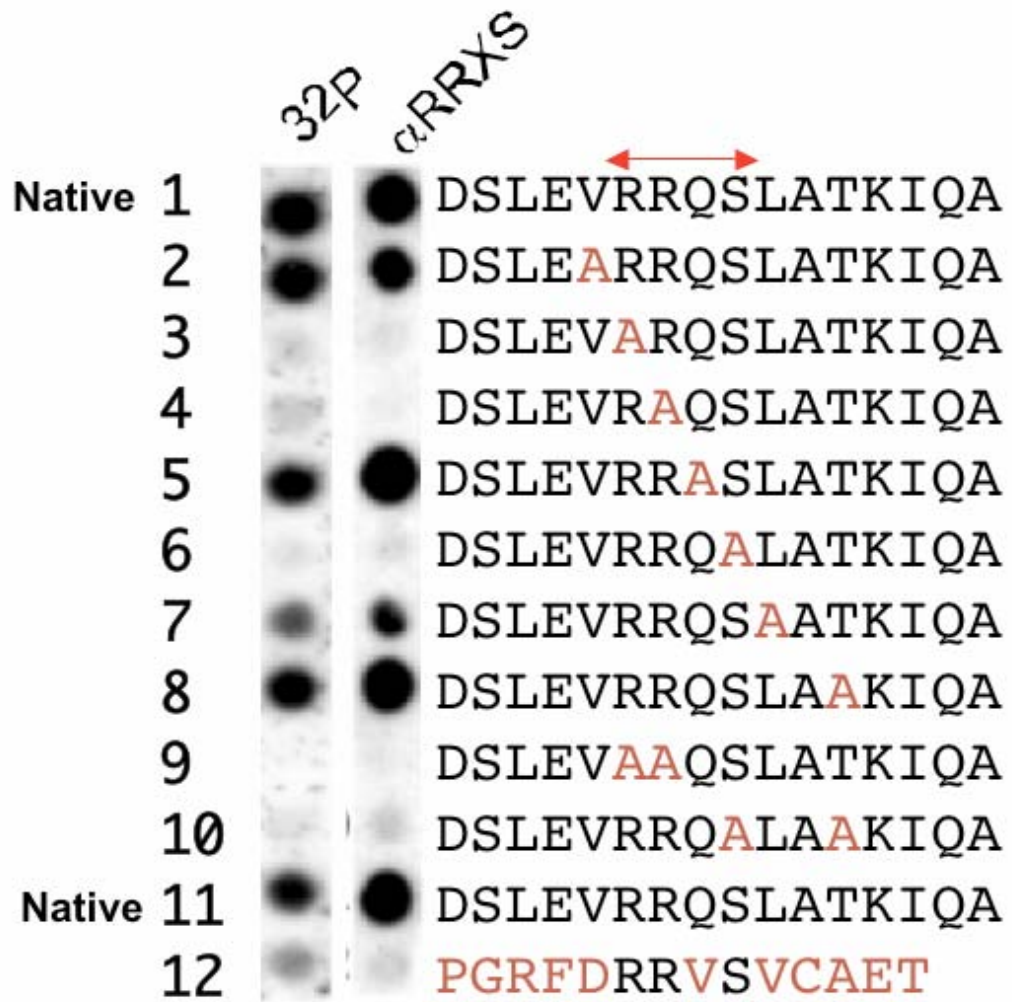
PKA Phosphorylation of S701

Because Myolc contains a consensus site for phosphorylation by PKA, we wanted to confirm that the rat S701 site could be phosphorylated by PKA in the context of its native surrounding amino acids (Figure 14). An array of 14-15 amino acid peptides was synthesized on cellulose membrane by an AutoSpot robot (AutoSpot ASP222, ABiMED, Langenfield, Germany). The AutoSpot-generated peptide arrays are useful for assessing kinase and phosphatase activities in relation to target substrates (Espanel X, 2002). An alanine scan was introduced to sequentially interrupt each amino acid in turn, including amino acids of the PKA consensus site (RRQS) in Myolc. When incubated in the presence of PKA, [γ - 32 P] ATP, and standard phosphorylation buffer, the native Myolc sequence became highly radioactive, indicating that it was strongly phosphorylated. Peptides with variations of the Myolc PKA sequence were also strongly phosphorylated when the RRQS site was preserved or when the surrounding amino acid sequence was not significantly altered. Peptide number 12 contained an ideal RII phosphorylation site, though was only moderately labeled. From these results we concluded that the S701 phosphorylation site within the Myolc sequence is an ideal PKA phosphorylation site.

To further support that the consensus sequences from the peptide arrays were phosphorylated, we probed the peptide array with an antibody that recognizes phosphorylated serine and threonine residues (Cell Signaling Technologies). The results obtained in this experiment were identical to those

results from PKA phosphorylation in the presence of [γ - ^{32}P] ATP, with the exception of lighter labeling of peptide 12. These results further verify that S701 MyoIc is a strong PKA phosphorylation site.

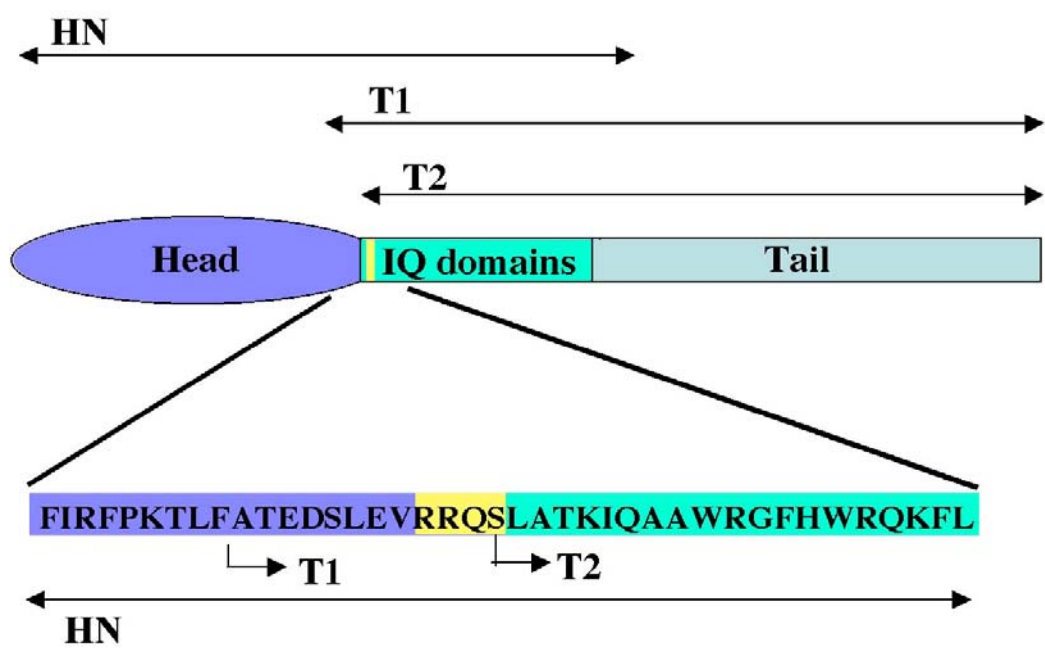
Figure 14. PKA phosphorylation of S701. MyoIc peptide arrays that included the RRXS PKA consensus site were strongly phosphorylated by PKA in the presence of [γ - 32 P] ATP. Alanine substitutions are labeled in red. The red arrow notes the PKA consensus site RRXS. The same peptides were recognized by a phospho-Ser/Thr antibody (α RRXS).



Myolc Constructs

We next wanted to determine if S701 could be phosphorylated by PKA in the context of longer protein fragments of Myolc, which closely mimic the native protein. Three rat Myolc constructs were expressed with a baculovirus expression system, and purified from Sf9 insect cells by Ni²⁺-NTA chromatography: Head-Neck (HN), Neck-Tail (NT), and Neck-Tail 701 (NT701) (Figure 15). The HN construct contains the head and neck (amino acids 1 - 791) regions of Myolc, while the NT construct contains the neck and tail regions of Myolc (amino acids 690 - 1028). Though NT701 (amino acids S701 - 1028) contains the neck, tail, and S701, this construct does not include the RRXS PKA consensus site required for serine phosphorylation. We used the NT701 construct as our negative control.

Figure 14. MyoIc constructs. Three rat MyoIc truncations are shown. The HN construct includes the head and neck domains. The NT construct includes the neck and tail. The NT701 includes the neck and tail but excludes the PKA consensus site.

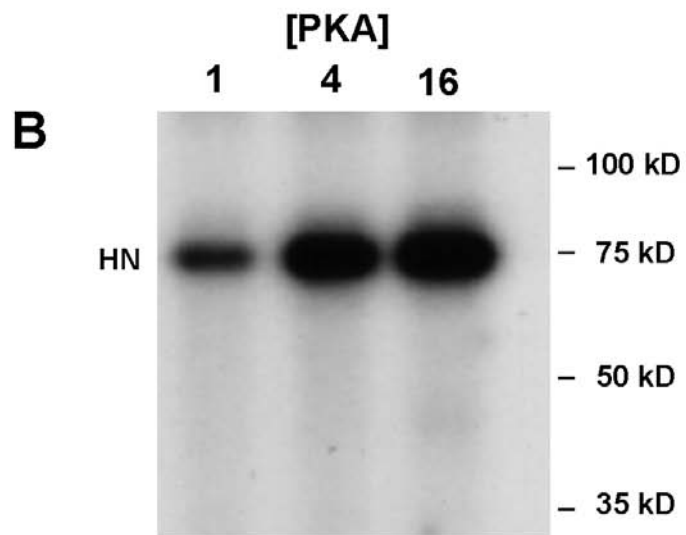
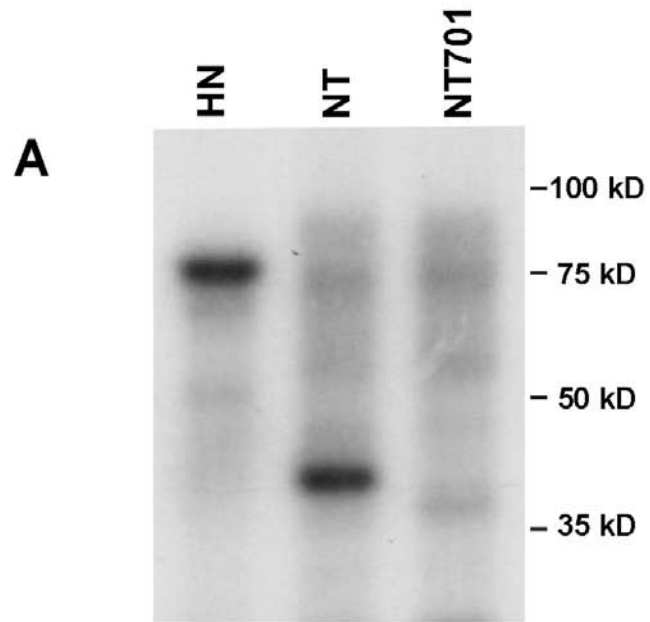


Myolc Constructs are Phosphorylated by PKA

To determine if S701 could be phosphorylated within the context of the longer protein fragments of Myolc, we incubated NT, HN, and NT701 for 30 minutes at 37°C with [γ -P³²] ATP, PKA, and standard phosphorylation buffer. The fragments that included the consensus PKA phosphorylation site at Myolc S701 (HN and NT) were phosphorylated, while the fragment that excluded the PKA consensus site preceding S701 (NT701) was not (Figure 16A). These results demonstrated that S701 is a key site of PKA phosphorylation in Myolc.

We wanted to determine if PKA has a dose-dependent effect on phosphorylation of the HN construct; this would provide additional support that Myolc is sensitive to PKA phosphorylation. The HN construct was phosphorylated with three concentrations of PKA in the presence of [γ -P³²] ATP, separated on an SDS-PAGE gel, and exposed to film. As expected, HN was phosphorylated by PKA in a dose-dependent manner (Figure 16B). Low amounts of PKA were able to phosphorylate HN, while higher concentrations of PKA resulted in greater phosphorylation, though only 15% of full phosphorylation was achieved.

Figure 16. Phosphorylation of Myoc constructs. A. HN and NT were phosphorylated by PKA in the presence of [γ - 32 P] ATP while NTS701 was not phosphorylated. B. HN is phosphorylated by PKA in a dose dependent manner, Concentrations of PKA are shown in [μ M].



DISCUSSION IA

Our results suggest that both short peptides and longer constructs of Myolc can be phosphorylated by PKA. Myolc contains a strong consensus site for PKA phosphorylation (RRXS), where (X) can be any amino acid and the PKA consensus site that includes S701 is RRQS. Phosphorylation of RRQS in the context of the native Myolc sequence on the peptide array shows that native Myolc can be phosphorylated by PKA. Sequences with substitutions of the arginines or serines in the consensus sequence were not phosphorylated. Peptide number 12 (PGRGDRRVSVCAET) contains an ideal recognition site for PKA RII phosphorylation. Though RRVS fits within the RRXS parameters for PKA phosphorylation, this sequence was only modestly phosphorylated. Peptide number 7 (DSLEVRRQSAATKIQA) also lacked the levels of robust phosphorylation seen in the other peptides. These two results taken together suggest that the native surrounding amino acids, especially the flanking leucine residue, may be required for strong phosphorylation of Myolc.

When the peptide array was probed with an antibody that recognizes phosphorylated serine and threonine residues, the results were nearly identical to those achieved in the presence of [γ -³²P] ATP. One minor difference was that scrambled peptide 12 showed even less labeling with the antibody. Again, this result supports the possibility that the amino acids surrounding RRQS of Myolc are required for robust phosphorylation by PKA. We do not have reason to believe there was any non-specific recognition by the antibody. Although this site

is also predicted to be phosphorylated by Ca^{2+} /calmodulin kinase II (CAMKII), the predicted likelihood of phosphorylation is not particularly high given a score of 0.725 by the ScanSite search, placing it in the "medium stringency" category (Obenauer et al., 2003).

Longer fragments of Myolc, HN and NT, were also phosphorylated by PKA, while NT701 was not. Though all three constructs contain S701, NT701 lacks the RRQ amino acids preceding the serine of the PKA consensus site. HN and NT contain the full RRQS site and both were phosphorylated in the presence of PKA, and [γ - ^{32}P] ATP. We also showed that HN is phosphorylated in a dose-dependent manner by PKA in the presence of [γ - ^{32}P] ATP and buffer.

To determine the extent of phosphorylation, the amount of [γ - P^{32}] ATP incorporation into Myolc from Figure 15A was quantified. The Myolc bands were cut out from the SDS-PAGE gel, incubated with H_2O_2 overnight, and counted with a scintillation counter. Though S701 is part of a strong PKA consensus site we found that, surprisingly, only 10-15% of the Myolc was phosphorylated using scintillation counting of phosphorylated Myolc bands (data not shown). Conditions affecting phosphorylation will be discussed in Results 1B.

Though these results demonstrate that S701 is the major site of PKA phosphorylation in Myolc, we cannot rule out other potential phosphorylation sites on this motor. Myolc may contain other weaker PKA consensus sites that could have produced the results we saw in Figure 16. Because the control construct NT701 was not phosphorylated by PKA, alternate PKA sites, if present, are more likely to exist in the head region. It is also possible that the Ni^{2+} -NTA

eluate of Myolc used in this experiment contained residual kinases that could have also phosphorylated Myolc. We believe this to be unlikely based on the general purity of our protein seen on Coomassie-stained SDS-PAGE gels. Also, protein that excluded exogenous PKA was not phosphorylated in control reactions. The NT phosphorylation compared to the lack of phosphorylation in NT701 strongly supports that S701 is a target of PKA in Myolc.

FUTURE DIRECTIONS IA

Though these results strongly support the contention that Myolc can be phosphorylated by PKA, there are a few experiments that would strengthen our hypothesis. Using a peptide array generated by the Auto-Spot robot, we would also like to test several other peptide combinations to determine the importance of amino acids flanking the PKA consensus site. To test if the amino acids closer to the N-terminus are crucial for phosphorylation, we would generate a peptide array with peptides 15 amino acids N-terminal to S701 along with an alanine scan. In a similar fashion we would like to test the importance of amino acids toward the C-terminal of RRQS. Using mutations of amino acids in the peptide array we would investigate the importance of the leucine residue at position 702. This target may be of importance as in the original probe of the peptide array (Figure 14). interruption of K702 appeared to decrease the robustness of S701 phosphorylation.

RESEARCH OBJECTIVES IB

Though Myolc could be phosphorylated by PKA, the stoichiometry was low. This section will explore the conditions that promote PKA phosphorylation of Myolc. Because S701 is located at the beginning of the first CaM-binding IQ domain of Myolc, we investigated how Ca^{2+} and CaM affect PKA phosphorylation. We determined that phosphorylation of an NT construct was Ca^{2+} -dependent, leading to the conclusion that the adjacent CaM-binding IQ domains may play a regulatory role. In short peptides that contain only the S701 PKA site and first IQ domain, phosphorylation was high in the presence of CaM. Increasing amounts of Ca^{2+} inhibited phosphorylation of the short peptide. Also, CaM bound with equal affinity to both phosphorylated and unphosphorylated IQ peptides. We propose that Myolc may require CaM bound to IQ1, but removal of the IQ2 CaM may be beneficial for phosphorylation of S701.

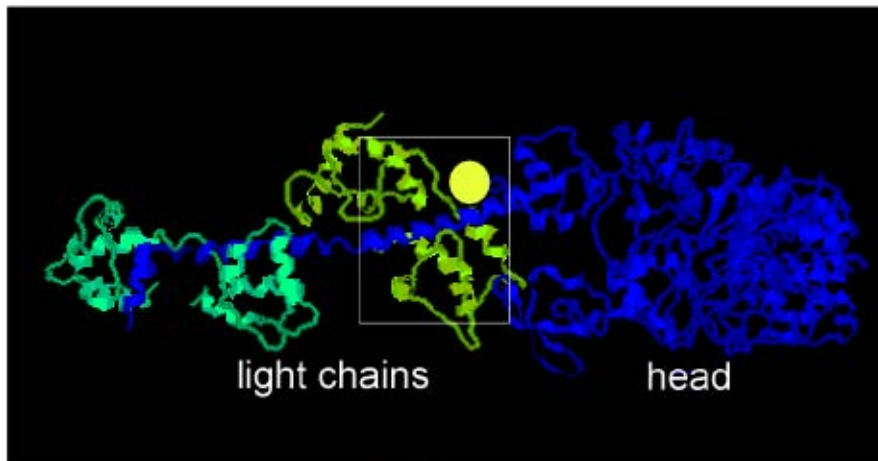
RESULTS IB

Phosphorylation of Myolc in the Presence of Vesicles

Because Myolc appears difficult to phosphorylate, phosphorylation conditions were considered. The involvement of interaction of lipid binding, Ca^{2+} , and CaM were investigated. Previous research had shown that Myolc binds to phospholipids (Reizes et al., 1994; Hirono et al., 2004). The CaM bound at IQ1 may prevent phosphorylation. It is possible that binding of phospholipids to Myolc's IQ domains may release CaM and expose the S701 site, as modeled in Figure 17. To examine if phosphoserine (PS) vesicles increased Myolc phosphorylation, Myolc was incubated with and without PS vesicles and Ca^{2+} under phosphorylating conditions. The results show that HN was phosphorylated in all conditions, but to a much greater level present when Ca^{2+} was included in the reaction (Figure 18). The presence of PS vesicles alone did not appear to increase PKA phosphorylation substantially.

Figure 17. Location of S701 in Myolc. A. The crystal structure of the myosin II head and neck (blue) domains and associated light chains (light and dark green) are illustrated along with a cartoon of the proposed location of a phosphate on Myolc S701 (yellow). S701 is located between the head and first IQ domain in Myolc. B. Modeling of the location of a phosphate at S701 (yellow), in relation to the neck (green) and first associated light chain (gray).

A



B

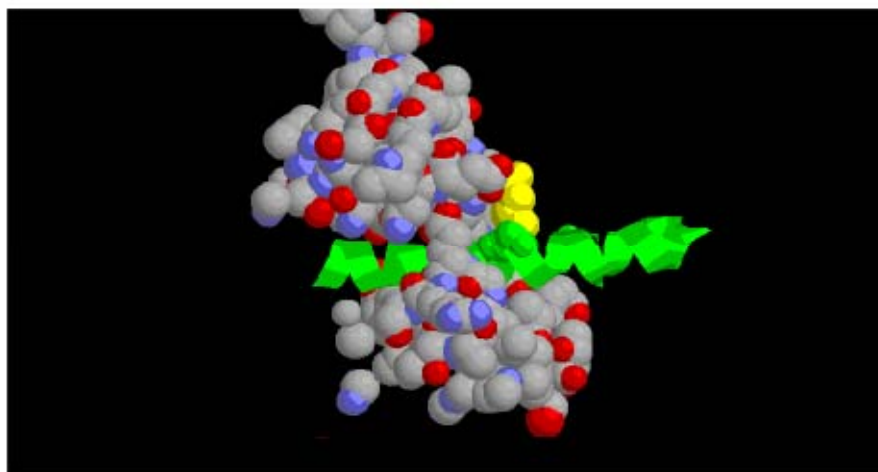
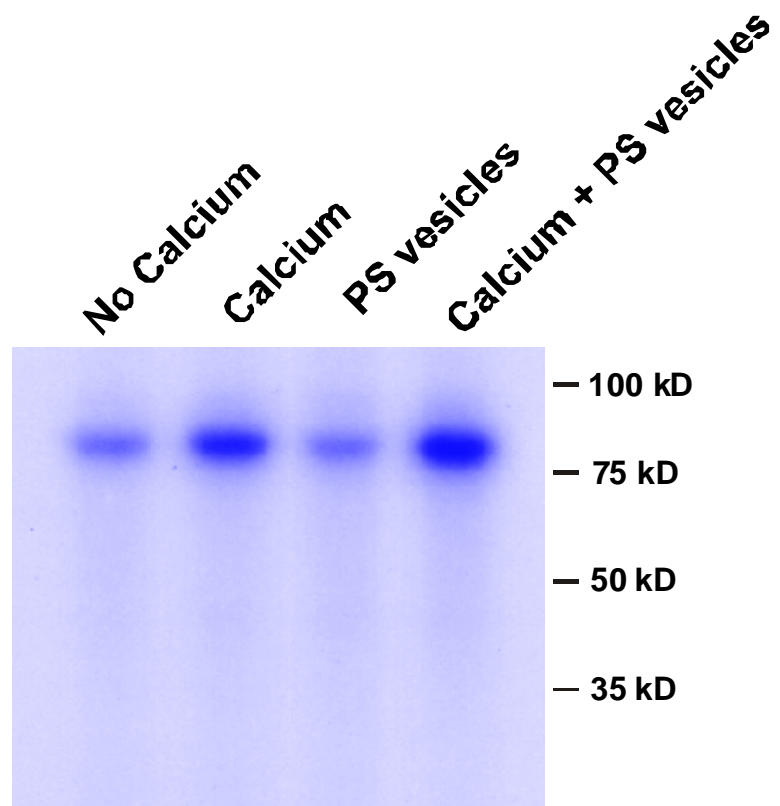


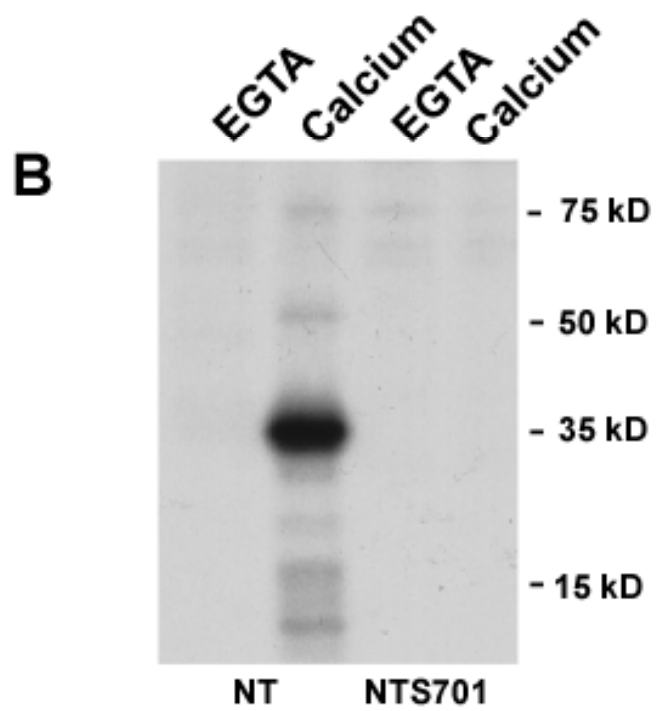
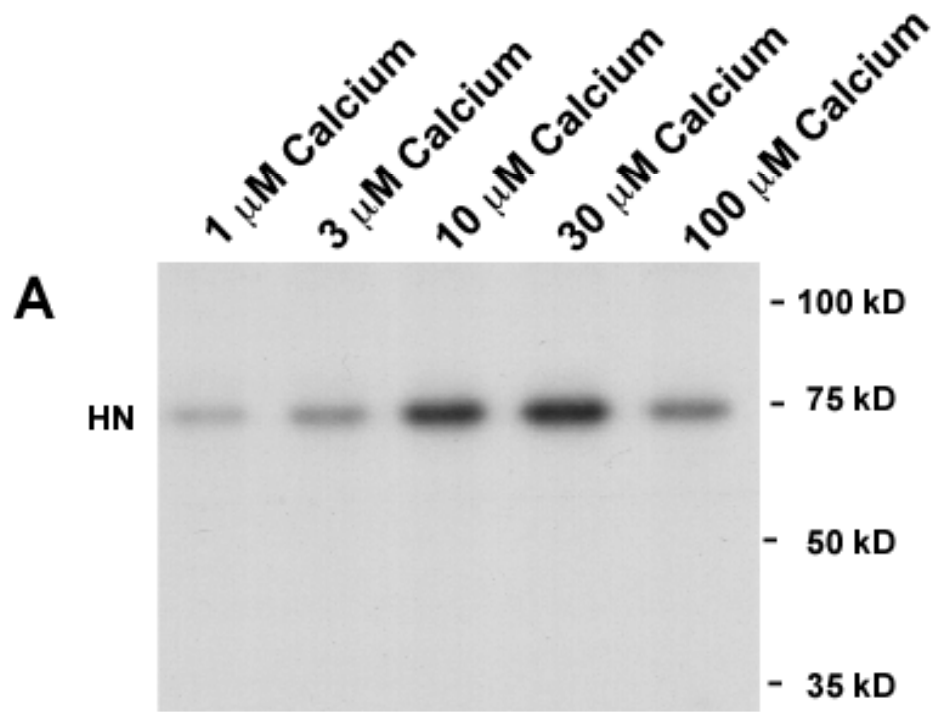
Figure 18. PS vesicles and MyoIc phosphorylation. PS vesicles were added to MyoIc phosphorylation reactions. HN was phosphorylated more strongly in reactions that included Ca^{2+} and PS vesicles or Ca^{2+} alone, and only slightly more when PS vesicles were included.



Calcium Promotes HN Phosphorylation

Because S701 site lies in close proximity to first IQ domain (IQ1) (Figure 17), we hypothesized that CaM at IQ1 may structurally block PKA access to S701; Ca²⁺ may bind to and release CaM from IQ1, thereby exposing S701. HN was incubated with a gradient of Ca²⁺ concentrations in the presence PKA and [γ -P³²] ATP. HN phosphorylation was sensitive to Ca²⁺ in a dose-dependent manner (Figure 19A). Ca²⁺ increased phosphorylation of HN by 2-3 fold though the ideal Ca²⁺ concentration for phosphorylation appeared to be 30 μ M. Interestingly, 100 μ M appeared to inhibit phosphorylation. To examine the Ca²⁺ dependence of NT, the protein was incubated with either Ca²⁺ or EGTA under phosphorylating conditions. Our control construct, NT701, was also exposed to identical conditions. There was robust phosphorylation of NT in the presence of Ca²⁺ and no phosphorylation with EGTA (Figure 19B). NT701 showed no phosphorylation in the presence of either Ca²⁺ or EGTA. This result confirms that Ca²⁺ is necessary for PKA phosphorylation of NT. Ca²⁺ may remove CaM and allow access of PKA to S701.

Figure 19. Calcium and Myolc phosphorylation. A. HN was phosphorylated in the presence of PKA, [γ - 32 P] ATP, and increasing amounts of Ca^{2+} . HN was phosphorylated in a dose dependent manner. B. Phosphorylation of NT and NTS701 was compared in the presence of PKA, [γ - 32 P] ATP, and Ca^{2+} . NT required Ca^{2+} for phosphorylation, while NT S701 was not phosphorylated.



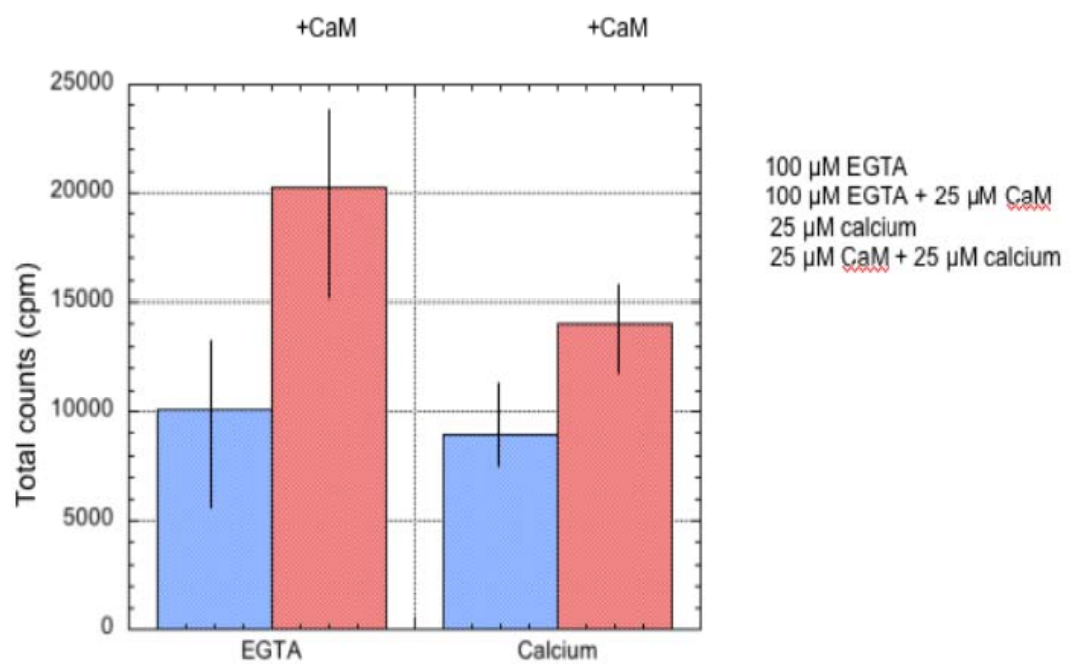
Calmodulin Promotes IQ1 Peptide Phosphorylation

To further examine if S701 phosphorylation is possible only in the CaM-free state of IQ1, a peptide containing the PKA consensus site and IQ1 were phosphorylated by PKA in the presence and absence of Ca^{2+} and CaM. Peptides that were incubated with CaM had significant [$\gamma\text{-P}^{32}$] ATP accumulation (Figure 20). Moreover, phosphorylation of the peptide is robust in the presence of EGTA, even with a saturating amount of CaM. Ca^{2+} had an inhibitory effect on phosphorylation when included in the reactions. When EGTA and EGTA/CaM were compared, results were statistically significant at a p value of 0.0026, while results from Ca^{2+} and Ca^{2+} /CaM has a p value of 0.0022. Contrary to our hypothesis, it appears that CaM bound at the IQ1 site *promotes* phosphorylation.

Figure 20. Phosphorylation of IQ1. A 30 amino acid peptide that included the PKA consensus site and first IQ domain (IQ1) was phosphorylated by PKA in the presence of [γ - 32 P] ATP and calcium, CaM, or EGTA. CaM promoted phosphorylation of IQ1 in both calcium and EGTA conditions, with the highest phosphorylation in the presence of EGTA and calcium.

Peptide: DSLEVRRQSLATKIQAAWRGFHWRQKFLRC

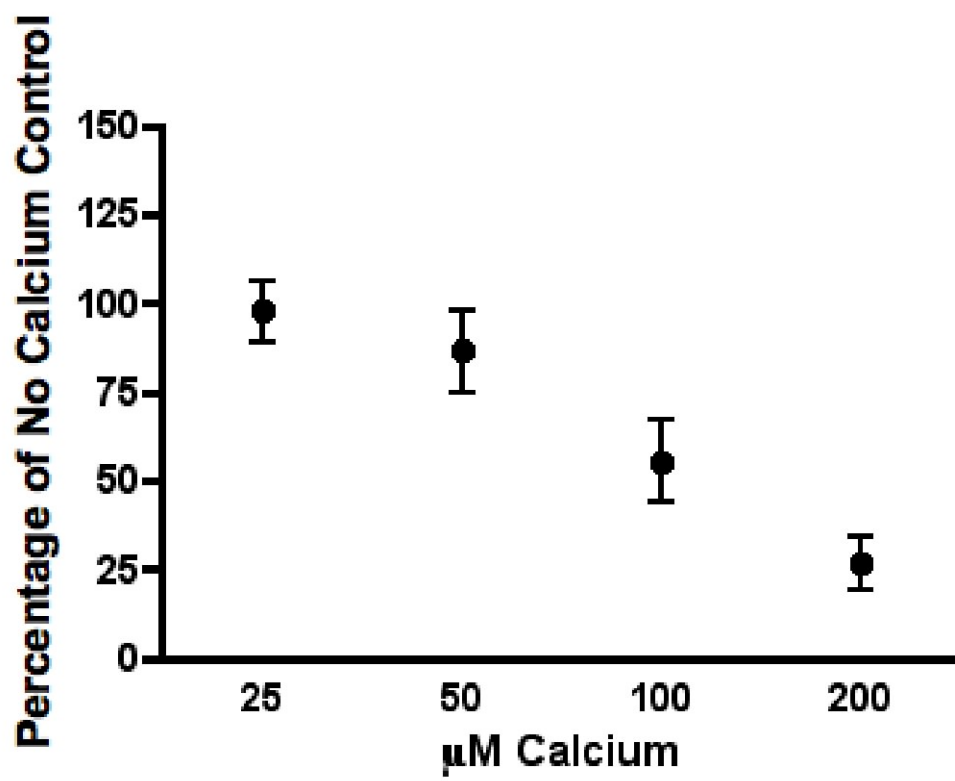
IQ1→



Calcium Inhibits IQ1 Phosphorylation

Because Ca^{2+} appeared to decrease phosphorylation of the IQ1 peptide, a Ca^{2+} titration was conducted to confirm the original observations in Figure 20. The IQ1 peptide was incubated with CaM and increasing concentrations of Ca^{2+} in the presence of PKA and $[\gamma\text{-P}^{32}]$ ATP. Incorporation of $[\gamma\text{-P}^{32}]$ ATP decreased as Ca^{2+} concentrations increased (Figure 21). Because Ca^{2+} binds to and removes CaM from IQ domains, this result suggests that the IQ1 peptide is phosphorylated when CaM is bound to IQ1.

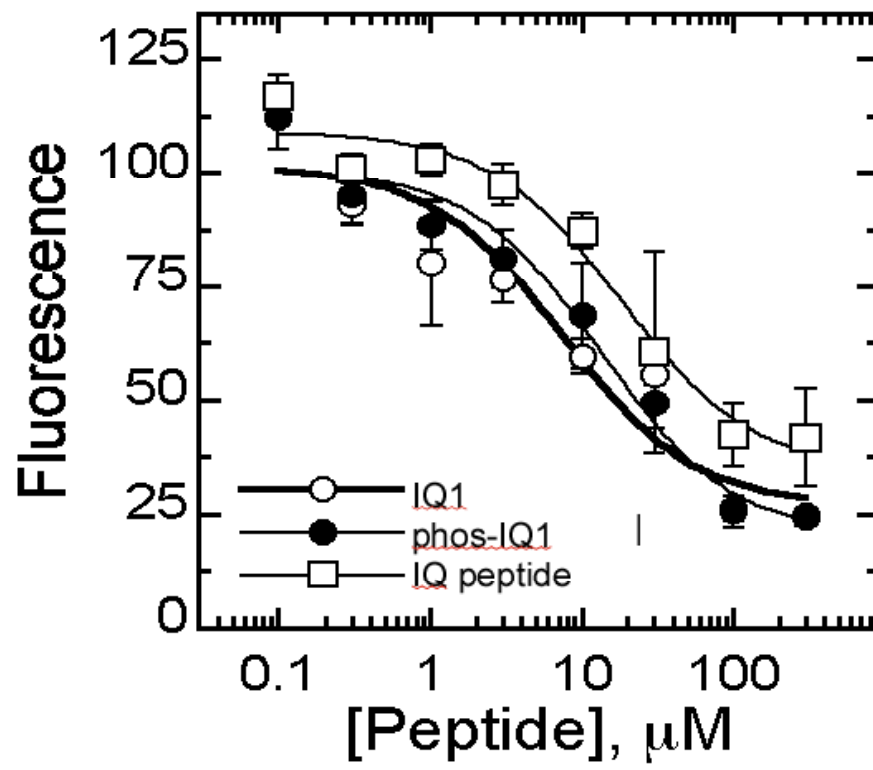
Figure 21. Calcium titration of IQ1 phosphorylation. IQ1 was phosphorylated by PKA in the presence of [γ - 32 P] ATP, CaM, and increasing amounts of calcium. Calcium inhibited PKA phosphorylation of IQ1. Error bars illustrate the standard error of the mean (SEM).



Alexa-Calmodulin Binding to IQ1 Peptides

The PKA consensus site is located five amino acids away from the beginning of IQ1, and therefore phosphorylation of S701 might be competitive with CaM binding. To investigate this scenario, the IQ1 peptide was synthesized with and without an added phosphate group at S701. The two synthesized peptides and a native IQ1 peptide were incubated with Alexa-CaM and buffer. Alexa-CaM bound equally well to Pi-modified and control peptides as indicated by a quench in fluorescence though was less robust for the native IQ1 peptide (Figure 22). The presence of a phosphate at S701 did not prevent binding of Alexa-CaM to the short peptide.

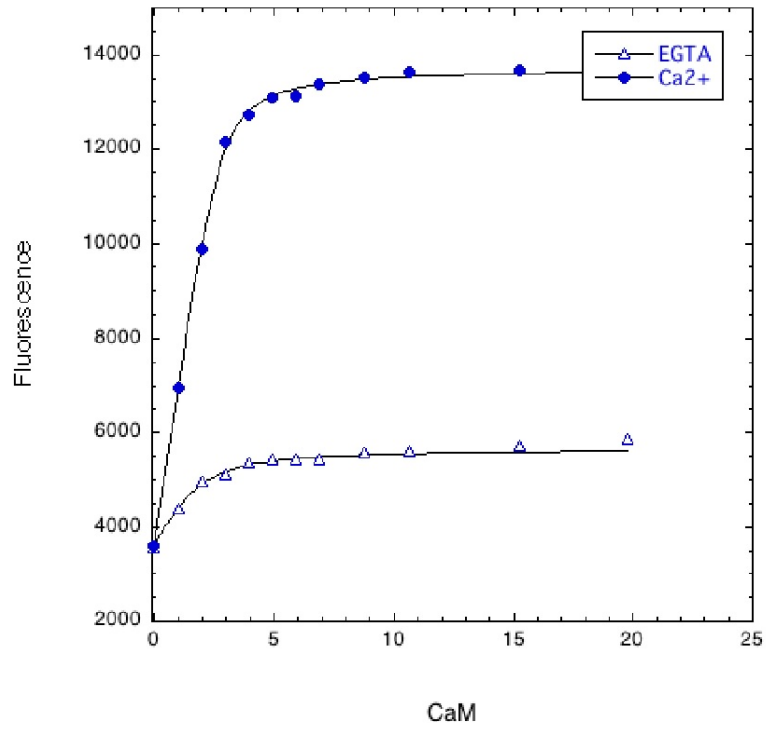
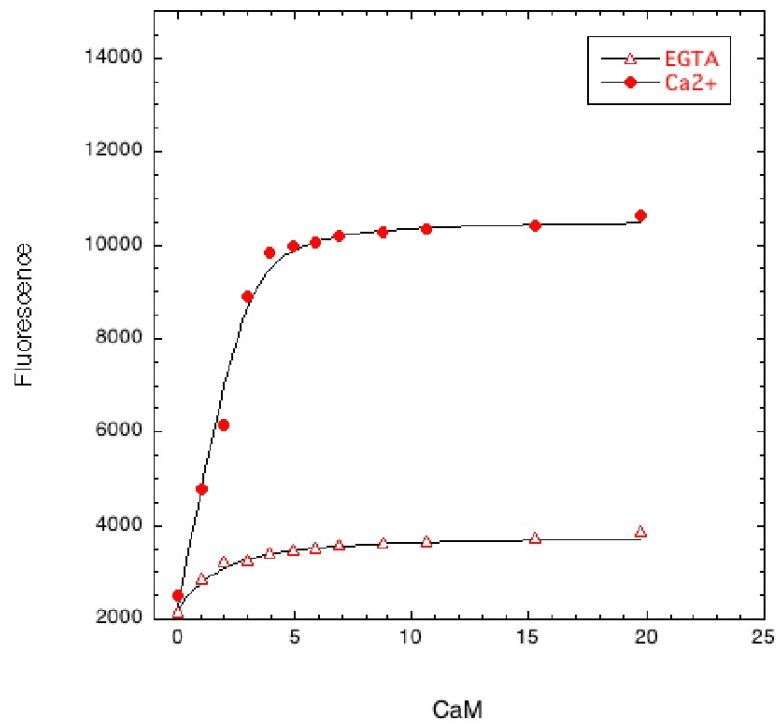
Figure 22. Alexa-CaM binding to IQ1 and phos-IQ1. Alexa-CaM was incubated with IQ1, phos-IQ1, and IQ1 native peptide and the fluorescence (in nm) was measured. Alexa-CaM bound equally well to both IQ1 and phos-IQ1.



Calmodulin Titration of IQ1 Peptides

The possibility that Alexa-CaM may not bind to MyoIc with the same affinity as native CaM was addressed in this experiment. Using native CaM, binding to phosphorylated and unphosphorylated IQ1 was investigated. We expected CaM to bind, as indicated by fluorescence dequenching of tryptophan residues on the peptides. Differences in the amount of quenching would indicate that CaM bound differently to one peptide compared to the other. Phosphorylated and unphosphorylated peptide were incubated with either EGTA or Ca^{2+} , and aliquots of CaM were added stepwise until binding saturation had been reached. Both phosphorylated and unphosphorylated peptides had similar changes in fluorescence emissions when incubated with CaM (Figure 23). Consistent with the Alexa-CaM data, these results suggest that the presence of a phosphate at S701 does not change the conformation or hinder the ability of CaM to bind to the phosphorylated peptide.

Figure 23. CaM titration of native CaM binding. IQ1 and phos-IQ1 were incubated with calcium and incremental amounts of CaM and the tryptophan fluorescence was measured. CaM bound with similar affinity to both Ser701-IQ1 (A) and phosphoSer701-IQ1 (B).

A**B**

DISCUSSION IB

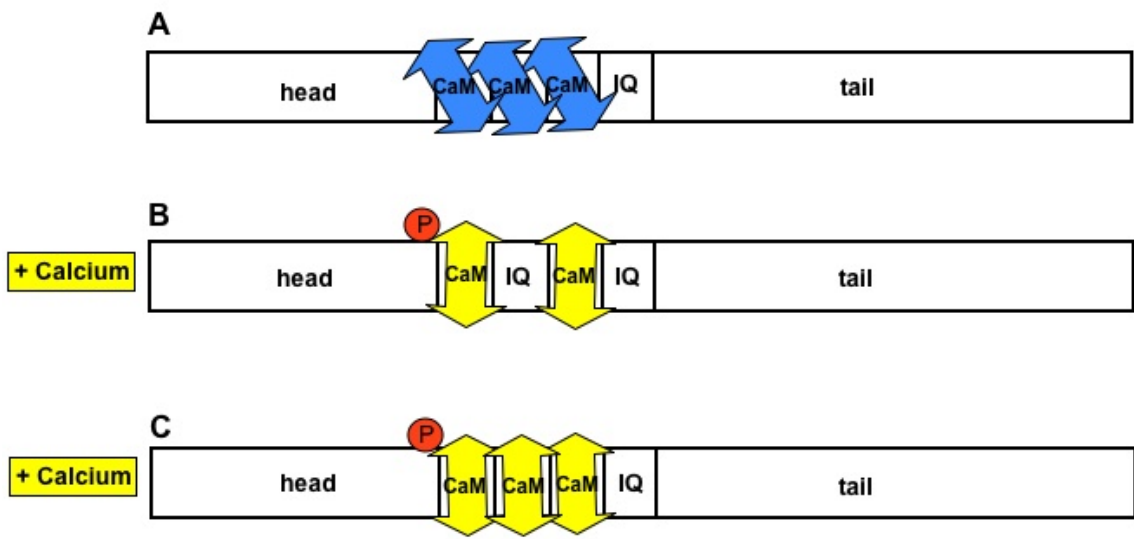
Though S701 is predicted to be a strong PKA phosphorylation site, these results reveal the difficulty in fully phosphorylating Myolc. Although PKA phosphorylation of Myolc fragments that include S701 is possible, the overall stoichiometry was low (~10-15%). HN and NT constructs had greater levels of phosphorylation in the presence of Ca^{2+} . Because S701 lies near the first CaM-binding IQ domain, we originally hypothesized that CaM binding to IQ1 was competitive with PKA and prevented phosphorylation. This hypothesis assumed that Ca^{2+} would bind to and remove CaM, exposing the phosphorylation site. Results from Figure 19 were consistent with this hypothesis. Ca^{2+} promoted phosphorylation in the HN construct up to 30 μM , and was a necessity for phosphorylation of NT. Phosphorylation decreased with 100 μM Ca^{2+} , suggesting the necessity of some bound CaM. To further investigate whether CaM was blocking the S701 site, the CaM inhibitor calmidazolium was added to phosphorylation reactions to remove CaM from the IQ domains which revealed a slight increase in HN phosphorylation by PKA (data not shown).

We further explored the IQ1:CaM interaction by exploiting peptides consisting of IQ1 and the PKA consensus site surrounding S701. When exposed to PKA and [$\gamma\text{-P}^{32}$] ATP, surprisingly the highest levels of phosphorylation were in the presence of CaM and EGTA, as demonstrated in Figure 20. When Ca^{2+} was added along with CaM, there was an inhibitory effect, as confirmed in Figure 21. Using Alexa-CaM and native CaM binding experiments (Figures 22 and 23), we determined that CaM could bind equally well to both phosphorylated and

unphosphorylated IQ1 peptides. CaM bound to IQ1 did not hinder PKA from phosphorylating S701. These results contradicted our original hypothesis that the IQ1 CaM interfered with phosphorylation. They suggest that CaM may, instead, be required to be bound to IQ1 for phosphorylation to take place. Ca^{2+} may play a regulatory role by binding to any of CaM's four Ca^{2+} binding sites, potentially changing the conformation of the bound CaM on the IQ1 motif itself. Because Ca^{2+} inhibits phosphorylation of the IQ1 peptide, phosphorylation is most likely favored when the IQ1 CaM is not fully occupied by Ca^{2+} .

With the longer constructs of Myolc, we showed that Ca^{2+} enhances phosphorylation. Studies by Gillespie and Cyr (2002) have suggested that when Ca^{2+} is low, CaM is bound to IQ1, IQ2, and IQ3. When Ca^{2+} is high, CaM bound to IQ2 is likely to be dissociated first, due to its weak association with Myolc. The IQ1 CaM will also dissociate, while the IQ3 CaM is predicted to stay bound to Myolc (Cyr et al., 2002). Similar dissociation of the CaM on IQ2 was demonstrated in MyoV (Trybus et al., 2007). Because CaM is more likely to dissociate from the IQ2 domain in the presence of Ca^{2+} , a strong possibility is that the conformation of the IQ1-CaM complex is constrained in native Myolc and neck-containing constructs. The presence of CaM on IQ2 may keep CaM on IQ1 in a position where it blocks accessibility of S701. Release of the IQ2 CaM may relieve a strained conformation which may expose S701 (Figure 24B). However, we cannot rule out the involvement of IQ3 or IQ4, as the CaM bound at these sites may have a similar inhibitory role.

Figure 24. Model for Ca^{2+} and CaM regulation. A. In the absence of Ca^{2+} phosphorylation is difficult due to molecular strain imposed by bound CaM. B. Low Ca^{2+} may bind and release CaM on IQ2, which in turn relieves an intermolecular strain. A conformational change may result and allow access of PKA to S701. C. Incomplete binding of Ca^{2+} to CaM may also cause a conformational change and permit S701 phosphorylation.



Another interpretation is that Ca^{2+} may promote unfolding of Myolc to reveal the phosphorylation site, as proposed by the results shown in Figure 19, where Ca^{2+} was required for NT phosphorylation. In the absence of Ca^{2+} , the tail could fold back on the protein, and require Ca^{2+} to relieve this obstruction. In MyoV, Ca^{2+} is required to unfold and activate the motor (Thirumurugan et al., 2006; Trybus et al., 2007). Similarly the head may block the phosphorylation site. Because both HN and NT were phosphorylated strongly in the presence of Ca^{2+} , it is unlikely that the head and tail are both playing an inhibitory role. Ca^{2+} may also bind incompletely to CaM without removing CaM and cause a conformational change in Myolc, similar to MyoV (Figure 24C) (Trybus et al., 2007). Another possibility is that Ca^{2+} binding to CaM could attract other binding partners that promote phosphorylation. This is unlikely, since such proteins would have to be present in the Myolc eluted from Ni^{2+} -NTA columns to address our observations.

There may still be other reasons why the S701 site is not strongly phosphorylated under our conditions. It is possible that in addition to Ca^{2+} , the motor may require other factors to be present for phosphorylation. Myosin's primary role is to produce force, so phosphorylation may require that Myolc is actively exerting force. A force-producing state of Myolc may stretch or unfold the protein in such a way that S701 is exposed for phosphorylation. A preliminary experiment used a stalling protein, NEM-S1, in the *in vitro* motility set-up to stall the motor. Myolc was eluted from the *in vitro* motility chambers, separated on a gel, and exposed to film. In the lane where Myolc was stalled with NEM-S1, there

was a faint band at 100 kD, near the size of Myolc. Subsequent experiments with NEM-SI and the actin-binding protein, α -actinin, were unable to confirm the initial observation. This result does not necessarily rule out this hypothesis. NEM-SI is activation-dependent and did not behave consistently in our hands, and the α -actinin experiments were only conducted once. With appropriate conditions, it is still a possibility that a force producing state may increase phosphorylation of Myolc.

FUTURE DIRECTIONS IB

The next step will be to further explore the interactions of the individual IQ domains with CaM, Ca^{2+} and the S701 site. One possibility is that Ca^{2+} may be required to be bound to CaM at IQ1, but not fully occupy all four binding sites on the CaM. Using CaM with mutations in 1, 2, 3, or all 4 of the binding sites could address this possibility. We proposed the idea that CaM at IQ2 may be inhibiting phosphorylation, so phosphorylation will be attempted with a Myolc construct with a non-functional IQ2 site. Mutations in IQ2 render this site unable to bind CaM. Similarly, Myolc with IQ2 deleted will be exposed to phosphorylating conditions. If phosphorylation is not increased, then this result would be a strong indication that the other IQ domains may be playing a role. Next, protein with mutant or deleted IQ3 and IQ4 will be used. If none of these conditions yield additional phosphorylation, then involvement of the head or tail domains will be investigated using a series of Myolc truncations.

RESEARCH OBJECTIVES IC

We wanted to determine the phosphorylation state of Myolc in hair cells. To do this we used COS-7 cells as a model system to determine the feasibility of phosphoserine Myolc immunoprecipitation. COS-7 cells were exposed to agents to stimulate and inhibit PKA. Cell lysates from treated and untreated cells were exposed to an antibody specific for phosphorylated S701 of Myolc to immunoprecipitate phosphorylated Myolc. Immunoblots of eluted protein were then probed with a Myolc antibody. PKA stimulated and inhibited conditions were compared with untreated cells to attain a relative estimation of endogenous phosphorylation levels. This protocol was also repeated with ionomycin-treated COS-7 cells and Sf9 cells. Unfortunately, no phosphorylated Myolc was immunoprecipitated. These experiments suggested that Myolc is unphosphorylated in COS-7 and Sf9 cells. From these experiments, I conclude that phosphorylation of S701 is not straightforward and may require specific CaM or Ca²⁺ interactions. We also hypothesize that the CaM bound to IQ2, IQ3, or IQ4 may play a key role in the availability of S701 for phosphorylation.

RESULTS IC

Phospho-MyolcS701 Antibody

To probe the phosphorylation state of Myolc in COS-7 cells, and potentially hair cells, an antibody, Phos-MyolcS701, was produced that recognizes phosphorylated S701 in the context of the native surrounding amino acids in Myolc. Phosphorylated and unphosphorylated peptide arrays including S701 were synthesized on a cellulose membrane with an AutoSPOT robot. These strips were then probed with Phos-MyolcS701 to test selectivity for phosphorylated residues. Phos-MyolcS701 recognized only the peptides with an added phosphate at S701 (Figure 25). Some staining of the unphosphorylated peptides was present; however, this was not deemed to be significant.

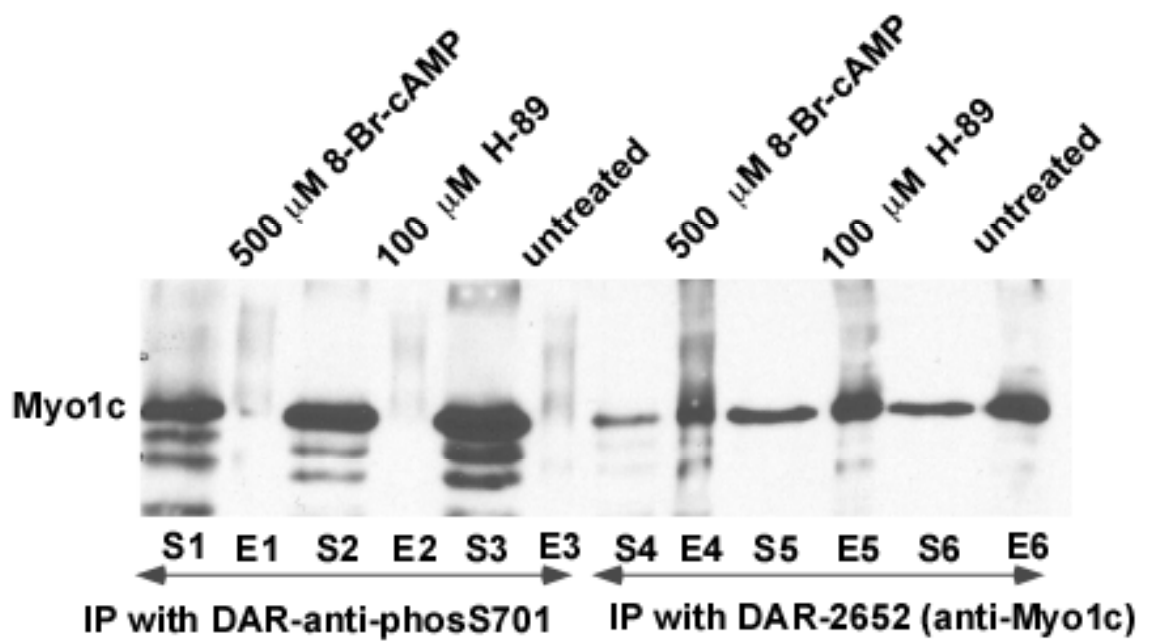
Figure 25. Phospho-MyolcS701 antibody. Myolc peptide arrays that included phosphorylated serine (r) were strongly recognized by the phospho-MyolcS701 antibody (7-11), while the unphosphorylated peptides were not labeled (1-6).

- 1 ● DSLEVRRQSLATKIOA
- 2 ● DSLEARRQSLATKIOA
- 3 ● DSLEVARQSLATKIOA
- 4 ● DSLEVRAQSLATKIOA
- 5 ● DSLEVRRASLATKIOA
- 6 ● DSLEVRRQALATKIOA
- 7 ● DSLEVRRQrLATKIOA
- 8 ● DSLEARRQrLATKIOA
- 9 ● DSLEVARQrLATKIOA
- 10 ● DSLEVRAQrLATKIOA
- 11 ● DSLEVRRArLATKIOA

Immunoprecipitation of Myolc from COS-7 Cells

To determine the phosphorylation state of Myolc in COS-7 cells, phosphorylated Myolc was immunoprecipitated (IP) from COS-7 cell lysates. Cells were treated with 8-Br-cAMP or H89 to increase or decrease phosphorylation levels respectively, while control cells were untreated. The cells were lysed and Myolc from the lysates was immunoprecipitated with donkey anti-rabbit (DAR)-Phos-MyolcS701 Sepharose. The Sepharose was separated from the lysate and washed. Immunoprecipitated protein was eluted from the Sepharose with 4x SB (IP eluate). Unbound protein in the lysate was precipitated with acetone (IP supernatant). Both IP eluates and IP supernatants were separated on an SDS-PAGE gels, transferred to membranes, and then the immunoblots were probed with 2652, a Myolc antibody. When exposed to DAR-Phos-MyolcS701 Sepharose, there was no IP of phosphorylated Myolc as seen in the E1, E2, and E3 (Figure 26). The majority of Myolc did not bind to the antibody and remained in the IP supernatant (S1, S2 and S3). To determine total amount of Myolc present, Myolc was also immunoprecipitated with DAR-2652 Sepharose, and immunoblots probed with 2652. In the control experiment DAR-2652 Sepharose bound Myolc as seen in the E4, E5, and E6, though a large amount of the Myolc remained in the IP supernatant (S4, S5, and S6).

Figure 26. IP of Myolc from COS-7 cells. COS-7 cell extracts from PKA stimulated, inhibited, and untreated cells were immunoprecipitated with DAR-anti-phosS701 and DAR-2652 Sepharose. IP eluates (E) of the immunoprecipitated protein along with IP supernatants (S) were separated on a gel and probed with 2652. No Myolc was immunoprecipitated with DAR-anti-phos-S701 (E1 - E3), but was present in the IP supernatants (S1 - S3).

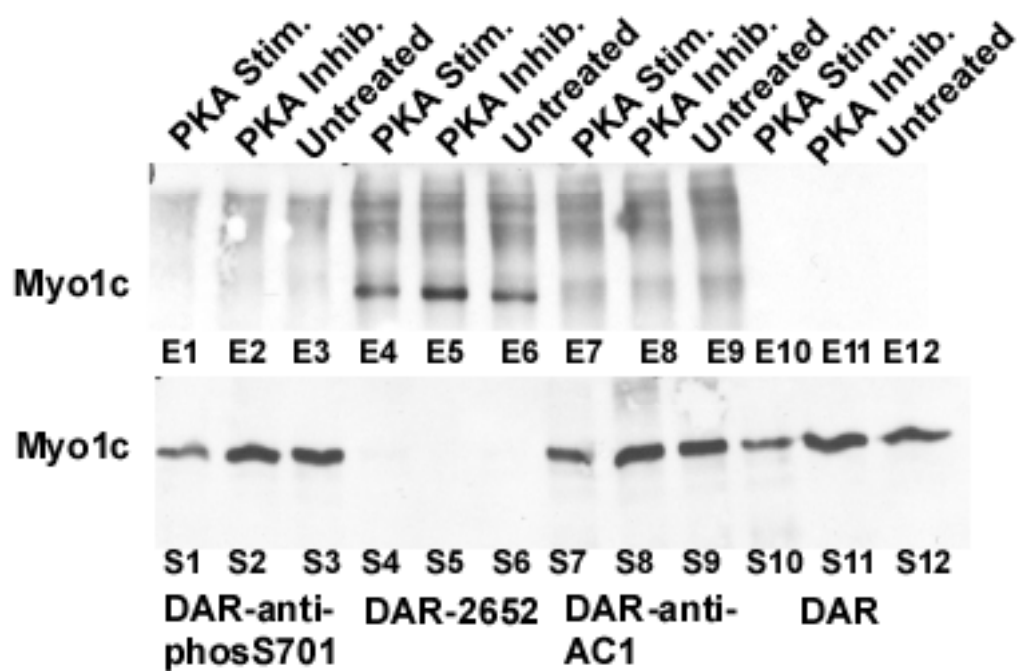


Probed with 2652 (anti-Myo1c)

Ionomycin Treated COS-7 Cells

Myolc was phosphorylated more strongly in the presence of Ca^{2+} , as discussed in Results IB. To stimulate phosphorylation, COS-7 cells were treated with 8-Br-cAMP, phosphatase inhibitors and the Ca^{2+} ionophore, ionomycin. H89 was added to inhibit phosphorylation in COS-7 cells, and a third set of cells remained untreated. Cells were lysed and Myolc from each of the three conditions was immunoprecipitated with DAR-Phos-MyolcS701 Sepharose. When immunoblots of the IP eluates were probed with 2652, no Myolc was detected (E1, E2 and E3), the Myolc remained unbound and present in the IP supernatant (S1, S2, and S3; Figure 27). To show the total amount of Myolc present, Myolc was immunoprecipitated with DAR-2652 Sepharose and the immunoblots probed with 2652. All COS-7 cell Myolc was present in the IP eluates by 2652 as seen in lanes E4, E5, and E6. Extracts from all three conditions were also exposed to negative control, DAR-anti-adenylyl cyclase 1 (anti-AC1) Sepharose and also to DAR Sepharose, and probed with 2652. DAR-anti-AC1 Sepharose and DAR Sepharose did not immunoprecipitate any Myolc (E7-E12); all Myolc was present in the IP supernatants (S7-S12).

Figure 27. IP of Myolc from ionomycin-treated cells. In addition to PKA stimulators and inhibitors, COS-7 cells were also treated with ionomycin. Extracts were exposed to DAR-anti-phosS701, run on a SDS-PAGE gel, and probed with 2652. No Myolc was present in the IP eluates (E1, E2, and E3).

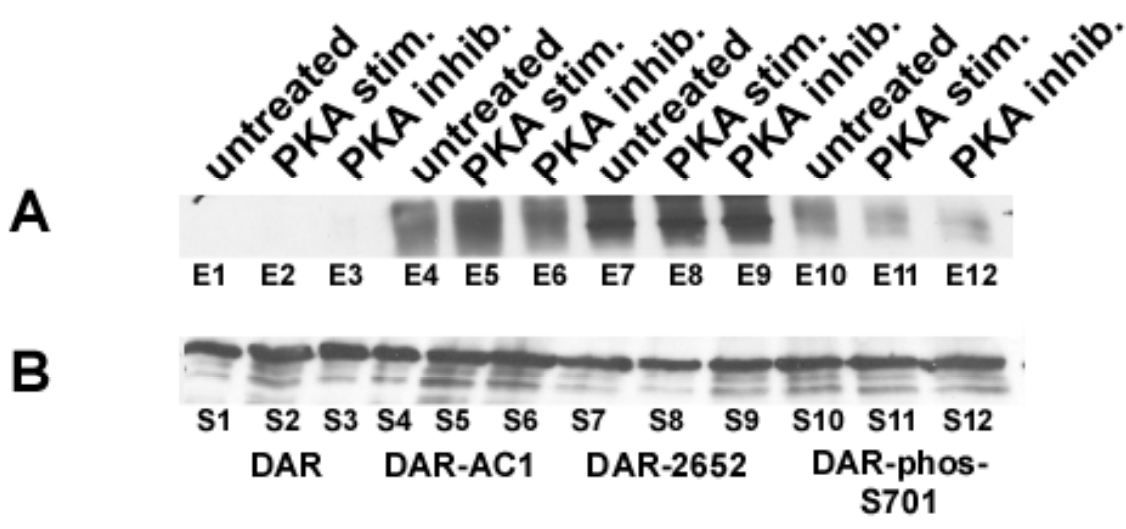


Probed with 2652

Immunoprecipitation of Myolc from Sf9 Cells

Myolc was difficult to phosphorylate in COS-7 cells, so immunoprecipitation was attempted with purified Myolc to simplify the experiment. To determine the phosphorylation state of Myolc in Sf9 cells, Myolc from Sf9 Ni²⁺-NTA eluates was immunoprecipitated with DAR-Phos-MyolcS701 Sepharose. Ni²⁺-NTA eluates were exposed to PKA, Ca²⁺ and phosphatase inhibitors to simulate phosphorylation, while another set of eluates was exposed to H89 and alkaline phosphatase to inhibit phosphorylation. A third set of eluates remained untreated. Myolc from the three conditions was immunoprecipitated with DAR-Phos-MyolcS701 Sepharose, and immunoblots were probed with 2652. No phosphorylated Myolc was present in the IP eluates with DAR-Phos-MyolcS701 Sepharose, (E10, E11, and E12) but there was a high amount of background protein present (Figure 28). Surprisingly, the majority of the Myolc remained in the IP supernatants (S10, S11, and S12). Similarly, the negative control antibody, DAR-anti-AC1 Sepharose, and DAR Sepharose alone, did not pull down any Myolc, as would be expected (E1 - E6). When immunoprecipitated with DAR-2652 Sepharose, approximately half the Myolc was extracted from the Ni²⁺-NTA eluates (E7, E8, and E9), while the residual Myolc was present in the IP supernatants (S7, S8, and S9).

Figure 28. IP of Myolc from Sf-9 eluates. Myolc was immunoprecipitated from Myolc eluates exposed to PKA stimulators and inhibitors. No Myolc was immunoprecipitated with DAR-phosS701 (E10, E11, and E12).



Probed with 2652

DISCUSSION IC

To probe the phosphorylation state of Myolc in COS-7 cells, Myolc was immunoprecipitated with Phos-MyolcS701, followed by detection with a Myolc antibody (2652). We chose COS-7 cells, a mammalian cell line, for our preliminary experiments because they are likely to model Myolc phosphorylation *in vivo*. The endogenous degree of phosphorylation of Myolc phosphorylation was compared with the degree of phosphorylation of Myolc from cells where PKA activity was inhibited or stimulated. This experimental design was intended to reveal a rough estimate of phosphorylation levels in the COS-7 cells. It was hoped that these techniques could be applied to hair cells, allowing us to estimate the endogenous Myolc phosphorylation state.

Unfortunately, no Myolc was pulled down in COS-7 cells or Sf9 cell eluates with Phos-MyolcS701 (Figures 27 and 28). Because the negative controls did not pull down any Myolc, and the 2652 antibody always pulled down Myolc, we believe the experimental design set-up and reagents were appropriate for semi-qualitative analysis. To confirm the reliability of the phospho-specific antibody, Figure 25 demonstrates that Phos-MyolcS701 recognizes proteins containing a phospho-serine701 in the context of native Myolc amino acids. Phos-MyolcS701 did not pull down any Myolc in the untreated conditions (Figures 26, 27 and 28). These results suggest that Myolc is in an unphosphorylated state when extracted from COS-7 cells or eluted from Sf9 cells. When Myolc and HN Sf9 immunoblots were probed with Phos-MyolcS701 or a general phospho Ser/Thr antibody, no Myolc was recognized, which further

supports this assumption (data not shown). Immunofluorescent staining of COS-7 with Phos-MyolcS701 also did not reveal any labeling (data not shown).

It would have been expected that PKA-stimulating conditions would have resulted in an increase in Myolc pull-down by Phos-MyolcS701. One consideration is that the chosen drugs or stimulating conditions were not ideal for Myolc phosphorylation. When stimulated with ionomycin, the released Ca^{2+} also may not have been in the vicinity of Myolc to facilitate phosphorylation. As an alternative to ionomycin, the Ca^{2+} ionophore A23187 could be used, which may display a greater effect.

One consideration to account for the low levels of phosphorylation is that Myolc may already be phosphorylated when expressed by Sf9 cells. However, using an antibody against phosphorylated S701 in Myolc, there was no evidence of endogenous phosphorylation. When Myolc constructs were incubated with various phosphatases before exposure to PKA and $[\gamma\text{-}^{32}\text{P}]$ ATP, there was no additional phosphorylation.

Its possible that Myolc expressed in Sf9 cells and Myolc in COS-7 cells require other Ca^{2+} or CaM concentrations for phosphorylation. Myolc may also be phosphorylated at high levels in hair cells, but may require hair-cell specific proteins or conditions that we were unable to replicate.

FUTURE DIRECTIONS IC

Most drugs are not absolute inhibitors or activators of desired target proteins, and may have nonspecific effects. Both H89 and 8-Br-cAMP affect other cAMP-dependent protein kinases, such as PKG, PKC μ , CaMKII, CKI, and MLCK (Davies SP, 2000). Other PKA inhibitors to be considered include PKI, H8, and KT 5720. General protein kinase inhibitors such as staurosporine may also be of value. It would also be ideal to inhibit other components of the protein kinase cascade. To promote phosphorylation, a combination of forskolin, IBMX, and phosphatase inhibitors to supplement 8-Br-cAMP may result in more robust phosphorylation. To further dephosphorylate MyoIc, a combination of adenylyl cyclase inhibitors, PKA inhibitors and phosphatases may have a greater effect than H89 alone.

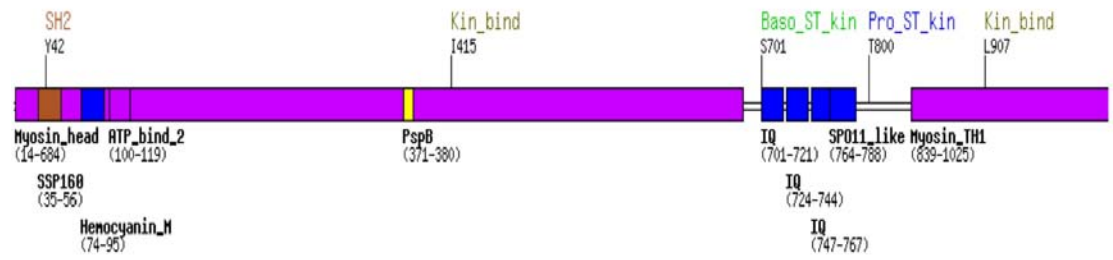
Another way to detect phosphorylation would be to stimulate hair cells with PKA in the presence of radioactive ATP. The hair cell lysates could then be run on a gel and exposed to film to determine if the MyoIc acquired radioactive phosphates. A direct method to determine the phosphorylation state of a protein is to run a mass spectrometry analysis of MyoIc isolated from hair cells. COS-7 cell-MyoIc, or Sf9-expressed MyoIc can be analyzed in a similar way.

Though MyoIc S701 can be phosphorylated in protein purified from Sf9 cell extracts can be various degrees, it is possible that endogenous MyoIc from COS-7 cells may not use the S701 site for phosphorylation. Other lower stringency phosphorylation sites will need to be investigated, as addressed in

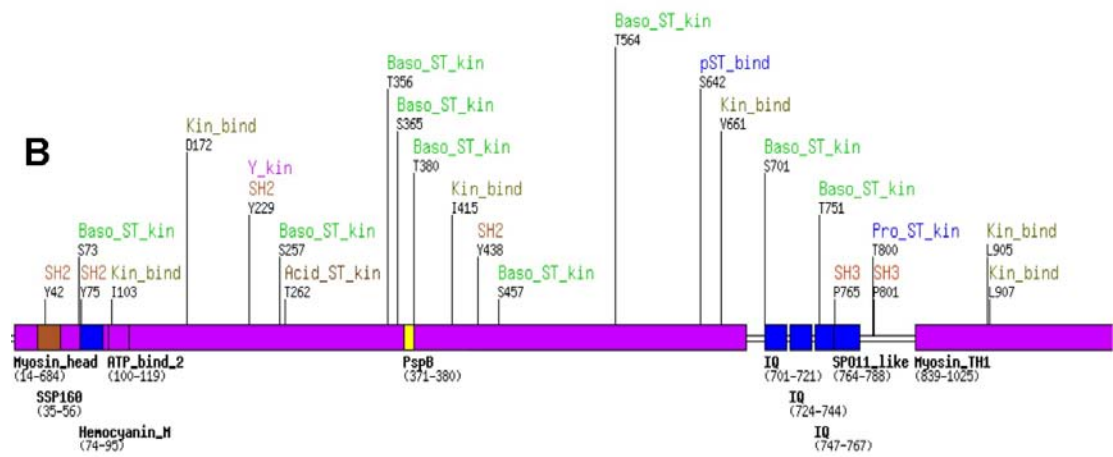
Results 1B. There are several PKC consensus sites present in HN that can be phosphorylated by PKC (Gillespie, P., unpublished). There are several lower-stringency phosphorylation sites in Myo1c including a potential ERK kinase phosphorylation site located at T800 that shows up on a high stringency Scansite search (Figure 29).

Figure 29. ScanSite Myolc phosphorylation sites. A high stringency search (A) and medium stringency search (B) of Myolc phosphorylation sites with Scan Site revealed several phosphorylation site candidates. S701 appears in both searches.

A



B



RESEARCH OBJECTIVES II

Results II investigates how S701 affects the function of Myolc. Point mutations at S701 were constructed to mimic the phosphorylated head neck S701A (HNS701A) and dephosphorylated (HNS701D) states of Myolc. I was able to show that compared to HN, ATPase rates were slower in HNS701D and *in vitro* motility rates are slower in both HNS701D and HNS701A. In an assay of motor force production, both HNS701A and HNS701D velocities were not inhibited by an actin binding protein, confirming the importance of the S701 site for Myolc mechanics.

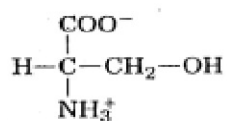
RESULTS II

S701 Amino Acid Substitutions

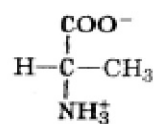
In the previous chapter, I determined that acquiring populations of MyoIc in fully phosphorylated and dephosphorylated states was unlikely. To overcome this obstacle, mutants of HN S701 were created to mimic the two phosphorylation states of MyoIc (Figure 30). To mimic a dephosphorylated state, alanine was substituted for S701. Alanine is a neutrally-charged amino acid, similar to an unphosphorylated serine. To mimic phosphorylation, aspartate was introduced at the 701 site. Aspartate carries an acidic group with a negative charge, similar to a phosphoserine. Both of these substitutions have been routinely used to mimic these two states of phosphorylation (Wagner N, 1993; Huang W, 1994; Smith SD, 2003).

Figure 30. Amino acid substitutions for S701. An alanine mutation was substituted for serine at 701 to mimic the dephosphorylated state of MyoIc, while aspartic acid was substituted for serine to mimic phosphoserine.

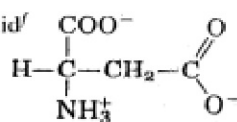
Serine



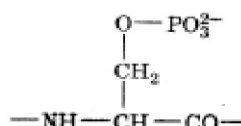
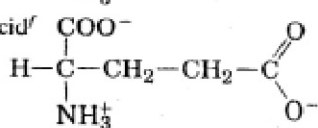
Alanine



Aspartic acid



Glutamic acid

**Phosphoserine**

***In Vitro* Motility of S701 Site Mutants**

Because it was hypothesized that the MyoIc S701 site is important for MyoIc mechanics, the MyoIc velocities of S701 site mutants were investigated. The *in vitro* motility assay was used to determine the rate of actin filament sliding over myosin bound to cover slips (Figure 31). The data were plotted using a cumulative probability graph. *In vitro* motility analysis of velocities revealed that both HNS701D (mean = 0.63 nm/sec) and HNS701A (mean = 1.14 nm/sec) had slower velocities than the native protein HN (mean = 1.52 nm/sec; Figure 32). HN701D had the slowest range of velocities, consistent with our prediction that a phosphorylation-mimicking mutant generates less force, and consequentially may translocate actin at a slower rate. This finding confirms that the 701 position in MyoIc is critical for MyoIc function

Figure 31. *In Vitro* Motility Assay A series of images of Rhodamine-phalloidin labeled actin propelled by MyoIc were captured by a camera linked to a microscope. Velocity of filaments was assessed by tracking movement of individual filaments and calculating an average velocity. Four frames showing tracking of four actin filaments (1 = red, 2 = yellow, and 3 = blue) is shown (A-D).

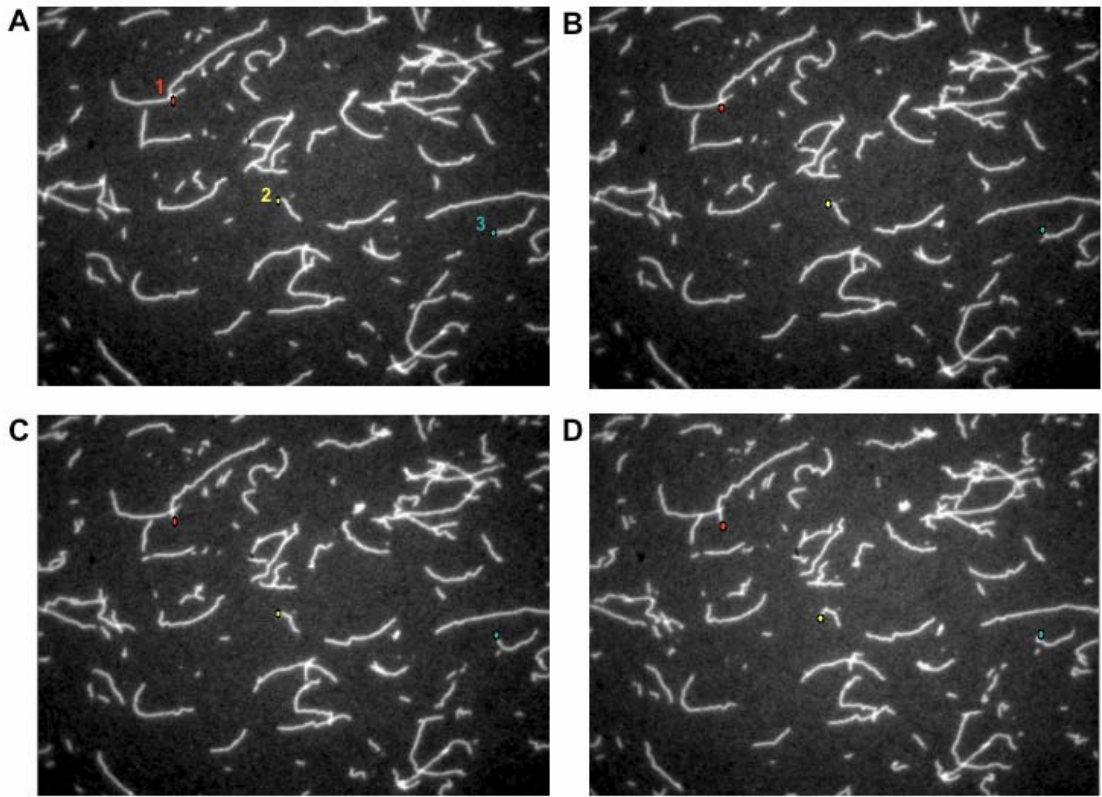
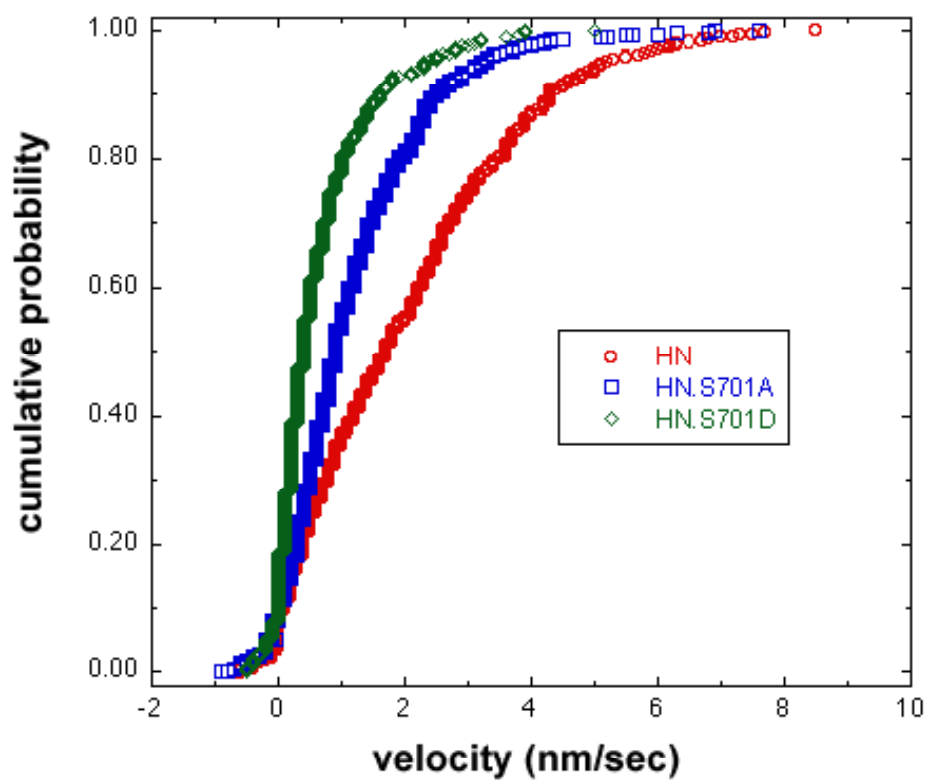


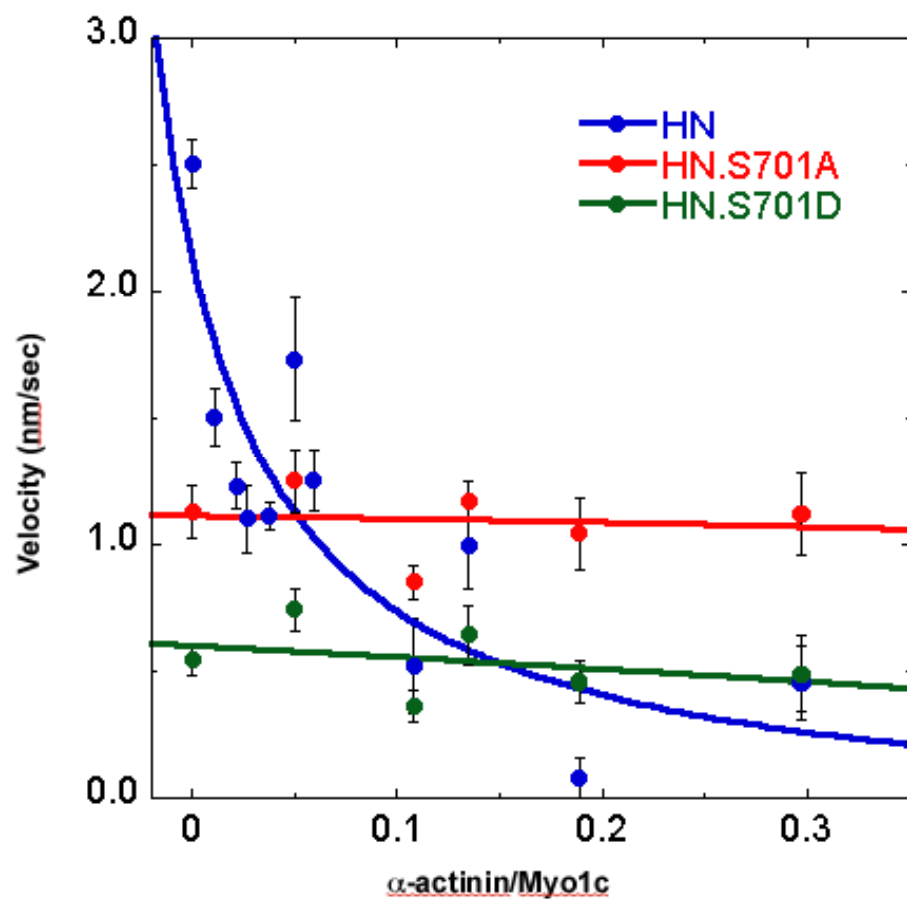
Figure 32. *In vitro* motility of S701 mutants. *In vitro* motility assays were used to assess the velocities of the S701 mutants of HN Myolc. Both HNS701A and HNS701D had a slower range of velocities than HN, with HNS701D displaying the slowest velocities.



***In Vitro* Motility in the Presence of α -Actinin**

The next step was to determine if the S701 site of MyoIc is specifically important for motor force production. Using the *in vitro* motility assay, the actin-binding protein α -actinin was included to introduce a mechanical load to the myosin (Bing W, 2000). Motors that exert more force should require more α -actinin to halt motility. With increasing amounts of α -actinin, the velocity of HN was predictably slower, as the load became too great to overcome (Figure 33). While the velocities of both HNS701A and HNS701D were initially slower with no added α -actinin, increasing amounts of α -actinin did not slow down actin translocation. These results imply that *both* HNS701A and HN701D are able to exert more force on actin than HN.

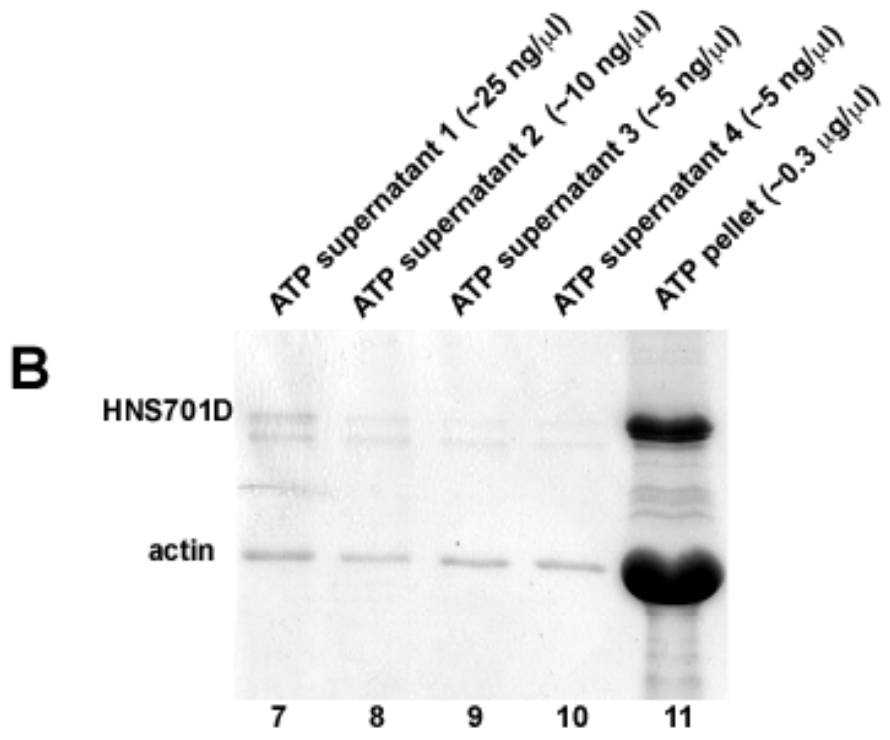
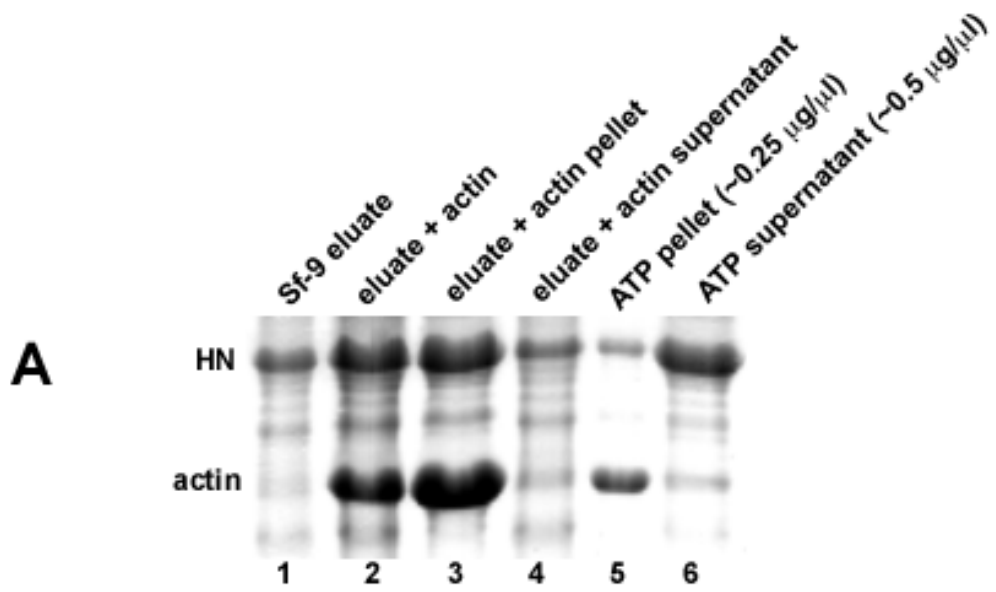
Figure 33. Force measurements of S701 mutants. To assess force production by the MyoIc S701 mutants, α -actinin was included in the *in vitro* motility assay to stall motor force production. The velocity of actin movement was recorded in relation to the ratio of α -actinin to MyoIc. While HN was inhibited by increasing amounts of α -actinin, neither HNS701A or HNS701D velocities were inhibited by α -actinin.



Actin Cycling of HNS701D Compared to HN

Preliminary experiments suggest that HNS701D has a slower ATPase rate than either HNS701A or HN. The slower ATPase and *in vitro* motility rates of HNS701D may be a result of a higher actin affinity. To investigate this possibility, the actin-cycling properties of HNS701D was compared with HN and HNS701A. HN was incubated with actin, followed by an ATP-dependent myosin release step. Samples were collected, run on an SDS-PAGE gel, and stained with Coomassie stain. Figure 33A demonstrates that HN binds actin readily in the absence of ATP (lane 2) and a majority of HN releases from actin upon addition of ATP (lane 6). HNS701D, by contrast, does not release readily from actin in the presence of 5 mM ATP (Figure 33B, lane 7). The residual HNS701D ATP pellet was resuspended with additional ATP three successive times followed by centrifugation. Lanes 8, 9, and 10 show that little additional HNS701D was released from the actin with each new ATP addition. Lane 11 shows the residual ATP pellet, where the majority of HNS701D remained bound to actin. HNS701A released actin readily in the presence of actin (data not shown). These results suggest that HNS701D has a high duty ratio, which is the fraction of time during the actin cycle that the myosin is bound to actin (Howard, 2001).

Figure 33. Actin cycling of HN and HNS701D. A. HN was actin-cycled and fractions from each step were run on an SDS-PAGE gel and Coomassie stained. Lane 6 shows that HN releases readily from actin in the presence of ATP. B. Lane 7 shows that little HNS701D is released from actin in the presence of ATP. A small amount of HNS701D was released with additional ATP addition, though most HNS701D remained bound to actin (lane 11).



DISCUSSION II

Initial electrophysiology data showed that PKA inhibitors and activators had a direct effect on open probability of the hair cell transduction channel (Geleoc et al., 2001). We hypothesize that Myo1c is the target of these agents and that phosphorylation of Myo1c alters force production by the adaptation motor. We proposed that when Myo1c is dephosphorylated, the motor applies more force to the tip link. To examine this hypothesis, site-mutants of the S701 site on Myo1c were constructed and their mechanical properties were investigated.

We determined that HNS701D, our site-mutant mimicking phosphorylation, had a slower range of velocities in the *in vitro* motility assay than HN. Based on the HNS701D and HN *in vitro* motility data, it is likely that HN is unphosphorylated at S701 when purified from Sf9 cells. It is possible that Sf9-purified HN is a mixed population of phosphorylated and unphosphorylated protein, though these *in vitro* motility data still imply that HN is largely unphosphorylated. It is interesting that HNS701A also translocates actin at slower velocities than HN. One would expect that HN701A velocities would be similar to HN. If HN is a mixed population, we hypothesize that HNS701A would translocate actin at a higher velocity than HN.

The *in vitro* motility assay has limitations; it is a measure of velocity and not direct force production. To measure force production of the mutants, α -actinin was introduced into the *in vitro* motility assay to act as a load; we predicted that

myosins producing more force would translocate actin in the presence of higher concentrations of α -actinin than myosin producing less force. The results of this assay showed that while HN velocities were slowed down with increasing amounts of α -actinin, velocities of HNS701D and HN701A remained relatively constant. These results show that both HN701A and HN701D produce more force than HN. It should be noted that in the presence of the highest molar ratio of α -actinin/MyoIc (0.3), velocities for both HN and S701A were similar (1.25 nm/sec. vs. 1.12 nm/sec).

Taken together, these results show that compared to HN both HNS701D and HNS701A produce greater force, but have slower velocities. The greater-force producing properties of HNS701A are consistent with our original hypothesis, but HNS701D also appears to produce greater force than HN. Figure 33 suggests that HNS701D eluates may be composed of a greater amount of myosin that does not release from actin in the presence of ATP, which may result in the slower velocity and greater force production. By staying attached to actin longer, these results imply that HNS701D has a greater duty ratio. Force production can be enhanced by prolonging the ADP-bound state (Howard, 2001). To further assess the limits of force production it would have been useful to introduce even higher molar ratios of α -actinin:MyoIc.

Mutations of S701 may not perfectly mimic the phosphorylated protein. There are subtle differences in amino acid structures and sizes that may affect protein function. Though both serine and alanine are small in size and neutral in charge, serine contains an additional hydroxyl group. Similarly, both aspartate

and phospho-serine are acidic but aspartate has a lower charge density than phosphoserine (Mathews and Van, 1996). These changes may cause the protein to fold differently, or possibly attract other binding partners, therefore affecting the protein's function (Mathews and Van, 1996). Moreover, mutations may also affect packing of Myolc molecules since the adaptation motor may act as a complex in the hair cell. To address these possibilities, other amino acid substitutions to S701 could be made in Myolc. Although alanine is typically used to mimic unphosphorylated serine, cysteine or methionine might be a better mimic (Mischak H, 1996). Glutamate may be a better mimic of phosphorylation, due to its acidic nature (Royo M, 2005).

As an alternative to HNS701D, the glutamate-based mutant, HNS701E, was constructed. In our hands, it was difficult to express and purify adequate amounts of HNS701E protein to use for *in vitro* motility and ATPase assays. It is likely that HNS701E was a poorly expressed protein, or the virus-titer was too low for robust production of protein in Sf9 cells. Similarly, full-length rat Myolc with S701D and S701A mutations were poorly expressed in Sf9 cells. Because mutating S701 affected ATPase rate, *in vitro* motility velocities, *in vitro* motility force production, and actin release, we can conclude that S701 does play an important role in the mechanics of Myolc. Existence of a pliant region between the motor and IQ domains was identified in scallop muscle myosin (Houdusse A, 2000). This region allows the position of the neck and tail domains to vary relative to the head. Mutations in the pliant region are predicted to play significant roles in the motor properties of the myosin as has been demonstrated in myosin

II; when a glycine residue is substituted for an arginine in the pliant region, the resulting mutant myosin displayed higher ATPase and motility rates (Yamashita H, 2000).

Evidence from another myosin-1E offers an appealing theory that could be applied to Myolc. The crystal structure of *Dictyostelium* myosin-1E illustrates a state in which the head's converter domain makes contact with and is stabilized by highly conserved tyrosine residues in the upper motor domain (Kollmar M, 2002). In myosin-1E, tyrosines 69 and 70 are aromatically stacked with another aromatic residue at phenylalanine 686 to stabilize an intermediate conformation (Kollmar M, 2002). In Myolc, S701 is located in a comparable residue to the F686 in myosin 1E, and a negatively charged phosphate at S701, as a result of phosphorylation, could interact with several positively charged arginine residues of the Myolc head at positions 65-70. Stabilization of an intermediate conformation in the myosin ATPase cycle by electrostatic interaction of a phosphate in the Myolc neck with the positively charged region in the myosin head may alter the motility and rate of ATP hydrolysis of the motor. Based on comparisons of Myolc and myosin-1E, phosphorylation of Myolc may stabilize the protein in an intermediate conformation and decrease the ATPase activity. It is predicted that an increase in myosin flexibility or stabilization of a structural intermediate can alter the speed of the motor and have significant effects on adaptation in the hair cell.

FUTURE DIRECTIONS II

To assess force, actin-binding proteins other than α -actinin could be used in the *in vitro* motility assay. Some commonly used proteins in such experiments include filamin and NEM-S1 (Janson LW, 1994; Bing W, 2000; Fitzsimons DP, 2001). We have also had preliminary success using an anti-actin antibody to stall actin translocation, and this method can also be used in conjunction with *in vitro* motility, similar to the α -actinin experiments. Given the resources, optical trapping would be the ideal method to access myosin force. Optical trapping allows measurements of single myosin molecules in the piconewton range by using a laser to trap the myosin.

Our experiments were limited by the ability to express and purify large amounts of protein. To overcome these difficulties, it would be ideal to express Myolc in bacteria because greater quantities of protein can be expressed on a shorter timescale than by Sf9 cells. Unfortunately, no one has expressed any active myosin in bacteria. To date, experiments with Myolc have been performed with Myolc protein expressed in Sf9 cells. The Sf9 cell protein expression system is not efficient; expression of a single protein from cloning to expression takes 6-8 weeks on average. To overcome some of these difficulties, it is possible to have the National Cell Culture Center, Minneapolis, Minnesota (NCCC) produce large quantities of desired proteins, which has been successful with expression of HN.

Investigating Myolc function in a fully phosphorylated form would address the problem of imperfect mutations. As addressed in Chapter IB, it is possible that CaM bound to IQ2 could be inhibiting full phosphorylation. If robust phosphorylation of the IQ2-mutant Myolc is achieved, then it would be ideal to look at motor mechanics of this mutant. Because mutating IQ2 may affect ATPase and *in vitro* motility rates, the unphosphorylated IQ2 mutant would need to be characterized and the ATPase and *in vitro* motility rates compared to the phosphorylated state. It is also possible that the IQ2 mutant may have slower motility and ATPase rates. This result would predict that CaM bound at IQ2 is necessary for Myolc motility or ATPase activity.

To confirm that Myolc is the sole downstream target of cAMP and PKA, alternative methods will be necessary. Using a Myolc knock-in mouse, endogenous Myolc could be replaced with a serine site-mutant mimicking phosphorylated or dephosphorylated Myolc. An alanine substitution is proposed as a suitable mimic of the dephosphorylated state, while either S701E or S701D may mimic the phosphorylated state of Myolc. Because we suspect native Myolc to be in a partially phosphorylated state, we initially proposed that experiments with a S701A knock-in would be the most informative so as to mimic dephosphorylated S701. If Myolc S701 is the target of PKA phosphorylation, H89 or 8-Br-cAMP should have no significant effects on open probability of the S701A mutant mouse. The resting open probability would also be expected to be higher than that of the wild-type mouse. Our α -actinin:Myolc data show that both S701A

and S701D produced greater force than HN *in vitro*, so we would predict that the S701A mouse would have a greater open probability than wild type mice.

Another method would be to take advantage of the Myo1c Y61G knock-in mutant mouse. Transduction currents in this mouse decrease upon adding the selective inhibitor NMB-ADP (Stauffer et al., 2005). If Myo1c is the selective target of 8-Br-cAMP or H89, then we would expect these agents to have no effect on currents when Myo1c is inhibited by NMB-ADP. Even a subtle effect on open probability by PKA-altering agents would suggest that there are other targets of PKA in the transduction apparatus.

RESEARCH OBJECTIVES III

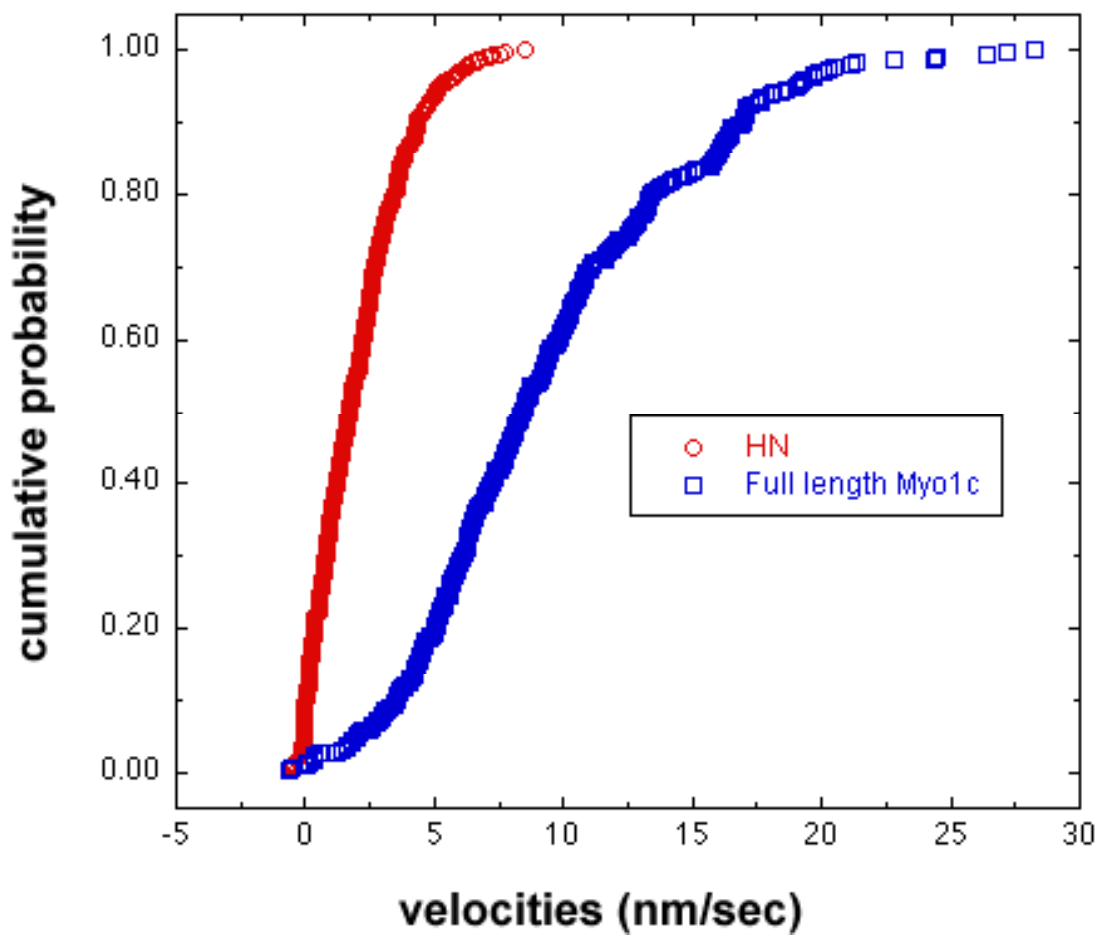
Results III reports data from two separate *in vitro* motility assays of Myolc function. The tail-less head neck (HN) construct of Myolc translocated actin at a slower speed compared with wild-type Myolc. To support data examining Myolc's role in fast adaptation, an *in vitro* motility assay with a mutant-specific inhibitor of mouse Myolc was conducted. *In vitro* motility analysis confirmed that Myolc velocity was halted by the Myolc-Y61G inhibitor NMB-ADP. It was also demonstrated that Ca^{2+} effectively slowed velocity of both Y61G and wtMyolc. NMB-ADP inhibited both fast and slow adaptation in mouse hair cells with the Y61G mutation in Myolc, therefore supporting the role of Myolc in both phases of adaptation.

RESULTS III

***In Vitro* Motility of HN Compared to WT MyoIc**

When *in vitro* motility rates of full-length rat MyoIc were compared to HN, an unexpected difference in velocities was noted. The rate of HN actin translocation, 2.0 ± 0.04 nm/sec ($n = 573$) (mean \pm standard error (SE), $n =$ actin filaments), was significantly slower than that of wild type MyoIc, which translocated actin at 9.4 ± 0.05 nm/sec ($n = 357$; Figure 35). Full length MyoIc is longer in length (1028 amino acids) than HN (791 amino acids), suggesting that the myosin tail may contribute to the observed greater velocity.

Figure 35. *In vitro* motility of HN and wt MyoIc. *In vitro* motility velocities were recorded for HN and full length rat MyoIc and fit with a cumulative velocity plot. Full length MyoIc had higher average velocities than the shorter HN.

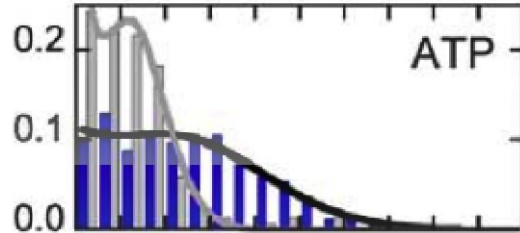


Inhibition of Mouse Y61G MyoIc by NMB-ADP

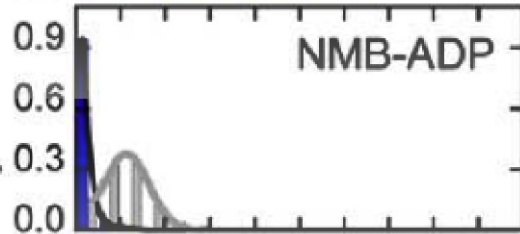
Mouse MyoIc was shown to play a key role in fast adaptation (Stauffer et al., 2005). The authors introduced a Y61G knock-in mutation into the ATP binding pocket of mouse MyoIc, rendering the protein selectively sensitive to the inhibitor N⁶-(2-methylbutyl) adenosine diphosphate (NMB-ADP). ATP and ATP analogs were introduced into a whole-cell recording pipette and the transduction currents of the hair cells were measured. When the inhibitor was introduced into hair cells of Y61G knock in mice, both fast and slow adaptation were inhibited. To support these findings, *in vitro* motility rates of Y61G MyoIc and wild-type protein were compared. In the presence of 1 mM EGTA, wild-type average velocity was 12.4 +/- 0.8 nm/sec (n = 323), while Y61G average velocity was 25.0 +/-0.9 nm/sec (n = 317); (Figure 36). In the presence of 2 mM ATP and 250 μM NMB-ADP, the average velocity of Y61G (2.7 +/- 0.1 nm/sec; n = 494) was inhibited while wild type (11.0 +/- 0.3 nm/sec; n = 363) remained essentially unaffected. With added Ca²⁺ both wild-type (6.2 +/- 0.3 nm/sec; n = 329), and Y61G (12.4 +/- 1.1 nm/sec; n = 243) were inhibited. NMB-ATP slowed motility for both wild type (5.6 +/- 0.3 nm/sec; n = 394) and Y61G: (4.2 +/- 0.6 nm/sec; n = 87).

Figure 36. *In vitro* motility of Y61G and wild-type Myolc. A. In the presence of ATP, Y61G mouse Myolc had a greater range of velocities than wild-type Myolc. B. NMB-ADP slowed Y61G Myolc actin translocation while wild-type Myolc was not affected. C. Ca^{2+} slowed both Y61G and wt Myolc velocities. D. NMB-ATP had an inhibitory affect on velocities of both Y61G and wtild-type Myolc.

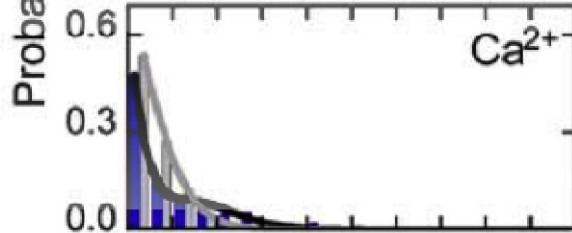
A



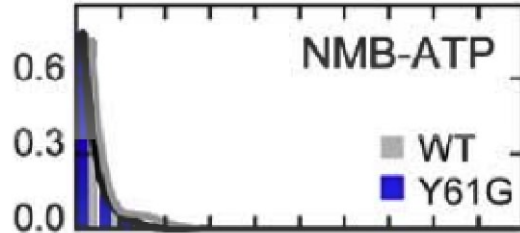
B



C



D



Rate (nm/s)

DISCUSSION III

These results show that wild-type rat Myolc translocated actin at a greater velocity than the truncated Myolc, HN. There was one notable difference: the full-length Myolc was attached to coverslips in the previous and current experiments with the 2652 antibody, which recognizes an epitope in the last 15 kDa of the tail. In the current experiment, HN was attached to coverslips with 9E10, an antibody that recognizes the myc tag at the distal C-terminal of the HN protein. Though the attachment points of the myosin were slightly different, wild-type Myolc maintained a longer tail than HN.

It is possible that attaching wild-type Myolc by mid-tail may have a steric effect on velocity or inhibit a part of the tail that normally speeds up velocity. There may be a spring-like component of the tail that is stabilized when attached to a substrate, explaining the greater velocity seen in the wild type. We cannot rule out the presence of a phosphorylation site or charge effect from the tail that is crucial for velocity. On a high stringency ScanSite analysis of Myolc, there is an ERK kinase-binding domain at L907 (see Figure 27). While this is an unlikely candidate to alter velocity, we cannot rule out the importance of this domain within the tail for myosin motility.

Other research has supported the hypothesis that myosin velocity is dependent on lever arm and tail length (Schott DH, 2002; Köhler D, 2003). The presence of a tail may allow Myolc to take a larger step or have a greater duty ratio which may translate to increased velocity (Schott DH, 2002). Research with

MyoV truncations show that myosins containing more IQ domains take larger steps along actin filaments and have faster velocities than shorter versions of the protein (Uyeda et al., 1996; Sakamoto T, 2005). Though little is known about the function of tails in unconventional myosins, the presence of a tail may add drag through ionic interactions and slow down motility (Guo B, 2004). Thirumurugan, (2006) proposed that binding of the MyoV tail to cargo unfolds and stabilizes the tail allowing a greater velocity. A similar effect may exist for wild-type Myolc, where binding of the tail to cargo or lipids stabilizes the motor to allow a faster propulsion rate.

It was determined that Myolc plays a strong role in both slow and fast adaptation. To support these findings, the effectiveness of the mutant-specific inhibitor NMB-ADP was tested with the *in vitro* motility assay. As seen with rat Y61G Myolc, the mouse Y61G had a greater velocity than wild-type Myolc. NMB-ADP was able to inhibit motility of mouse Y61G while wild-type Myolc was unaffected. Ca^{2+} slowed velocities of both the wild-type and Y61G Myolc. We hypothesize that Myolc generates less force in the presence of Ca^{2+} and cannot overcome the load of immobile Myolc on the surface of the coverslip. Unexpectedly, NMB-ATP inhibited both wild-type and Y61G. This may be a result of the hydrolysis product, NMB-ADP, inhibiting the myosin, resulting in more force production.

FUTURE DIRECTIONS III

To further investigate the role of tail length on Myo1c velocity, several other truncations of Myo1c could be evaluated. It will be crucial to investigate how truncations that exclude or mutate the potential Erk kinase-binding domain affect motility. Expressing wild-type rat Myo1c with a C-terminal myc-tag would rule out any doubt based on the tag. Comparing HN and wild-type velocities in the presence of α -actinin would be a good starting point for force assessment of the motors. Using more involved techniques such as laser trapping would more definitively determine how the tail affects force production.

SUMMARY AND CONCLUSIONS

Nearly 30 million people experience some form of deafness or vestibular abnormality (Kroenke, 1989; Kroenke, 1990). Hair cells of the ear have the key responsibility of transducing auditory and vestibular information into electrical signals. Although identities of several key proteins within the hair cell have been determined, far less is known about how any one protein is functionally regulated by processes such as phosphorylation. Phosphorylation, a known “on-off” switch for many proteins, is likely to be a key regulator for Myo1c and may be a determining factor of whether a hair cell's transduction channel is open or closed. The goal of this thesis was to determine the consequences of S701 phosphorylation on the biochemical properties of Myo1c and also determine the conditions that promote phosphorylation. Understanding the regulation of Myo1c by phosphorylation in the hair cell will shed light on the molecular mechanics of the adaptation motor and further our understanding of deafness and vestibular abnormalities, perhaps permitting development of more effective therapies.

Research by David Corey reported that the open probability of hair cell transduction channels could be changed by agents that alter PKA activity (Geleoc et al., 2001). Consistent with these results was the identification of a strong PKA phosphorylation site at S701 in Myo1c, a key force-producer in tip-link tension. This site lies at the junction between the head and neck domain; a prime location to affect motor mechanics and function. We demonstrated that S701 could be phosphorylated by PKA, and that phosphorylation levels were sensitive

to Ca^{2+} . Ca^{2+} promoted phosphorylation in long Myolc constructs, suggesting that CaM bound to Myolc IQ domains may have an inhibitory role on PKA access to S701. Experiments with short peptides containing only the PKA consensus site and IQ1 demonstrated that the presence of CaM at IQ1 did not have an inhibitory effect on phosphorylation. Surprisingly, Ca^{2+} had an inhibitory effect on phosphorylation of the IQ1 peptide. CaM also bound equally well to short peptides that contained a phosphate at S701 and peptides without a phosphate. These experiments point to the involvement of other Myolc IQ domains in Ca^{2+} facilitation of phosphorylation.

To determine the relative phosphorylation state of Myolc in hair cells, we first immunoprecipitated Myolc from COS-7 cells and Sf9 cell expressed protein. Unfortunately, no phosphorylated protein was recognized. We are fairly confident, however, that endogenous Myolc is in an unphosphorylated state. These experiments have shown that Myolc is difficult to phosphorylate, or requires other factors to be present that we have yet to introduce. Myolc phosphorylation is more complex than originally thought.

Our experiments investigating the impact of mutated S701 on Myolc function have illustrated the importance of this site. Preliminary ATPase assay results suggest that HNS701D may have slower ATPase rates, though these results will need to be confirmed. *In vitro* motility experiments determined that both mutants HNS701A and HNS701D translocated actin slower than HN. In an assay of force production, however, both HNS701A and HN701D velocities were not inhibited by high concentrations of an actin-binding protein, suggesting that

both these mutants produce greater force. The HNS701A result was consistent with the earlier hypothesis that MyoIc with mutations mimicking dephosphorylated S701 would be the greatest force-producers. Though both mutations had similar biomechanical properties, they both significantly differed from that of HN. We can conclude, however, that the S701 site is critical for MyoIc mechanics.

Lastly, it was also determined that wild type MyoIc translocates actin at a faster velocity than the tail-less HN construct. Whether this is due to the involvement of a yet-unidentified tail domain or phosphorylation site, or binding partner is not known. The final set of experiments supports the finding that MyoIc is a key component of fast adaptation. *In vitro* motility assays showed that NMB-ADP was able to inhibit motility of mouse Y61G MyoIc while having no effect on wild type MyoIc activity.

Taken together, these results show the importance of the S701 site in MyoIc. Ca^{2+} and CaM may be important regulatory mechanisms for PKA phosphorylation of MyoIc, and may play a larger role in the control of hair cell adaptation. The studies with S701 mutant confirm the hypothesis that S701 is important for MyoIc mechanics. These studies further our understanding of MyoIc phosphorylation and how this significant motor may regulate hair cell channel sensitivity.

REFERENCES

- Ahmed, Z. M., Goodyear, R., Riazuddin, S., Lagziel, A., Legan, P. K., Behra, M., Burgess, S. M., Lilley, K. S., Wilcox, E. R., Riazuddin, S., Griffith, A. J., Frolenkov, G. I., Belyantseva, I. A., Richardson, G. P., Friedman, T. B. 2006. The tip-link antigen, a protein associated with the transduction complex of sensory hair cells, is protocadherin-15. *J Neurosci* 26: 7022-7034
- Anderson DW, P. F. J., Belyantseva IA, Fridell RA, Beyer L, Martin DM, Wu D, Kachar B, Friedman TB, Raphael Y, Camper SA. 2000. The motor and tail regions of myosin XV are critical for normal structure and function of auditory and vestibular hair cells. *Hum Mol Genet* 9: 1729-1738
- Art, J. J., Crawford, A. C., Fettiplace, R., Fuchs, P. A. 1985. Efferent modulation of hair cell tuning in the cochlea of the turtle. *J Physiol (Lond)* 360: 397-421
- Assad, J. A., Corey, D. P. 1992. An active motor model for adaptation by vertebrate hair cells. *J. Neurosci.* 12: 3291-3309
- Assad, J. A., Shepherd, G. M. G., Corey, D. P. 1991. Tip-link integrity and mechanical transduction in vertebrate hair cells. *Neuron* 7: 985-994
- Avraham, K. B., Hasson, T., Steel, K. P., Kingsley, D. M., Russell, L. B. 1995. The mouse Snell's waltzer deafness gene encodes an unconventional myosin. *Nature Genetics* 11: 369-375

Batters, C., Arthur, C. P., Lin, A., Porter, J., Geeves, M. A., Milligan, R. A., Molloy, J. E., Coluccio, L. M. 2004a. Myo1c is designed for the adaptation response in the inner ear. *EMBO J.* 23: 1433-1440

Batters, C., Wallace, M. I., Coluccio, L. M., Molloy, J. E. 2004b. A model of stereocilia adaptation based on single molecule mechanical studies of myosin I. *Philos. Trans. R. Soc. Lond. B Biol. Sci.* 359: 1895-1905

Bautista, D. M., Jordt, S. E., Nikai, T., Tsuruda, P. R., Read, A. J., Poblete, J., Yamoah, E. N., Basbaum, A. I., Julius, D. 2006. TRPA1 mediates the inflammatory actions of environmental irritants and proalgesic agents. *Cell* 124: 1269-1282

Baylor, D. A., Fettiplace, R. 1975. Light path and photon capture in turtle photoreceptors. *J Physiol (Lond)* 248: 433-464

Berg, J. S., Powell, B. C., Cheney, R. E. 2001. A millennial myosin census. *Mol. Biol. Cell* 12: 780-94.

Bing W, K. A., Marston SB. 2000. A simple method for measuring the relative force exerted by myosin on actin filaments in the in vitro motility assay: evidence that tropomyosin and troponin increase force in single thin filaments. *Biochem J* 350 Pt 3: 693-699

Bose, A., Guilherme, A., Robida, S. I., Nicoloso, S. M., Zhou, Q. L., Jiang, Z. Y., Pomerleau, D. P., Czech, M. P. 2002. Glucose transporter recycling in response to insulin is facilitated by myosin Myo1c. *Nature* 420: 821-824

Bosher, S. K., Warren, R. L. 1978. Very low calcium content of cochlear endolymph, an extracellular fluid. *Nature* 273: 377-378

Cheney, R. E., O'Shea, M. K., Heuser, J. E., Coelho, M. V., Wolenski, J. S., Espreafico, E. M. 1993. Brain myosin-V is a two-headed unconventional myosin with motor activity. *Cell* 75: 13-23

Coelho MV, L. R. E. 1993. Ca(2+)-dependent phosphorylation of the tail domain of myosin-V, a calmodulin-binding myosin in vertebrate brain. *Braz J Med Biol Res* 26: 465-472

Corey, D. P., Hudspeth, A. J. 1983. Kinetics of the receptor current in bullfrog saccular hair cells. *J. Neurosci.* 3: 962-976

Corey, D. P., Garcia-Anoveros, J., Holt, J. R., Kwan, K. Y., Lin, S. Y., Vollrath, M. A., Amalfitano, A., Cheung, E. L., Derfler, B. H., Duggan, A., Geleoc, G. S., Gray, P. A., Hoffman, M. P., Rehm, H. L., Tamasauskas, D., Zhang, D. S. 2004. TRPA1 is a candidate for the mechanosensitive transduction channel of vertebrate hair cells. *Nature* 432: 723-730

Cyr, J. L., Dumont, R. A., Gillespie, P. G. 2002. Myosin-1c interacts with hair-cell receptors through its calmodulin-binding IQ domains. *J. Neurosci.* 22: 2487-2495

Davare MA, H. M. C., Hell JW. 2000. Protein phosphatase 2A is associated with class C L-type calcium channels (Cav1.2) and antagonizes channel phosphorylation by cAMP-dependent protein kinase. *J Biol Chem* 275: 39710-39717

Davies SP, R. H., Caivano M, Cohen P. 2000. Specificity and mechanism of action of some commonly used protein kinase inhibitors. *Biochem J* 351: 95-105

Drescher MJ, K. K. M., Beisel KW, Karadaghy AA, Hatfield JS, Kim SY, Drescher AJ, Lasak JM, Barretto RL, Shakir AH, Drescher DG. 1997. Expression of adenylyl cyclase type I in cochlear inner hair cells. *brain res mol Brain Res* 45: 325-330

Dumont, R. A., Lins, U., Filoteo, A. G., Penniston, J. T., Kachar, B., Gillespie, P. G. 2001. Plasma membrane Ca²⁺-ATPase isoform 2a is the PMCA of hair bundles. *J. Neurosci.* 21: 5066-5078

Eatock, R. A., Corey, D. P., Hudspeth, A. J. 1987. Adaptation of mechano-electrical transduction in hair cells of the bullfrog's sacculus. *J. Neurosci.* 7: 2821-2836

Espanel X, H.-R. M., Van Huijsduijnen RH. 2002. The SPOT technique as a tool for studying protein tyrosine phosphatase substrate specificities. *protein sci* 11: 2326-2334

Fain, G. L. 1999. *Molecular and Cellular Physiology of Neurons* (Cambridge, MA; Harvard University Press).

Fettiplace, R. 1992. The role of calcium in hair cell transduction. *Soc Gen Physiol Ser* 47: 343-356

Fiol CJ, M. A. M., Wang Y, Roeske RW, Roach P 1987. Formation of protein kinase recognition sites by covalent modification of the substrate. Molecular mechanism for the synergistic action of casein kinase II and glycogen synthase kinase 3. *j biol chem* 262: 14042-14048

Fitzsimons DP, P. J. R., Campbell KS, Moss RL. 2001. Cooperative mechanisms in the activation dependence of the rate of force development in rabbit skinned skeletal muscle fibers. *j gen Physiol* 117: 133-148

Friedman, T. B., Sellers, J. R., Avraham, K. B. 1999. Unconventional myosins and the genetics of hearing loss. *Am J Med Genet* 89: 147-157

Geleoc, G. S. a. C., D. P. 2001. Modulation of mechanoelectrical transduction by protein kinase A in utricular hair cells of neonatal mice. *Assoc Res Otolaryngol Abs* 865:

Gillespie, P. G., Corey, D. P. 1997. Myosin and adaptation by hair cells. *Neuron* 19: 955-958

Gillespie, P. G., Gillespie, S. K., Mercer, J. A., Shah, K., Shokat, K. M. 1999. Engineering of the myosin-I β nucleotide-binding pocket to create selective sensitivity to N(6)-modified ADP analogs. *J. Biol. Chem.* 274: 31373-31381

Gillespie, P. G., Hasson, T., Garcia, J. A., Corey, D. P. 1996. Multiple myosin isozymes and hair-cell function. *Cold Spring Harb. Symp. Quant. Biol.* 61: 309-318

Gillespie, P. G., Cyr, J. L. 2002. Calmodulin binding to recombinant myosin-1c and myosin-1c IQ peptides. *BMC Biochem.* 3: 31

Gillespie, P. G., Cyr, J. L. 2004. Myosin-1c, the hair cell's adaptation motor. *Annu. Rev. Physiol.* 66: 521-545

Goodyear, R. J., Marcotti, W., Kros, C. J., Richardson, G. P. 2005. Development and properties of stereociliary link types in hair cells of the mouse cochlea. *J Comp Neurol* 485: 75-85

Guo B, G. W. H. 2004. The tail of myosin reduces actin filament velocity in the in vitro motility assay. *Cell Motil Cytoskeleton* 59: 264-272

Hasson, T., Gillespie, P. G., Garcia, J. A., MacDonald, R. B., Zhao, Y., Yee, A. G., Corey, D. P. 1997. Unconventional myosins in inner-ear sensory epithelia. *J. Cell Biol.* 137: 1287-1307

Hasson, T., Mooseker, M. S. 1994. Porcine myosin-VI: characterization of a new mammalian unconventional. *Journal of Cell Biology* 127: 425-440

Hirono, M., Denis, C. S., Richardson, G. P., Gillespie, P. G. 2004. Hair cells require phosphatidylinositol 4,5-bisphosphate for mechanical transduction and adaptation. *Neuron* 44: 309-320

Holt, J. R., Gillespie, S. K., Provance, D. W., Shah, K., Shokat, K. M., Corey, D. P., Mercer, J. A., Gillespie, P. G. 2002. A chemical-genetic strategy implicates myosin-1c in adaptation by hair cells. *Cell* 108: 371-381

Homma K, Y. M., Saito J, Ikebe R, Ikebe M 2001. The core of the motor domain determines the direction of myosin movement. *nature* 412: 831-834

Houdusse A, S.-G. A. G., Cohen C. 2000. Three conformational states of scallop myosin S1. *Proc Natl Acad Sci U S A*. 97: 11238-11243

Howard, J., Ashmore, J. F. 1986. Stiffness of sensory hair bundles in the sacculus of the frog. *Hear Res* 23: 93-104

Howard, J. 2001. *Mechanics of Motor Proteins and the Cytoskeleton*. 367

Howard, J., Hudspeth, A. J. 1987. Mechanical relaxation of the hair bundle mediates adaptation in mechano-electrical transduction by the bullfrog's saccular hair cell. *Proc. Natl. Acad. Sci. USA* 84: 3064-3068

Howard, J., Hudspeth, A. J., Vale, R. D. 1989. Movement of microtubules by single kinesin molecules. *Nature* 342: 154-158

Howard, J., Roberts, W. M., Hudspeth, A. J. 1988. Mechano-electrical transduction by hair cells. *Ann. Rev. Biophys. Biophys. Chem.* 17: 99-124

Huang W, E. R. L. 1994. Constitutive activation of Mek1 by mutation of serine phosphorylation sites. *proc natl Acad Sci U S A* 91: 8960-8963

Hudspeth, A. J. 1992. Hair-bundle mechanics and a model for mechano-electrical transduction by hair cells. *Soc. Gen. Physiol. Ser.* 47: 357-370

Hudspeth, A. J., Gillespie, P. G. 1994. Pulling springs to tune transduction: adaptation by hair cells. *Neuron* 12: 1-9

Hudspeth, A. J., Jacobs, R. 1979. Stereocilia mediate transduction in vertebrate hair cells (auditory system/cilium/vestibular system). *Proc. Natl. Acad. Sci. USA* 76: 1506-1509

Jacobs, R. A., Hudspeth, A. J. 1990. Ultrastructural correlates of mechano-electrical transduction in hair cells of the bullfrog's internal ear. *Cold Spring Harb. Symp. Quant. Biol.* 55: 547-561

Janson LW, T. D. L. 1994. Actin-crosslinking protein regulation of filament movement in motility assays: a theoretical model. *biophys J* 67: 973-982

Kachar, B., Parakkal, M., Kurc, M., Zhao, Y., Gillespie, P. G. 2000. High-resolution structure of hair-cell tip links. *Proc. Natl. Acad. Sci. USA* 97: 13336-13341

Kelley MW, O. C. K., Corwin JT. 1992. Maturation of kinocilia in amphibian hair cells: growth and shortening related to kinociliary bulb formation. *hear Res* 59: 108-115

Kennedy, H. J., Evans, M. G., Crawford, A. C., Fettiplace, R. 2003. Fast adaptation of mechano-electrical transducer channels in mammalian cochlear hair cells. *Nat. Neurosci.* 6: 832-836

Köhler D, R. C., Meyhöfer E, Bähler M. 2003. Different degrees of lever arm rotation control myosin step size. *J Cell Biol.* 161: 237-241

Kollmar M, D. U., Kliche W, Manstein DJ, Kull FJ. 2002. Crystal structure of the motor domain of a class-I myosin. *EMBO J* 21: 2517-2525

AV, K. 2001. Models of the dynamics of otolithic membrane and hair cell bundle mechanics. *J Vestib Res* 11: 33-42

Kroenke, M., and Manglesdorff, A. D. 1989. Common symptoms in ambulatory care: incidence, evaluation, therapy, and outcome. *Am J Med Genet* 86: 262-266

Kroenke, M., Arrington, M. E., and Manglesdorff, A. D 1990. The prevalence of symptoms in medical outpatients and the adequacy of therapy. *Arch Intern Med* 150: 1685-1689

Kros, C. J., Marcotti, W., van, N. S. M., Self, T. J., Libby, R. T., Brown, S. D., Richardson, G. P., Steel, K. P. 2002. Reduced climbing and increased slipping adaptation in cochlear hair cells of mice with *Myo7a* mutations. *Nat. Neurosci.* 5: 41-47

- Kumagami H, B. E., Wild K, Zenner HP, Ruppertsberg JP, Schultz JE. 1999. Expression pattern of adenylyl cyclase isoforms in the inner ear of the rat by RT-PCR and immunochemical localization of calcineurin in the organ of Corti. *hear Res* 132: 69-75
- Küssel-Andermann P, E.-A. A., Safieddine S, Hardelin JP, Nouaille S, Camonis J, Petit C. 2000. Unconventional myosin VIIA is a novel A-kinase-anchoring protein. *J biol chem* 275: 29654-29659
- Kwan, K. Y., Allchorne, A. J., Vollrath, M. A., Christensen, A. P., Zhang, D. S., Woolf, C. J., Corey, D. P. 2006. TRPA1 contributes to cold, mechanical, and chemical nociception but is not essential for hair-cell transduction. *Neuron* 50: 277-289
- Lewis, E. R., Leverenz, E L, Bialek, B S 1985. *The Vertebrate Inner Ear* (Boca Raton, FL; CRC Press).
- Lim, D. J. 1986. Functional structure of the organ of Corti: a review. *Hear Res* 22: 117-146

Lister, I., Roberts, R., Schmitz, S., Walker, M., Trinick, J., Veigel, C., Buss, F., Kendrick-Jones, J. 2004. Myosin VI: a multifunctional motor. *Biochemical Society Transactions* 32: 684-688

Martin, P., Bozovic, D., Choe, Y., Hudspeth, A. J. 2003. Spontaneous oscillation by hair bundles of the bullfrog's sacculus. *J. Neurosci.* 23: 4533-4548

Martin, P., Hudspeth, A. J. 1999. Active hair-bundle movements can amplify a hair cell's response to oscillatory mechanical stimuli. *Proc. Natl. Acad. Sci. USA* 96: 14306-14311

Martin, P., Mehta, A. D., Hudspeth, A. J. 2000. Negative hair-bundle stiffness betrays a mechanism for mechanical amplification by the hair cell. *Proc. Natl. Acad. Sci. USA* 97: 12026-12031

Mathews, C. K., Van, H., K. E 1996. *Biochemistry*. xxvii, 1159 p

Mermall, V., Post, P. L., Mooseker, M. S. 1998. Unconventional myosins in cell movement, membrane traffic, and signal. *Science* 279: 527-533

Metcalf, A. B., Chelliah, Y., Hudspeth, A. J. 1994. Molecular cloning of a myosin I beta isozyme that may mediate adaptation by hair cells of the bullfrog's internal ear. *Proc. Natl. Acad. Sci. USA* 91: 11821-11825

Mischak H, S. T., Janosch P, Eulitz M, Steen H, Schellerer M, Philipp A, Kolch W. 1996. Negative regulation of Raf-1 by phosphorylation of serine 621. *mol cell biol* 16: 5409-5418

Montcouquiol M, K. M. W. 2003. Planar and vertical signals control cellular differentiation and patterning in the mammalian cochlea. *j neurosci* 23: 9469-9478

Mooseker, M. S., Cheney, R. E. 1995. Unconventional myosins. *Ann. Rev. Cell Devel. Biol.* 11: 633-675

Nagata, K., Duggan, A., Kumar, G., Garcia-Anoveros, J. 2005. Nociceptor and hair cell transducer properties of TRPA1, a channel for pain and hearing. *J Neurosci* 25: 4052-4061

Nascimento, A. A. C., Cheney, R. E., Tauhata, S. B. F., Larson, R. E. 1996. Enzymatic characterization and functional domain mapping of brain myosin-V. *Journal of Biological Chemistry* 271: 17561-17569

O'Hagan R, C. M., Goodman MB. 2005. The MEC-4 DEG/ENaC channel of *Caenorhabditis elegans* touch receptor neurons transduces mechanical signals. *nat neurosci* 8: 43-50

Obenauer JC, C. L. C., Yaffe MB. 2003. Scansite 2.0: Proteome-wide prediction of cell signaling interactions using short sequence motifs. *nucleic Acids Res* 31: 3635-3641

Oliver, T. N., Berg, J. S., Cheney, R. E. 1999. Tails of unconventional myosins. *Cell Mol Life Sci* 56: 243-57.

Pickles, J. O., Comis, S. D., Osborne, M. P. 1984. Cross-links between stereocilia in the guinea pig organ of Corti, and their possible relation to sensory transduction. *Hearing Res.* 15: 103-112

Reizes, O., Barylko, B., Li, C., Südhof, T. C., Albanesi, J. P. 1994. Domain structure of a mammalian myosin I. *Proc. Natl. Acad. Sci. USA* 91: 6349-6353

Ricci, A. J., Fettiplace, R. 1997. The effects of calcium buffering and cyclic AMP on mechano-electrical transduction in turtle auditory hair cells. *J. Physiol. (Lond.)* 501: 111-124

Ricci, A. J., Wu, Y. C., Fettiplace, R. 1998. The endogenous calcium buffer and the time course of transducer adaptation in auditory hair cells. *J. Neurosci.* 18: 8261-8277

Royo M, D. S. C., Fitzpatrick PF. 2005. Effects of mutations in tyrosine hydroxylase associated with progressive dystonia on the activity and stability of the protein. *proteins* 58: 14-21

Rusch, A., Hummler, E. 1999. Mechano-electrical transduction in mice lacking the alpha-subunit of the epithelial sodium channel. *Hear Res* 131: 170-16.

Rzadzinska AK, S. M. E., Davies C, Riordan GP, Kachar B. 2004. An actin molecular treadmill and myosins maintain stereocilia functional architecture and self-renewal. *J cell biol.* 164: 887-897

Sakamoto T, Y. A., Selvin PR, Sellers JR. 2005. Step-size is determined by neck length in myosin V. *biochemistry* 44: 16203-16210

Schneider, M. E., Dose, A. C., Salles, F. T., Chang, W., Erickson, F. L., Burnside, B., Kachar, B. 2006. A new compartment at stereocilia tips defined by spatial and temporal patterns of myosin IIIa expression. *J Neurosci* 26: 10243-10252

Schott DH, C. R. N., Bretscher A. 2002. Secretory vesicle transport velocity in living cells depends on the myosin-V lever arm length. *J Cell Biol.* 156: 35-39

Sellers JR, V. 2006. Walking with myosin V. *Curr Opin Cell Biol* 18: 68-73

Sellick, P. M., Patuzzi, R., Johnstone, B. M. 1982. Measurement of basilar membrane motion in the guinea pig using the Mössbauer technique. *J. Acoust. Soc. Am.* 72: 131-141

Shepherd, G. M. G., Assad, J. A., Parakkal, M., Kachar, B., Corey, D. P. 1992. Movement of the tip-link attachment is correlated with adaptation in bullfrog saccular hair cells. *J. Gen. Physiol.* 98: 25a

Shotwell, S. L., Jacobs, R., Hudspeth, A. J. 1981. Directional sensitivity of individual vertebrate hair cells to controlled deflection of their hair bundles. *Ann. N.Y. Acad. Sci.* 374: 1-10

Sidi, S., Friedrich, R. W., Nicolson, T. 2003. NompC TRP channel required for vertebrate sensory hair cell mechanotransduction. *Science* 301: 96-99

Siemens, J., Lillo, C., Dumont, R. A., Reynolds, A., Williams, D. S., Gillespie, P. G., Müller, U. 2004. Cadherin 23 is a component of the tip link in hair-cell stereocilia. *Nature* 428: 950-955

Smith SD, J. Z., Huynh KK, Wells A, Elce JS. 2003. Glutamate substitutions at a PKA consensus site are consistent with inactivation of calpain by phosphorylation. *feBS Lett* 542: 115-118

Solc, C. K., Derfler, B. H., Duyk, G. M., Corey, D. P. 1994. Molecular cloning of myosins from bullfrog saccular macula: a candidate for the hair cell adaptation motor. *Auditory Neurosci.* 1: 63-75.

Sollner, C., Rauch, G. J., Siemens, J., Geisler, R., Schuster, S. C., Muller, U., Nicolson, T. 2004. Mutations in cadherin 23 affect tip links in zebrafish sensory hair cells. *Nature* 428: 955-959

Stauffer, E. A., Scarborough, J. D., Hirono, M., Miller, E. D., Shah, K., Mercer, J. A., Holt, J. R., Gillespie, P. G. 2005. Fast adaptation in vestibular hair cells requires myosin-1c activity. *Neuron* 47: 541-553

Stowers, L., Holy, T. E., Meister, M., Dulac, C., Koentges, G. 2002. Loss of sex discrimination and male-male aggression in mice deficient for TRP2. *Science* 295: 1493-1500

Tilney, L. G., Bonder, E. M., Coluccio, L. M., Mooseker, M. S. 1983. Actin from Thyone sperm assembles on only one end of an actin filament: a. *Journal of Cell Biology* 97: 112-124

Tilney, L. G., DeRosier, D. J., Mulroy, M. J. 1980. The organization of actin filaments in the stereocilia of cochlear hair cells. *J. Cell Biol.* 86: 244-259

Uyeda, T. Q., Abramson, P. D., Spudich, J. A. 1996. The neck region of the myosin motor domain acts as a lever arm to generate movement. *Proc Natl Acad Sci U S A* 93: 4459-4464

Veigel C, W. F., Bartoo ML, Sellers JR, Molloy JE 2002. The gated gait of the processive molecular motor, myosin V. *Nat cell Biol* 4: 59-65

Veigel, C., Coluccio, L. M., Jontes, J. D., Sparrow, J. C., Milligan, R. A., Molloy, J. E. 1999. The motor protein myosin-I produces its working stroke in two steps. *Nature* 398: 530-533

Volkman N, O. G., Trybus KM, DeRosier DJ, Lowey S, Hanein D 2003. Myosin isoforms show unique conformations in the actin-bound state. *proc natl Acad Sci U S A* 100: 3227-3232

G., v. B. 1960. Experiments in Hearing (New York; McGraw-Hill Inc.).

Wagner N, E. P., Tedder TF. 1993. Regulation of the tyrosine kinase-dependent adhesion pathway in human lymphocytes through CD45. *J Immunol* 150: 4887-4899

Walker, R. G., Hudspeth, A. J. 1996. Calmodulin controls adaptation of mechano-electrical transduction by hair cells of the bullfrog's sacculus. *Proc. Natl. Acad. Sci. USA* 93: 2203-2207

Walker, R. G., Willingham, A. T., Zuker, C. S. 2000. A *Drosophila* mechanosensory transduction channel. *Science* 287: 2229-2234

Wang, F. S., Wolenski, J. S., Cheney, R. E., Mooseker, M. S., Jay, D. G. 1996. Function of myosin-V in filopodial extension of neuronal growth cones. *Science* 273: 660-663

Wangemann P, L. J., Marcus DC. 1995. Ion transport mechanisms responsible for K⁺ secretion and the transepithelial voltage across marginal cells of stria vascularis in vitro. *hear Res* 84: 19-29

Wells AL, L. A. W., Chen LQ, Safer D, Cain SM, Hasson T, Carragher BO, Milligan RA, Sweeney HL 1999. The kinetic mechanism of myosin V. *Proc natl Acad Sci U S A* 96: 13726-13731

Wu, Y. C., Ricci, A. J., Fettiplace, R. 1999. Two components of transducer adaptation in auditory hair cells. *J. Neurophysiol.* 82: 2171-2181

Yamashita H, T. M. J., Warshaw DM, Lowey S, Trybus KM. 2000. Functional consequences of mutations in the smooth muscle myosin heavy chain at sites implicated in familial hypertrophic cardiomyopathy. *J Biol Chem* 275: 28045-28052

Yamoah, E. N., Lumpkin, E. A., Dumont, R. A., Smith, P. J., Hudspeth, A. J., Gillespie, P. G. 1998. Plasma membrane Ca^{2+} -ATPase extrudes Ca^{2+} from hair cell stereocilia. *J. Neurosci.* 18: 610-624

Zhao, Y., Yamoah, E. N., Gillespie, P. G. 1996. Regeneration of broken tip links and restoration of mechanical transduction in hair cells. *Proc. Natl. Acad. Sci. USA* 93: 15469-15474

Zheng, J., Shen, W., He, D. Z., Long, K. B., Madison, L. D., Dallos, P. 2000. Prestin is the motor protein of cochlear outer hair cells. *Nature* 405: 149-55.

Zhu T, S. M., Ikebe M. 1996. Functional expression of mammalian myosin I beta: analysis of its motor activity. *biochemistry* 35: 513-522

Zhu, T., Sata, M., Ikebe, M. 1996. Functional expression of mammalian myosin I beta: analysis of its motor activity. *Biochemistry* 35: 513-522